UNIVERSITY OF HAWAII
LIBRARY
JUL 13 '59

The
Philosophical Magazine

FIRST PUBLISHED IN 1798

A Journal of Theoretical
Experimental and Applied Physics

Vol. 4 May 1959 No. 41
Eighth Series

£1 5s. 0d., plus postage
Annual Subscription £13 10s. 0d., payable in advance

ALERE FLAMMAM

Printed and Published by
TAYLOR & FRANCIS LTD
RED LION COURT, FLEET STREET, LONDON, E.C.4

THE PHILOSOPHICAL MAGAZINE

Editor
Professor N. F. Mott, M.A., D.Sc., F.R.S.

Editorial Board
Sir Lawrence Bragg, O.B.E., M.C., M.A., D.Sc., F.R.S.
Sir George Thomson, M.A., D.Sc., F.R.S.
Professor A. M. Tyndall, C.B.E., D.Sc., F.R.S.

Authors wishing to submit papers for publication in the Journal should send manuscripts directly to the Publishers.

Manuscripts should be typed in *double* spacing on one side of quarto (8 × 10 in.) paper, and authors are urged to aim at absolute clarity of meaning and an attractive presentation of their texts.

References should be listed at the end in alphabetical order of authors and should be cited in the text in terms of author's name and date. Diagrams should normally be in Indian ink on white card, with lettering in soft pencil, the captions being typed on a separate sheet.

A leaflet giving detailed instructions to authors on the preparation of papers is available on request from the Publishers.

Authors are entitled to receive 25 offprints of a paper in the Journal free of charge, and additional offprints can be obtained from the Publishers.

The *Philosophical Magazine* and its companion journal, *Advances in Physics*, will accept papers for publication in experimental and theoretical physics. The *Philosophical Magazine* publishes contributions describing new results, letters to the editor and book reviews. *Advances in Physics* publishes articles surveying the present state of knowledge in any branch of the science in which recent progress has been made. The editors welcome contributions from overseas as well as from the United Kingdom, and papers may be published in English, French and German.

A new International Journal

ERGONOMICS

HUMAN FACTORS IN WORK, MACHINE CONTROL AND EQUIPMENT DESIGN

General Editor
A. T. WELFORD
University of Cambridge, Psychological Laboratory, Downing Place, Cambridge

Associate Editor (Anatomy and Physiology)
W. F. FLOYD

Assistant Editor
Miss H. M. CLAY

Editorial Board

H. Bastenier, *Belgium*; R. B. Bromiley, *Canada*; R. Bonnardel, Bernard Metz, *France*; E. A. Müller, *Germany*; M. G. Bennett, W. E. Hick, Sir Charles Lovatt Evans, L. G. Norman, *Great Britain*; F. H. Bonjer, *Netherlands*; S. P. M. Forssman, *Sweden*; E. Grandjean, *Switzerland*; H. S. Belding, P. M. Fitts, *U.S.A.*

Contents of February, 1959

Symposium on Training

Introductory Address. By P. H. St. J. Wilson, C.B., C.B.E., Chief Industrial Commissioner, Ministry of Labour and National Service
Physiological Bases of Training. By Albert Hemingway, Department of Physiology, School of Medicine, University of Leeds
Training Operatives in Industry. By W. Douglas Seymour, Clent, Worcestershire
The Training of Shoe-Machinists. By W. T. Singleton, The British Boot, Shoe and Allied Trades Research Association, Kettering
A Theory of the Acquisition of Speed-Skill. By E. R. F. W. Crossman, Department of Psychology, Reading University, England
Practice and Knack : Some Comments on Learning and Training in Industry. By Isabel Blain, National Institute of Industrial Psychology
The Operator as a Self-Regulating System: A Factory Experiment. By S. David M. King, Organization & Training (Consultants) Limited, 19 Bolton Street, London, W.1
Note on Current Trends in Literature on Training. By Ezra V. Saul, Institute for Applied Experimental Psychology, Tufts University, Medford, Massachusetts
Circuit Training. By G. T. Adamson, Department of Physical Education, The University, Leeds
The Limitations of a ‘ Procrustean ’ Approach to the Optimization of Man–Machine Systems. By F. V. Taylor and W. D. Garvey, U.S. Naval Research Laboratory, Washington, D.C.
Physical Training in Relation to the Energy Expenditure of Walking and to Factors Controlling Respiration During Exercise. By J. E. Cotes and F. Meade, Medical Research Council, Pheumoconiosis Research Unit, Llandough Hospital, Penarth, Glamorgan, Wales
Problems of Training of the Cardiovascular System. By M. J. Karvonen, Institute of Occupational Health, Helsinki, Finland
Training Muscle Strength. By E. A. Müller, Max-Planck-Institut für Arbeitsphysiologie, Dortmund, Germany
Abstracts of other Papers Delivered at the Symposium

Price £1 5s. 0d. per part plus postage
Subscription price per volume £4 15s. 0d. post free, payable in advance

Printed and Published by
TAYLOR & FRANCIS LTD
RED LION COURT, FLEET STREET, LONDON, E.C.4

Orders originating in U.S.A. and Canada should be sent to the
Academic Press Inc., 111 Fifth Avenue, New York, 3, N.Y., U.S.A.

INTERNATIONAL JOURNAL OF
RADIATION BIOLOGY
and related studies in Physics, Chemistry and Medicine

Editor
W. M. Dale, M.D., D.Sc.
Dept. of Biochemistry, Christie Hospital & Holt Radium Institute, Withington, Manchester, 20

Assistant Editor
John Wakefield, B.A., F.Z.S.

Editorial Board
Charlotte Auerbach, *U.K.;* J. H. Baxendale, *U.K.;* D. W. van Bekkum, *Holland;* E. H. Betz, *Belgium;* H. A. S. van den Brenk, *Australia;* A. A. Buzzatti-Traverso, *Italy;* J. Coursaget, *France;* F. Devik, *Norway;* M. Haissinsky, *France;* A. Hollaender, *U.S.A.;* B. F. Kaufmann, *U.S.A.;* G. Klein, *Sweden;* H. Langendorff, *Germany;* M. Magat, *France;* M. Nakaidzumi, *Japan;* E. Paterson, *U.K.;* H. Ulrich, *Switzerland;* M. Westergaard, *Denmark.*

Contents of April, 1959

Impairment of Fertility by Whole-body Irradiation of Female Mice. By R. H. Mole, Medical Research Council, Radiobiological Research Unit, Atomic Energy Research Establishment, Harwell, Berks, England

Some Effects of X-rays on Dividing Cells in the Testis and Bone Marrow of the Marsupial *Potorous Tridactylus*. By G. B. Sharman, M.R.C. Radiobiological Research Unit, A.E.R.E., Harwell, Berks, England

The Effect of Cysteamine on the Survival of Spermatogonia after X-irradiation. By Anita M. Mandl, Department of Anatomy, University of Birmingham

Identification and Follow-up of Homologous and Heterologous Bone-marrow Transplants in Radiation-chimeras. By W. Welling, O. Vos, W. W. H. Weyzen and D. W. van Bekkum, Medical Biological Laboratory of the National Defence Research Council TNO, Rijswijk (Z.H.), Netherlands

The Effect of Colloidal ^{198}Au on the Bone Marrow and its Replacement in Rabbits. By J. M. Garvan, E. P. George, F. A. Rocke, St. Vincent's Hospital, Darlinghurst, N.S.W., Australia, and S. Vince, Institute of Child Health, Royal Alexandra Hospital for Children, Camperdown, N.S.W., Australia

The Viability of Near-normal Irradiated Chromosomes. By A. J. Bateman, Christie Hospital and Holt Radium Institute, Manchester, England

Response of Megakaryocytes on the ' August ' Rat of X-irradiation. By Shirley M. Simpson, Physics Department (Downs Branch), Institute of Cancer Research, Royal Cancer Hospital, Fulham Road, London, S.W.3

Further Observations on the Radiation Chemistry of Aqueous Solutions of Thiourea. By W. M. Dale and J. V. Davies, Department of Biochemistry, Christie Hospital, Manchester 20

Price per part £1 0s. 0d. plus postage
Subscription per volume (4 issues) £3 15s. 0d. post free, payable in advance

Printed and Published by
TAYLOR & FRANCIS LTD
RED LION COURT, FLEET STREET, LONDON, E.C.4

Orders originating in U.S.A. and Canada should be sent to the
Academic Press Inc., 111 Fifth Avenue, New York 3, N.Y., U.S.A.

Journal of Electronics and Control

A Philosophical Magazine Associated Journal

Editor:
J. THOMSON, M.A., D.Sc., M.I.E.E., F.Inst.P.
Consultant Editor:
Professor N. F. MOTT, F.R.S.
Editorial Board:
Professor P. AIGRAIN (France)
Professor H. B. G. CASIMIR (Holland)
J. F. COALES (U.K.)
Professor K. G. EMELEUS (U.K.)
D. W. FRY (U.K.)
Dr. W. KLEIN (Germany)
Dr. R. KOMPFNER (U.S.A.)

Contents of March, 1959

Electronics Section

New Experimental Results for Plasma Electron Oscillations. By D. W. Mahaffey, Physics Department, Queen's University of Belfast

The Measurement of the Temperature Dependence of the Mobility and Effective Lifetime of Minority Carriers in the Base Region of Silicon Transistors. By D. M. Evans, Official communication from the D.S.I.R. Radio Research Station, Slough

Kinetic Theory of Space-Charge II: Electron Collisional Damping in the Magnetron (and Diode). By Louis Gold, Lincoln Laboratory, Massachusetts Institute of Technology, Lexington, Massachusetts

The Space Charge Field Emission Hypothesis Applied to Hayashi Data on Discharges through Gases. By Herman Ritow, Highland Park, Illinois

The Effect of Trigger Pulse Polarity on the Anode Breakdown Time of the Cold Cathode Arc Conduction Tetrode. By R. Feinberg, Ferranti Ltd., seconded to The Manchester College of Science and Technology

Control Section

Measurement of Magnetic Flux Density by Paramagnetic Resonance. By C. P. Allen and M. Sherry, Communication from the Staff of the Research Laboratories of The General Electric Company Limited, Wembley, England

The Faraday Effect in Anisotropic Semiconductors. By I. G. Austin, Communication from the Staff of the Research Laboratories of The General Electric Company Limited, Wembley, England

The Differential Transformer (Displacement Pick-Up) in Polymer Testing. By A. R. Payne and A. E. Eagles, Research Association of British Rubber Manufacturers Shawbury, Shrewsbury, Shropshire

---

Price per part £1 5s. plus postage
Price per volume £7 post free, payable in advance
6 monthly issues per volume

Printed and Published by

TAYLOR & FRANCIS LTD
RED LION COURT, FLEET STREET, LONDON, E.C.4

Orders originating in U.S.A. and Canada should be sent to the
Academic Press Inc., 111 Fifth Avenue, New York, 3, N.Y., U.S.A.

Physics in Medicine and Biology

A Taylor & Francis Journal published in association
with The Hospital Physicists' Association

Editor: J. E. ROBERTS, D.Sc.
Consultant Editor: Professor N. F. MOTT, F.R.S.

Editorial Board

R. Bonet-Maury, *Paris*; J. Dainty, *Edinburgh*; H. E. Johns, *Toronto*; W. A. Langmead. *London*; D. A. McDonald, *London*; J. S. Mitchell, *Cambridge*; G. J. Neary, *Harwell*; B. Rajewsky, *Frankfurt*; J. Rotblat, *London*; S. Rowlands, *London*; H. P. Schwan, *Philadelphia*; R. Sievert, *Stockholm*; F. W. Spiers, *Leeds*; J. F. Tait, *Massachusetts*; A. J. H. Vendrik, *Nijmegen*.

Contents of January, 1959

The Measurement of Exposure Dose for High Energy Radiation with Cavity Ionization Chambers. By T. E. Burlin, B.Sc., Physics Department, Hammersmith Hospital, London, W.12

The Energy Response of a Victoreen Condenser Ionization Chamber. By A. J. D. Szilvasi, Ph.D. and G. N. Whyte, Ph.D., National Research Council, Ottawa, Canada

An Analysis of Clasp Design in Partial Dentures. By J. A. Warr, M.A.(Cantab.), B.Sc. (London), B.D.S.(London), L.D.S.R.C.S.Eng., Department of Prosthetics, The London Hospital Medical College, Turner Street, London, E.1

A Study of the External Gamma-ray Field Arising from a Radioactive Source Situated in Air and in a Scattering Medium. By H. A. B. Simons, M.A., Ph.D. and S. Chomet, M.Sc., Physics Department, The Royal Free Hospital School of Medicine, 8 Hunter Street, London, W.C.1

A Wide Range Direct Reading X-Ray Dosemeter. By S. Stuart, Electronic Instruments Ltd., Richmond, Surrey and S. B. Osborn, B.Sc., A.Inst. P., University College Hospital, London, W.C.1

Pulmonary Diffusion of Oxygen. By B. F. Visser, Ph.D. and A. H. J. Maas, M.Sc., Pulmonary Function Laboratory, State University Hospital, Utrecht, Netherlands

The Influence of the Anomalous Viscosity of Blood upon its Oscillatory Flow. By M. G. Taylor, M.D., Physiology Department, Medical College of St. Bartholomew's Hospital, London

Subscription price per volume £3 10s. post free, payable in advance
4 parts per volume—£1 per part plus postage

Printed and Published by

TAYLOR & FRANCIS, LTD

RED LION COURT, FLEET STREET, LONDON, E.C.4

Orders originating in U.S.A. and Canada should be sent to the
Academic Press Inc., 111 Fifth Avenue, New York, 3, N.Y., U.S.A.

A new International Journal

Molecular Physics

Editor: **H. C. LONGUET-HIGGINS, F.R.S.**
Associate Editor: **J. H. VAN DER WAALS**

Editorial Board:

J. Bjerrum, *Copenhagen*; G. Careri, *Padua*; C. A. Coulson, *Oxford*; F. H. C. Crick, *Cambridge;* P. J. W. Debye, *Cornell*; D. Hadži, *Ljubljana*; O. Hassel, *Oslo*; W. Heitler, *Zürich*; J. O. Hirschfelder, *Wisconsin*; D. F. Hornig, *Princeton*; J. A. A. Ketelaar, *Amsterdam*; J. G. Kirkwood, *Yale*; R. Kronig, *Delft*; J.W. Linnett, *Oxford*; A. Liquori, *Rome*; Dame Kathleen Lonsdale, *London* ; P-O. Löwdin, *Uppsala* ; M. Magat, *Paris* ; R. S. Mulliken, *Chicago ;* A. Münster, *Frankfurt*; L. J. Oosterhoff, *Leiden*; L. E. Orgel, *Cambridge*; J. A. Pople, *Teddington*; I. Prigogine, *Brussels*; R. E. Richards, *Oxford*; J. S. Rowlinson, *Manchester*; G. S. Rushbrooke, *Newcastle upon Tyne*; L. E. Sutton, *Oxford*; H. W. Thompson, *Oxford*; B. Vodar, *Bellevue, Paris.*

Contents of April, 1959

The Colours of Transition Metal Hexafluorides. By the late W. Moffitt, G. L. Goodman, Chemistry Department, Harvard University, M. Fred and B. Weinstock, Argonne National Laboratory, Lemont, Illinois

Intensities in Inorganic Complexes. III. Octahedral Complexes of Ni(II) and V(III). By C. J. Ballhausen and Andrew D. Liehr, Bell Telephone Laboratories, Incorporated, Murray Hill, New Jersey

Theory of Anisotropic Hyperfine Interactions in π-electron Radicals. By Harden M. McConnell, Gates and Crellin Laboratories of Chemistry, California Institute of Technology, Pasadena, California and John Strathdee, Shell Development Company, Emeryville, California

The Electronic Structure of Hydrogen Fluoride. By R. A. Ballinger, National Physical Laboratory, Teddington, Middlesex

Molecular-orbital Treatment of a New Type of Heteroaromatic Compound. By R. D. Brown and B. A. W. Coller, Chemical Laboratories, University of Melbourne, Carlton, N.3, Victoria, Australia

Statistical Mechanics of Solid and Liquid Mixtures of Ortho- and Para-hydrogen. By A. Bellemans and Agnessa Babloyantz, Faculty of Sciences, Université Libre de Bruxelles, Belgium

On the Motion of a Particle Coupled to Lattice Vibrations. By Thor A. Bak, M. Goche and F. Henin, Faculté des Sciences, Université Libre de Bruxelles, Belgium

The Singularities of the Integrals in Mayer's Ionic Solution Theory. By Harold L. Friedman, Faculté des Sciences, Université Libre de Bruxelles

Calculation of Vibrational Relaxation Times in Gaseous Cyanogen. By P. G. Dickens, Inorganic Chemistry Laboratory, Oxford

Thermodynamic Properties of Clathrates. I. The Heat Capacity and Entropy of Argon in the Argon Quinol Clathrates. By N. G. Parsonage and L. A. K. Staveley, Inorganic Chemistry Laboratory, Oxford

Price per part £1 5s. 0d. plus postage
Subscription per volume (4 issues) £4 15s. 0d. post free, payable in advance

Printed and Published by
TAYLOR & FRANCIS LTD
RED LION COURT, FLEET STREET, LONDON, E.C.4

Orders originating in U.S.A. and Canada should be sent to the
Academic Press Inc., 111 Fifth Avenue, New York, 3, N.Y., U.S.A.

Advances in Physics

A Quarterly Supplement of the Philosophical Magazine

Editor:
PROFESSOR N. F. MOTT, M.A., D.Sc., F.R.S.

Editorial Board:
SIR LAWRENCE BRAGG, O.B.E., M.C., M.A., D.Sc., F.R.S.
SIR GEORGE THOMSON, M.A., D.Sc., F.R.S.
PROFESSOR A. M. TYNDALL, C.B.E., D.Sc., F.R.S.

Contents of January, 1959

The Theory of Superconductivity. By C. G. Kuper, Department of Natural Philosophy, St. Salvator's College, St. Andrews

The Modern Theory of Superconductivity. By I. M. Khalatnikov and A. A. Abrikosov, Institute of Physical Problems, Kaluzhskove Shosse, 32 Moscow, U.S.S.R.

Price per part £1 plus postage

Price per annum £3 15s. post free

Printed and Published by

TAYLOR & FRANCIS LTD

RED LION COURT, FLEET STREET, LONDON, E.C.4

INTERNATIONAL JOURNAL

OPTICA ACTA

European Journal of Optics **Journal Européen d'Optique** **Europäische Zeitschrift für Optik**

English Editor: C. G. Wynne, 13 Elwill Way, Beckenham, Kent, U.K.

Rédacteur Français: A. Maréchal, 3 Boulevard Pasteur, Paris, France

Deutscher Herausgeber: G. Franke, Laufdorfer Weg 2, Wetzlar, Germany

Editorial Board

J. M. Otero y Navascues, *Madrid;* R. W. Ditchburn, *Reading;* A. Arnulf, *Paris;* A. Biot, *Gand;* J. Cabannes, *Paris;* P. Fleury, *Paris;* F. Gabler, *Vienna;* G. Hansen, *Oberkochen;* E. Ingelstam, *Stockholm;* H. Korte, *Braunschweig;* W. S. Stiles, *London;* G. Toraldo di Francia, *Florence;* A. C. S. van Heel, *Delft.*

Contents of April, 1959

Correction Approchée de l'Effet de Lobe en Radioastronomie. Par J. Arsac, Observatoire de Meudon

Colour Perception with the Peripheral Retina. By J. D. Moreland and A. Cruz, Technical Optics Section, Imperial College, London

A Fourier Analyser for Optical Frequency Response Determinations. By J. M. Naish, Royal Aircraft Establishment, Hampshire England

Photo-sensitive Reactions in Foveae of Normal and Cone-monochromatic Observers. By R. A. Weale, Visual Research Division, Ophthalmological Research Unit, (Medical Research Council), Institute of Ophthalmology, Judd Street, London, W.C.1

Contrast Transfer in the Grating Spectrograph. By A. Lohmann, Institute of Optical Research, Stockholm 70, Sweden

Doppelbrechungs-interferenzfarben sehr dünner Plättchen. Von S. Rösch, Wetzlar

Price per part £1 (1375 fr.), (DM 11.75), ($2.80), plus postage

Subscription price per volume (4 parts) £3 15s. (5155 fr.), (DM 44), ($10.50), post free, payable in advance

Printed and Published by

TAYLOR & FRANCIS LTD

RED LION COURT, FLEET STREET, LONDON, E.C.4

A HISTORY OF MATHEMATICS

from antiquity to the early nineteenth century

by J. F. SCOTT, B.A., D.Sc., Ph.D.
Vice-Principal of St. Mary's College,
Strawberry Hill, Twickenham,
Middlesex

Author of *The Scientific Work of René Descartes* (1596–1650), *Mathematical Work of John Wallis, D.D., F.R.S.* (1616–1703), and other works.

CONTENTS : Mathematics in Antiquity—Greek Mathematics—The Invention of Trigonometry—Decline of Alexandrian Science and the Revival in Europe—Mathematics in the Orient—Progress of Mathematics during the Renaissance—New Methods in Geometry—The Rise of Mechanics—The Invention of Decimal Fractions and of Logarithms—Newton and the Calculus—Taylor and Maclaurin, the Bernoullis and Euler, Related Advances—The Calculus of Variations, Probability, Projective Geometry, Non-Euclidean Geometry—Theory of Numbers—Lagrange, Legendre, Laplace, Gauss.

This volume is intended primarily to help students who desire to have a knowledge of the development of the subject but who have too little leisure to consult original works and documents. The author has availed himself of the facilities afforded by the Royal Society and other learned Societies to reproduce extracts from manuscripts and many scarce works.

9¾ × 6¾ Price 3 guineas

Printed and Published by
TAYLOR & FRANCIS LTD.
RED LION COURT, FLEET STREET,
LONDON, E.C.4

THE SCIENTIFIC WORK OF RENÉ DESCARTES 1596-1650

BY

J. F. SCOTT, B.A., M.SC., PH.D.

With a Foreword by

H. W. TURNBULL, M.A., F.R.S.

This book puts the chief mathematical and physical discoveries of Descartes in an accessible form and fills an outstanding gap upon the shelf devoted to the history of philosophy and science. There is to be found in this volume the considerable contribution that Descartes made to the physical sciences, which involved much accurate work in geometrical optics and its bearing upon the practical problem of fashioning lenses, as also the deeper problems of light and sight and colour. The careful treatment that Dr. Scott has accorded to the work of Descartes is very welcome. The book is well worth reading and will be an asset to all libraries. This publication is recommended and approved by the Publication Fund Committee of the University of London.

212 *pp.* 7 × 10 *amply illustrated*

PRICE £1–0–0 NET

Printed and Published by
TAYLOR & FRANCIS LTD.
RED LION COURT, FLEET STREET,
LONDON, E.C.4

Yield Point Phenomena in Alpha Brass and other Face-Centred Cubic Metals†

By G. F. Bolling
Department of Physical Metallurgy, University of Birmingham‡

[Received September 26, 1958 ; and in revised form November 19, 1958]

Abstract

The characteristics of yield points which may be produced in a 70 : 30 alpha brass have been observed at several temperatures. The yield point phenomena were produced by various techniques which included ageing under stress, unloading and combinations of the two. The effects arising from ageing under stress are compared to experiments on repeated yielding. The particular results in brass are supported by various experiments with a range of face-centred cubic metals. From the evidence presented it seems that the process of ageing is more complex than hitherto supposed.

§ 1. Introduction

The existence of a yield point in single crystals of alpha brass, arising from a strain-ageing treatment, has been shown by Ardley and Cottrell (1953). Subsequently Piercy *et al.* (1955) and Adams (1958) have used this effect in making observations pertinent to deformation. From the results of these investigations it may be concluded that the movement of dislocations can be influenced by a suitable annealing treatment. The formation of solute atmospheres at dislocations impedes the initiation of plastic flow but permanent hardening is absent and therefore a yield effect arises.

Recently the experiments of Haasen and Kelly (1957) and Makin (1957, 1958) have shown that a yield point effect may be produced in single crystals of aluminium, copper and nickel simply by the process of unloading and reloading. The general nature of this phenomenon led Haasen and Kelly to suggest that the generation of sessile dislocations during unloading may be the process which is responsible for the production of a yield point. Makin (1958) has put forward a model postulating the appearance of new sessile dislocations which explains most of his extensive observations on copper single crystals.

It will be shown in this investigation that the yield point produced by unloading is also a general phenomenon in polycrystalline face-centred cubic metals and alloys. This observation complicates the analysis of yield points arising from strain-ageing. Thomas (1958) has recently shown that in an aluminium–zinc alloy there is an interaction between the two yield effects at temperatures at which stress accelerates recovery. Similarly, the present work in alpha brass indicates that a simple ageing experiment is not free from the effects produced by unloading at temperatures where recovery is not an important process. Any specimen which is deformed, unloaded and aged, and then tested for a yield point always exhibits the unloading effect in addition to any ageing effect.

---

† Communicated by the Author.

‡ Now at Westinghouse Research Laboratories, Pittsburgh, Pennsylvania, U.S.A.

Following this observation it seemed necessary to study the nature of strain-ageing in the absence of unloading for any accurate analysis of the processes involved. Accordingly, experiments have been performed using ageing under stress. The results may be compared to those from some simple experiments determining the onset of repeated yielding.

The main set of observations concerns the yield effects in polycrystalline samples of a 70 : 30 alpha brass. In addition, a summary of observations on reasonably pure face-centred cubic metals and alloys is given to support the general trend of results specifically noted for the brass.

§ 2. EXPERIMENTAL METHOD

Tensile tests were performed on a 'hard' Polanyi machine at a strain rate in the range $\sim 10^{-4}\,\mathrm{sec}^{-1}$, varying slightly with beam flexure. The load was recorded using the output from a system of strain gauges mounted on the beam; a strip-chart recorder was arranged to measure with an accuracy of 0·04% in the mid-range of load. (Full deflection on the recorder corresponded to only a fraction of the total applied stress.) The movement of the strip-chart was coupled by a servomechanism to the strain-imposing drive of the machine such that elongation could be measured with an accuracy of 0·04% and load-elongation curves were automatically plotted. The specimen holder was constructed so that baths at different temperatures from 77°K to 398°K could be used to surround a specimen.

Brass wires were prepared from the high purity stock at the University of Birmingham, previously made by Ardley and Cottrell (1953) of a composition nearly 70 : 30. The wires were annealed to a fine grain size and then soldered into brass grips, leaving a free length of 50 mm of 0·75 mm wire. (Other types of grips were also used to ensure that no different results were obtained.) When other metals were investigated, suitable wires were prepared and similarly mounted.

§ 3. EXPERIMENTS

3.1. *Brass—Ageing Without Unloading*

3.1.1. *Experiments*

The experiments concerning ageing under stress are presented first to show the general nature of the yield points concerned. The experimental method involved the deformation of a specimen to some strain at the imposed strain rate, the removal of this imposed rate for a specified length of time, and the continuation of the same imposed rate after this time.

The sequence of events is illustrated in fig. 1. Part ‘ A ’ is a representation from a load-elongation curve, and part ‘ C ’ the derived stress–strain curve; part ‘ B ’ shows the sequence of events with time, during which transient creep occurs.

Fig. 1

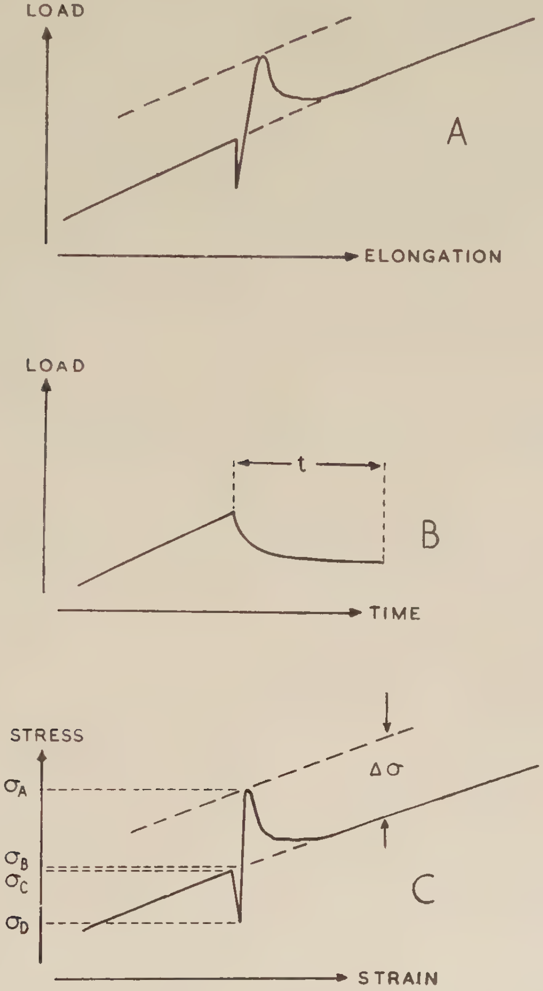

Part ‘A’ is a representation from a load–elongation curve showing the yield point effect developed from ageing under stress ; part ‘ B ’ shows the load drop with time, and ‘ C ’ the derived stress–strain curve.

It can be seen that when the imposed rate was removed a stress relaxation ensued with an accompanying additional strain; as evident on the time-based curve this small amount of strain has the nature of transient creep. In order to define the magnitude of the yield point effect this creep strain must be considered. An apparent hardening equal to or less than $\sigma_B - \sigma_C$ results from this strain increment and is observed even in metals showing no yield effect. (The hardening might be less than $\sigma_B - \sigma_C$ because the strain rate under which it is achieved is less than that at which σ_B is reached by extrapolation.) Therefore, the recoverable hardening shown by the yield point is best defined as $\Delta\sigma = \sigma_A - \sigma_B$. This is the increase in flow stress above the stress–strain curve which would have been derived during uninterrupted deformation. The ratio σ_A/σ_B is then the relative amount of hardening.

The stress relaxation, $\sigma_C - \sigma_D$, which occurred during the maximum ageing times at any temperature was always $< 3\%$ of the stress level and it was found that this amount of unloading was inappreciable in producing any unloading effect. Therefore, no attempt was made to keep the specimen at a constant load level by manipulating the machine drive. The procedure is similar to that employed by Westwood and Broom (1957).

Fig. 2

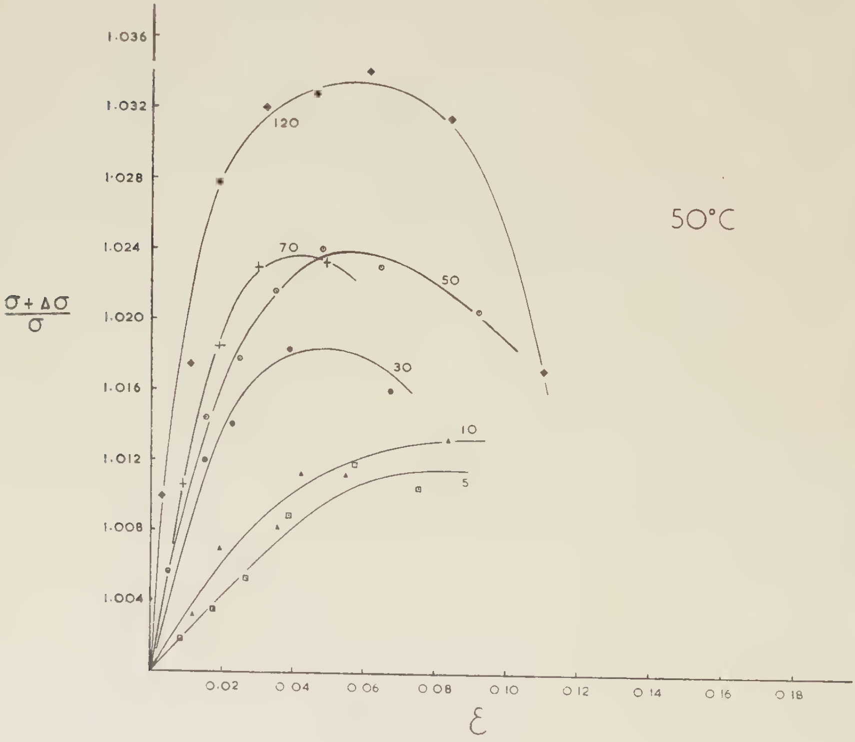

(*a*)

The relative hardening at the yield point is plotted against strain for tests at 50°c.

Time in seconds: 120—◆. 70—+. 50—⊙. 30—●. 10—△. 5—⊡.

Fig. 2 (*continued*)

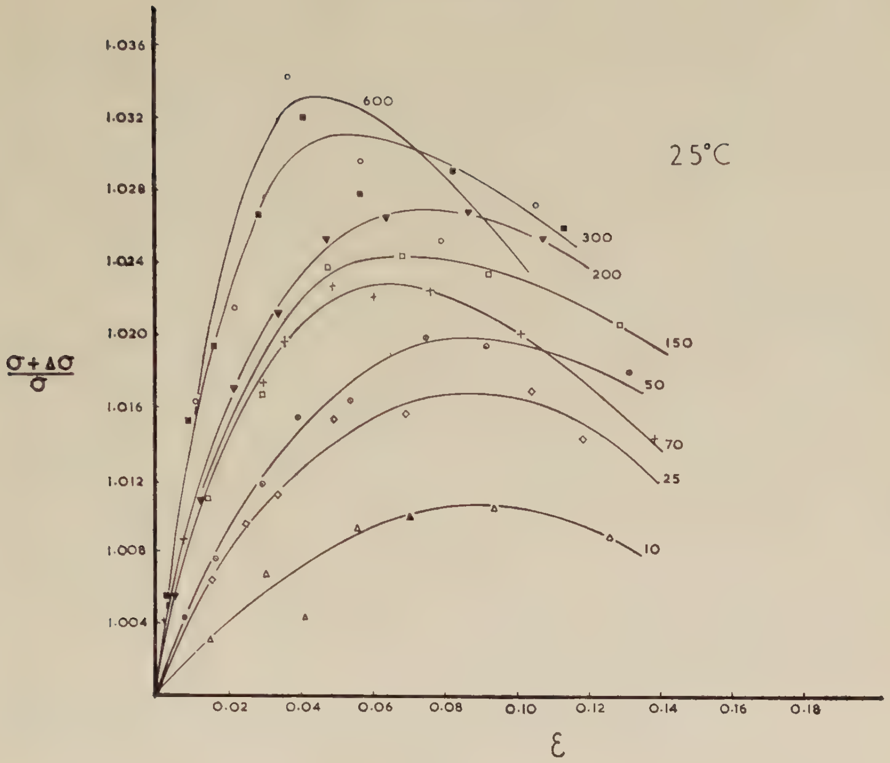

(*b*)

Time in seconds : 600—○. 300—■. 200—▼. 150—□.
70—+. 50—⊙. 25—◇. 10—△.

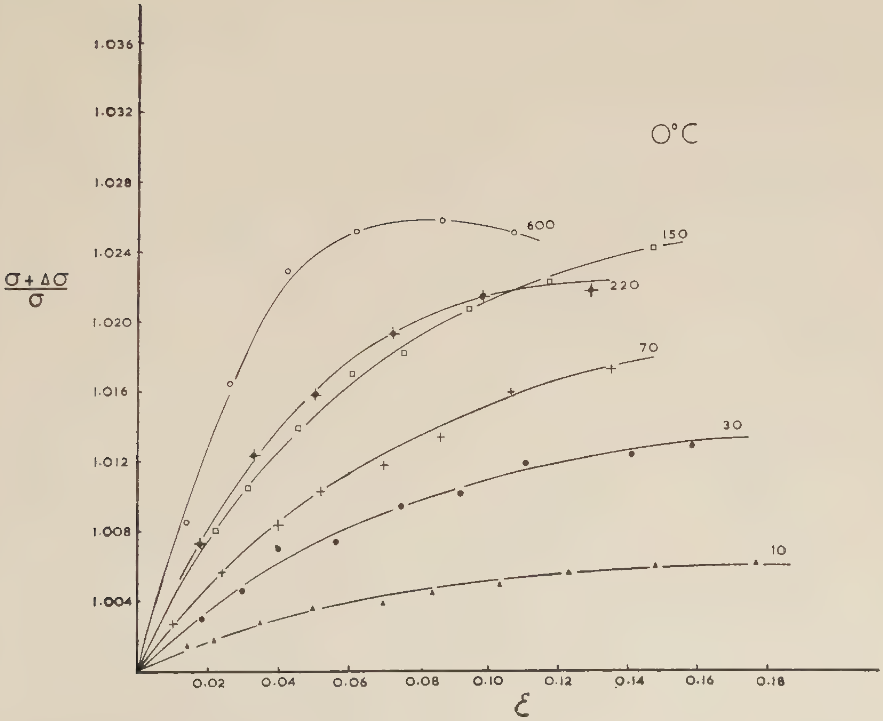

(*c*)

Time in seconds : 600—○. 220—❋. 150—□. 70—+. 30—●. 10—△.

Fig. 2 *(continued)*

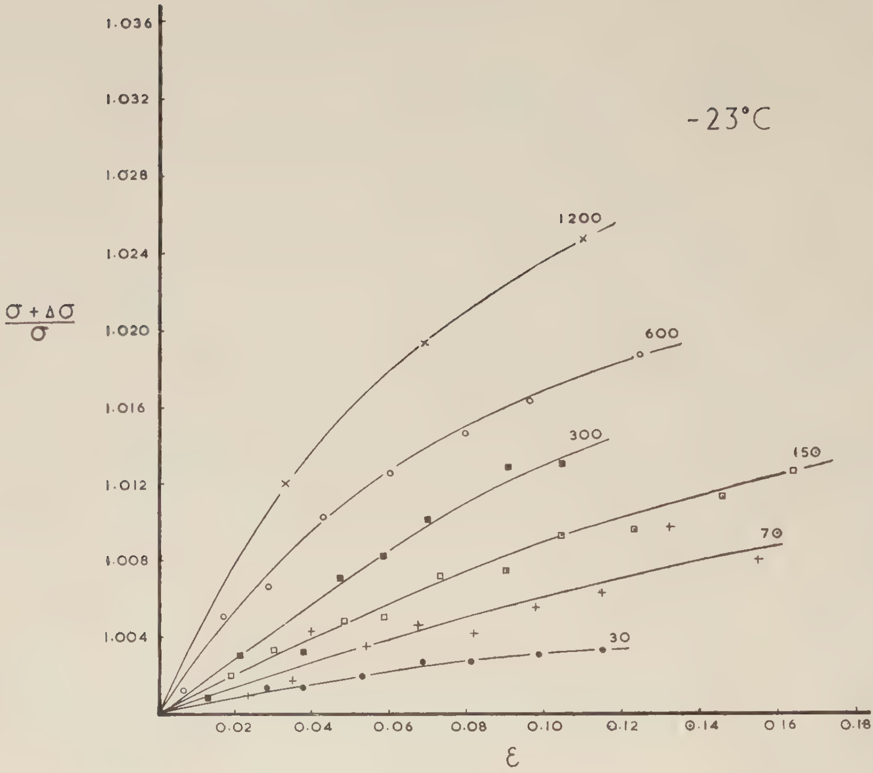

(*d*)

Time in seconds : 1200—×. 600—○. 300—■. 150—□. 70—+. 30—●.

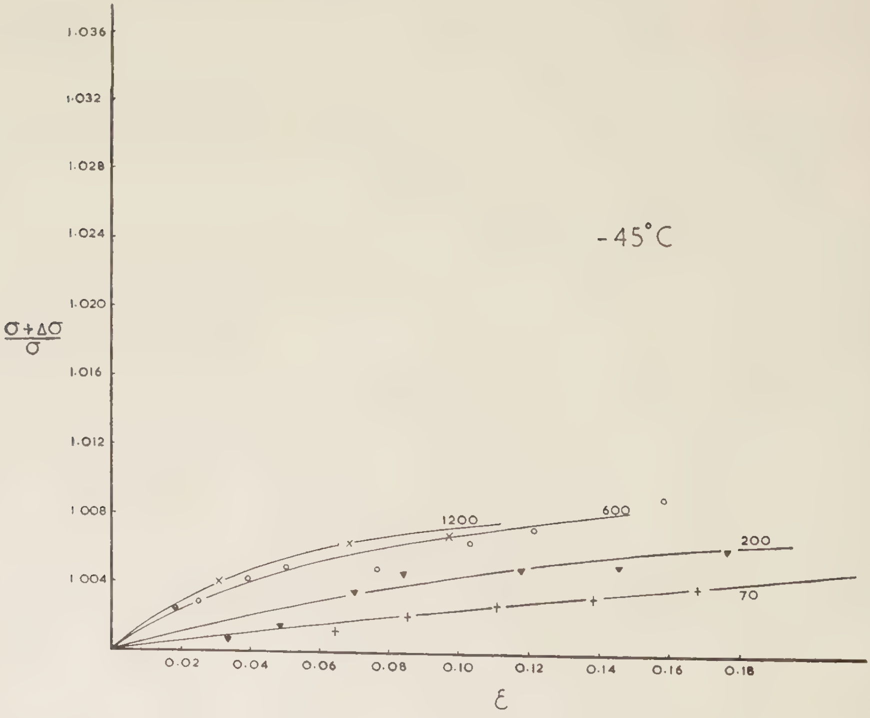

(*e*)

Time in seconds : 1200—×. 600—○. 200—▼. 70—+.

It was found that the exact shape of the yield point depended on the extent of the deformation at which the test was made. At lower stresses and small strains a plateau yield with no yield drop was obtained, but after greater deformation the yield drop developed and this region exhibited a fine structure or a tendency to repeated yielding, which had a greater lifetime, the greater the deformation. Several experiments were done to show that the magnitude of a yield point was independent of preceding tests on the specimen if the irregular region after the yield was avoided. It was thus possible to perform several tests on one specimen.

The ageing under the stress was done on many specimens at different times and temperatures. It was not desirable to deform at one standard temperature and age at another because some unloading is involved in any such experiment. In general one ageing time was used in repeated tests on one specimen. The primary results of these experiments are shown in figs. 2 (*a*)–(*e*). Here the relative amount of hardening, σ_A/σ_B, is plotted against the strain at which the test was made.

The families of curves which are thus obtained seem more self-consistent than if the absolute yield effect, $\Delta\sigma$, is plotted. A maximum hardening is obtained which is related to the appearance of repeated yielding or jerky flow. At the lower temperatures of investigation no maximum is reached and the tendency for repeated yielding in the yield drop region after a test is slight. At higher temperatures when a maximum is observed repeated yielding appears distinctly after any test and over a considerable range of strain. Above 50°c repeated yielding occurs after small strains and does not disappear. At these temperatures neither creep nor any appreciable additional yield is obtained if ageing under stress is done at the high levels of a serrated stress–strain curve. Therefore, the process of ageing under stress seems to produce yield points of the same nature as repeated yielding and should decrease when repeated yielding ensues.

In the procedure which will be used to derive an activation energy for the effect the two methods of plotting would be equivalent if all the specimens had been identical. This is because the same stress level would have been obtained for any sample at a given strain. However, there was a variation in initial flow stress among the specimens and it was found that identical tests on different specimens were more similar in terms of the relative hardening than the absolute hardening.

3.1.2. *Activation energy I*

An investigation of the time variation of the relative hardening for a given strain and temperature suggests that a law close to $t^{2/3}$ applies. Cottrell and Bilby (1949) have derived an expression for the number of solute atoms which will arrive at unit length of an edge dislocation to lower the strain energy of the system, namely,

$$n(t)=\alpha n_0\left(\frac{ADt}{kT}\right)^{2/3} \qquad (1)$$

where n_0 is the number of atoms originally in solid solution and A is a parameter concerned with the interaction between the solute and dislocations; α, D, k and T have their usual meanings. Harper (1951) has modified this law to take into account the depletion of the bulk by the segregation. This cannot be directly applied to an alloy containing 30% solute. Instead, if a maximum number, n, of solute atoms segregate, the fraction segregated, $f=n(t)/n$, may be defined; and if we assume that the rate of segregation is proportional to the fraction unsegregated,

$$\frac{\partial f}{\partial t}=(1-f)\phi(t),$$

where $\phi(t)$ is a function to be determined. This may be solved under the condition that the equation of Cottrell and Bilby applies at short times. A relation similar to Harper's is derived, namely,

$$f=1-\exp\left[-\frac{\alpha n_0}{n}\left(\frac{ADt}{kT}\right)^{2/3}\right]. \quad . \quad . \quad . \quad . \quad . \quad (2)$$

In order to use this relation it must now be assumed that the fractional hardening is proportional to the number of solute atoms per unit length of dislocation; i.e.

$$\left(\frac{\Delta\sigma}{\sigma_B}\right)\propto n(t) \quad \text{and} \quad \left(\frac{\Delta\sigma}{\sigma_B}\right)_{\max}\propto n.$$

Then

$$f=\frac{\Delta\sigma}{\sigma_B}\bigg/\left(\frac{\Delta\sigma}{\sigma_B}\right)_{\max}.$$

It must also be assumed that n is independent of temperature in the range considered.

The greatest hardening obtained in any experiment gave $\sigma_A/\sigma_B=1{\cdot}035$ and therefore $\Delta\sigma/\sigma_B=0{\cdot}035$. Figure 3 shows a plot of log $(1-f)$ versus $t^{2/3}$. The points are calculated from the curves of figs. 2 (*a*)–(*e*) for the value of strain, $\epsilon=0{\cdot}02$. Choosing another higher strain intercept gave similar lines except that closer proximity to the maximum of a curve gave more unreliable points.

Reasonable straight lines are obtained from this plot and an activation energy for the process may be calculated. In fig. 4 the logarithms of the slopes from fig. 3 times $T^{2/3}$ are plotted against the reciprocal absolute temperature. The straight line yields an activation energy of 0·42 ev with an error of about 20%.

3.1.3. *Vacancy concentration*

Since the yield points produced during the ageing appeared in very short times, the diffusion which occurred must have been rapid. This rapid diffusion may be attributed to an excess vacancy concentration produced by the strain. The excess concentration may be assumed to have the form $c = A\epsilon^m$, where A and m are constants, and in the following way m may be derived from the experiments.

The diffusion rate may be written as

$$D = D_0\left(\exp\left(-\frac{Q_f}{kT}\right) + c\right)\exp\left(-\frac{Q_m}{kT}\right) \quad . \quad . \quad . \quad (3)$$

where Q_f and Q_m are respectively the activation energies for formation and for movement of vacancies. In the ranges of temperature and strain used in the experiments it is reasonable to assume that $c \gg \exp(-Qf/kT)$ in accordance with Seitz (1952) and Mott (1953). Then

Fig. 3

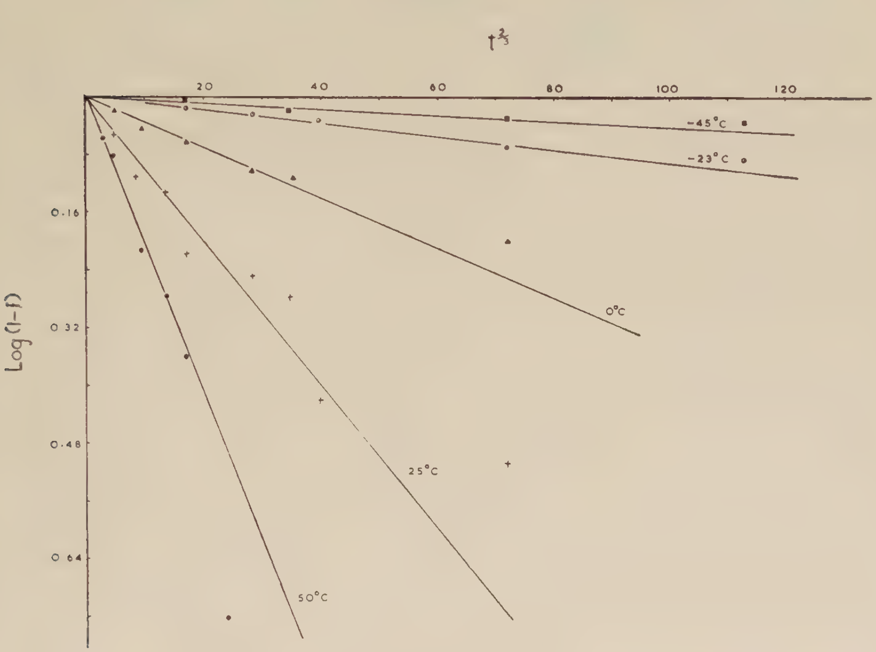

A plot similar to Harper's (1951) formula is shown. The points were calculated from the curves of fig. 2 at a strain $\epsilon = 0{\cdot}02$, assuming a maximum hardening $\Delta\sigma/\sigma_B = 0{\cdot}035$.

Temperature : 50°c— ●. 25°c—+. 0°c—▲. −23°c—⊙. −45°c—■.

$$D = D_0 c \exp(-Q_m/kT). \quad . \quad . \quad . \quad . \quad . \quad . \quad . \quad (4)$$

Substituting (4) in (2) it may be seen for a constant temperature and for a particular value of the hardening at the yield that

$$ct = A\epsilon^m t = \text{constant}. \quad . \quad . \quad . \quad . \quad . \quad . \quad . \quad (5)$$

The data were examined at all temperatures for values of $\sigma_A/\sigma_B = 1{\cdot}004$ and $1{\cdot}008$. Logarithmic plots of strain versus time were made but the slopes of the lines used to obtain m were scattered. An average obtained from these values is not as valid as one obtained in the following manner. In fig. 5 the data at each temperature and relative hardening value has been 'normalized' so that the value of the strain for 70 sec is constant. From the slope of the straight line it is found that $m = 1{\cdot}3(6)$.

Fig. 4

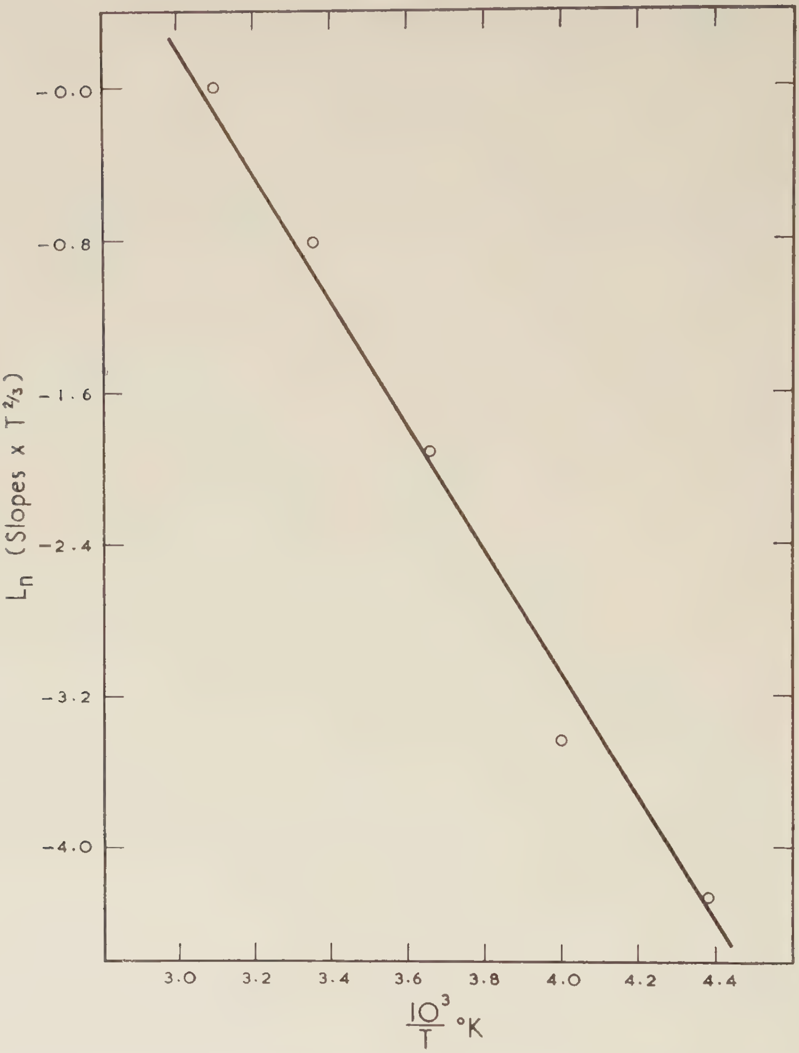

To obtain an activation energy the slopes of the lines from fig. 3 corrected for temperature have been plotted against the reciprocal absolute temperature.

This observation is in accord with the theory put forward by van Bueren (1955) predicting $1{\cdot}25 \leqslant m \leqslant 2$, the extremes being determined in the cases of single or multiple glide respectively. It also agrees with the viewpoint of van Bueren and Jongenburger (1955) about experiments observing resistivity changes produced by annealing after deformation. Seitz (1952) predicted that c was of the order of $\sim 10^{-4}\epsilon$; in order for agreement between this and $c \sim A\epsilon^{1\cdot 3(6)}$, A must be larger than 10^{-4}.

3.1.4. *Activation energy II*

The preceding method used in deriving the dependence of the vacancy concentration upon strain does not really depend on the form of the time law for the ageing process. Basically, the only assumption needed is that the diffusion rate and time of ageing enter any expression for the magnitude of the ageing process only as the product Dt.

Fig. 5

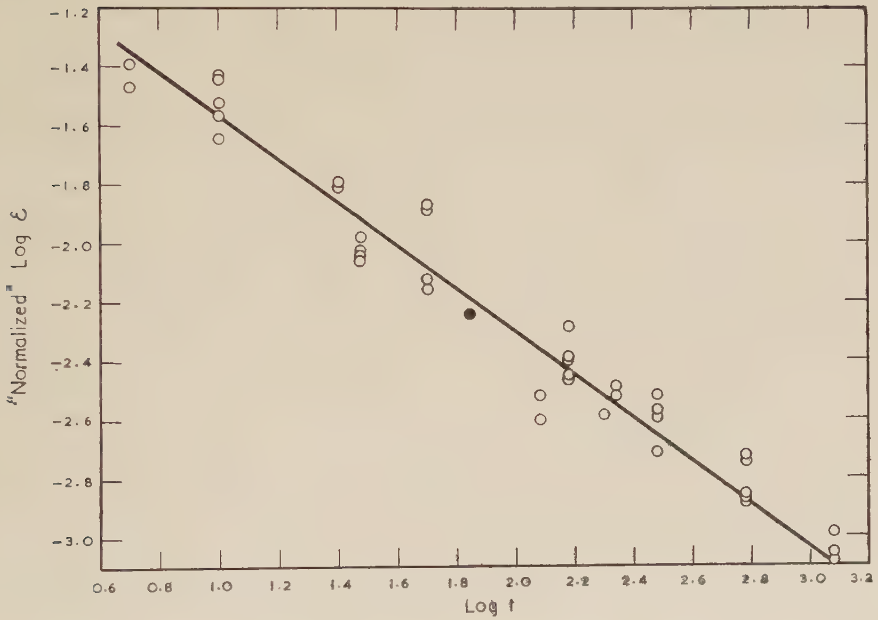

The points represent the strain obtained from constant values of $\sigma_A/\sigma_B = 1\cdot 004$ and $1\cdot 008$ in figs. 2 (*a*)–(*e*) plotted against time. However, the range of strain has been 'normalized' so that the strain values at 70 sec are all the same as that for 50°c and $\sigma_A/\sigma_B = 1\cdot 008$. (Not all curves provide an intersection which could be plotted.)

Over the small temperature range investigated a similar procedure may be followed using this one assumption to obtain an activation energy. In fig. 6 the curves for 70 sec tests at the various temperatures are plotted together. For a constant yield point effect the product Dt will be constant.

Therefore, at constant time

$$A\epsilon^{m}\exp(-Q_m/kT)=\text{constant}. \quad . \quad . \quad . \quad . \quad . \quad . \quad . \quad (6)$$

In fig. 7, curve A, $\ln \epsilon$ is plotted against $1/T$ for an effect of 1·004 magnitude in fig. 6. Using the value of $m=1{\cdot}3$ (6) from the preceding section an activation energy $Q_m=0{\cdot}42$ ev is obtained. There is good agreement between this value and the one obtained from the particular time law.

Fig. 6

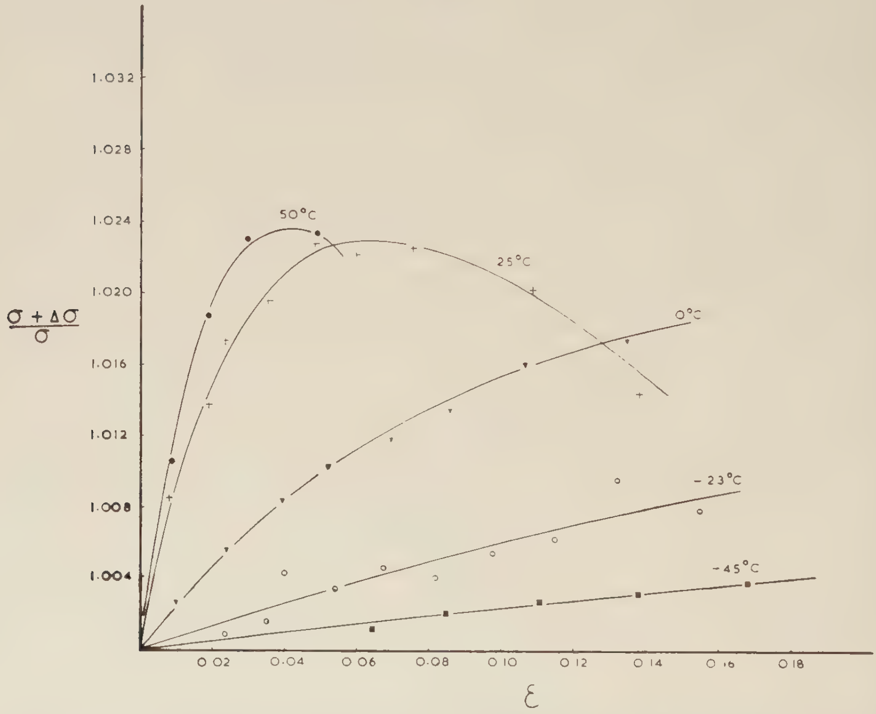

To illustrate the effect of temperature, curves from figs. 2 (*a*)–(*e*) for seventy second tests at the various temperatures are plotted together.
Temperature : 50°c—●. 25°c—+. 0°c—▼. −23°c—⊙. −45°c—■.

3.1.5. *Low temperatures*

Some final observations obtained from tests at ~154°K and 77°K are directly pertinent to the nature of ageing under stress. The investigation was not extensive because the results are similar to those put forward by Westwood and Broom (1957). Moreover, at 77°K the creep encountered during the times of ageing was sufficiently great so that the machine drive had to be employed to keep the stress relaxation < 3% of the original stress level. Some results on two specimens are shown in table 1.

From comparison with the results at higher temperatures it is obvious that a process with the same activation energy cannot be responsible for the effect at the low temperatures. Westwood and Broom have proposed that interstitials may be the source of both diffusion and locking at similar temperatures in aluminium and copper.

3.2. *Brass—Repeated Yielding*

Several wires of alpha brass were deformed continuously to the limit of the machine at temperatures in the range 0°C to 124°C. The load–elongation curves showed that a stepwise, or serrated deformation occurred after some strain had been reached and that it increased in magnitude, or frequency at higher strains.

Cottrell (1953) has related the onset of this Portevin–Le Chatelier or repeated yielding effect to the stage of deformation where diffusion rates

Fig. 7

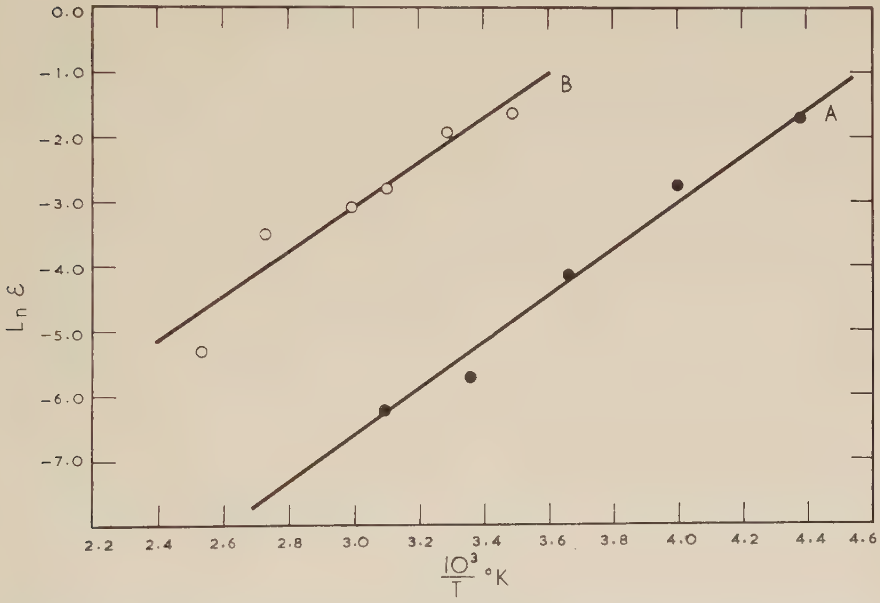

Two curves for activation energies are shown. ‘ A ’ has been prepared from the data of fig. 6. ‘ B ’ shows the results from experiments on repeated yielding.

Table 1

Temperature (°K)	Time of test (t) sec	Strain (ϵ)	Relative amount of hardening, σ_A/σ_B
77	6480	0·120	1·0030
”	2000	0·136	1·0019
”	1020	0·150	1·0019
154	540	0·096	1·0011
”	510	0·126	1·0016

are high enough to allow the diffusion of solute to moving dislocations. When the relation $c \sim 10^{-4}\epsilon$ for the concentration of vacancies produced during the deformation is used, a correlation between the strain at the onset of repeated yielding and temperature at a constant strain rate is found to fit reasonably well.

This is

$$\epsilon = B' \exp\left(-\frac{Q_m'}{kT}\right)$$

where B' is a constant depending on the lattice, the strain rate, etc., and Q_m' is the activation energy for vacancy movement.

If the relation $c = A\epsilon^m$ is used for the concentration of vacancies, the same form is derived,

$$\epsilon = B \exp\left(-\frac{Q_m}{mkT}\right)$$

but $Q_m = mQ_m'$.

Curve B of fig. 7 shows the results of plotting $\ln\epsilon$ versus $1/T$ for the strain at the onset of repeated yielding. Using the value of $m = 1{\cdot}3$ (6) the activation energy for the process is found to be $\sim 0{\cdot}40$ ev. A correlation between repeated yielding and the phenomenon of the first experiment has been noted. As well both processes are similar because some type of ageing process is occurring at stress.

Below 15°c repeated yielding was not observed at the strain rate used, and above 125°c it seemed that repeated yielding was always present. The determination of the onset of repeated yielding is difficult experimentally and the results have a limited reliability for this reason. It should also be noted that the onset is denoted by a value of $\Delta\sigma$ that is sufficient for perception of the effect, and not σ_A/σ_B as for curve A of fig. 7. When the data of fig. 6 are replotted in terms of $\Delta\sigma$ versus ϵ the activation energy which may be derived is in fact $< 0{\cdot}40$ ev; however, the curves are positively or negatively curved depending on the temperature of test, and this is not understood.

There is much better agreement between the activation energy from ageing under stress and that from repeated yielding than might be expected with an estimated error of about 20% in each experiment. If the two processes are the same the value of the activation energy should be in range $0{\cdot}41 \pm 0{\cdot}08$ ev.

3.3. *Brass—Unloading Tests*

3.3.1.

At room temperature the onset of the ageing effect at stress is so rapid that a smooth unloading and reloading of a specimen at the machine rate is accompanied by both creep and ageing at the high stress levels. It was therefore necessary to carry out experiments with abrupt unloading in addition to those with smooth unloading in order to investigate any unloading effect. In fig. 8 three curves are plotted for unloading tests on one sample. (For convenience in representation $\Delta\sigma$ has been plotted against σ_B as was done by Haasen and Kelly (1957).) Smooth unloading took more time at higher deformations, and abrupt unloadings were made

(a) with unloaded times of the same order as in the smooth unloading tests and (b) with a constant, short unloaded time. These tests are respectively represented by curves U_S, U_{At} and U_A for whose points the time values are listed in table 2. The abrupt unloading was accomplished by directly overloading the beam enough to allow complete relaxation of the specimen. It was then necessary to reverse the straining mechanism a sufficient distance so that a smooth passage through the yield point would be obtained on reloading. It is important to note that some smooth reloading was then necessary.

Fig. 8

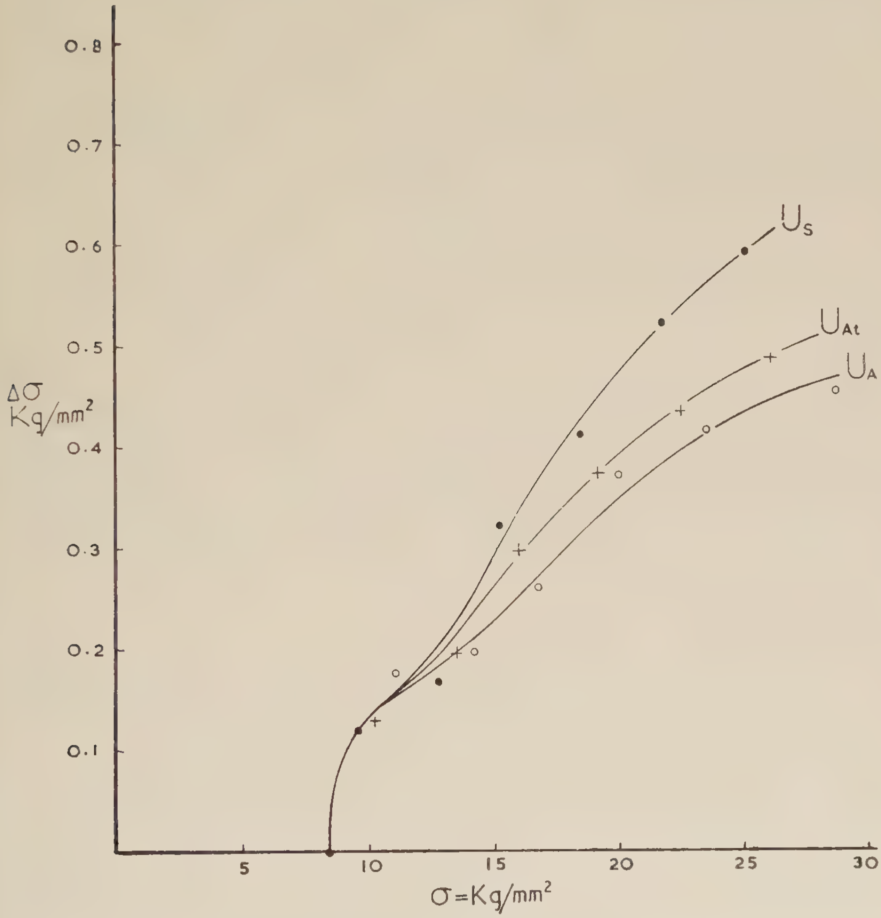

The manner of unloading tests affects the yield points derived. Curves are plotted for the values of the yield effect from unloading tests at room temperature. U_S, ●, represents smooth unloading; U_{At}, +, represents abrupt unloading, aged for an unloaded time equal to that for smooth unloading; U_A, ○, represents abrupt unloading. The times taken during the tests are listed in table 1.

The value of $\Delta\sigma$ for fig. 8 was defined in the same manner as in the ageing tests; the hardening due to creep, $\sigma_B - \sigma_C$, is therefore not included. It is first notable that the curves for abrupt unloading are both lower than that for smooth unloading and reloading. Secondly, the difference between the two 'abrupt' curves is constant; whereas, for the 'smooth' curve the difference increases with stress and thus with unloading time. Since ageing should be induced at the high stress levels the increasing difference between the 'smooth' and the 'abrupt' curves is easily understood. The difference between the two 'abrupt' curves is not time-dependent and could arise from the experimental method. Since some smooth reloading was done, both curves should include some ageing and it will be shown in the next section that this is additive to the unloading yield effect.

Table 2. (*t*) sec

U_s Unloading time	U_{At} Unloaded time	U_A Unloaded time
220	220	20
270	270	20
320	320	20
390	390	20
450	450	20
500	500	20

Another type of test was performed at room temperature. At similar strains, specimens were abruptly unloaded and aged from 10 to $\sim 10^4$ sec. Upon abrupt reloading (with a smooth passage through the yield point) no appreciable difference was obtained in the value of the yield effect with unloaded time. However, ageing at stress for similar times gave very much larger yield effects.

3.3.2.

At 77°K the yield effect arising from ageing at stress does not appear until times of the order of $\sim 10^3$ sec at large deformations. It is thus possible to investigate the unloading yield effect more easily.

A simple test shows that the magnitude of the unloading yield effect is not time-dependent.

Another observation is of interest. First it must be noted that although no effect appears after short ageing times the creep rate is considerable at high stress; therefore, creep occurs during smooth unloading and reloading. There is then a difference between the unloading effect as defined by Haasen and Kelly (1957) and that by Makin (1958). Referring to fig. 1, it seems that the former workers defined $\sigma_{HK} = \sigma_A - \sigma_B$, whereas the latter defined $\Delta\sigma_M = \sigma_A - \sigma_C$. Over a range of stress for polycrystalline specimens $\Delta\sigma_{HK}$ and $\Delta\sigma_M$ vary only very slightly. However, when the size of the yield effect is related to the percentage unloading made, only

$\Delta\sigma_M$ is nearly linear with unloading. $\Delta\sigma_{HK}$ is not of any great magnitude until 40–50% unloading is done.

This matter of definition explains the small disagreement between the two observers. At small unloading relatively larger amounts of creep occur, increasing the value of $\Delta\sigma_M$.

Fig. 9

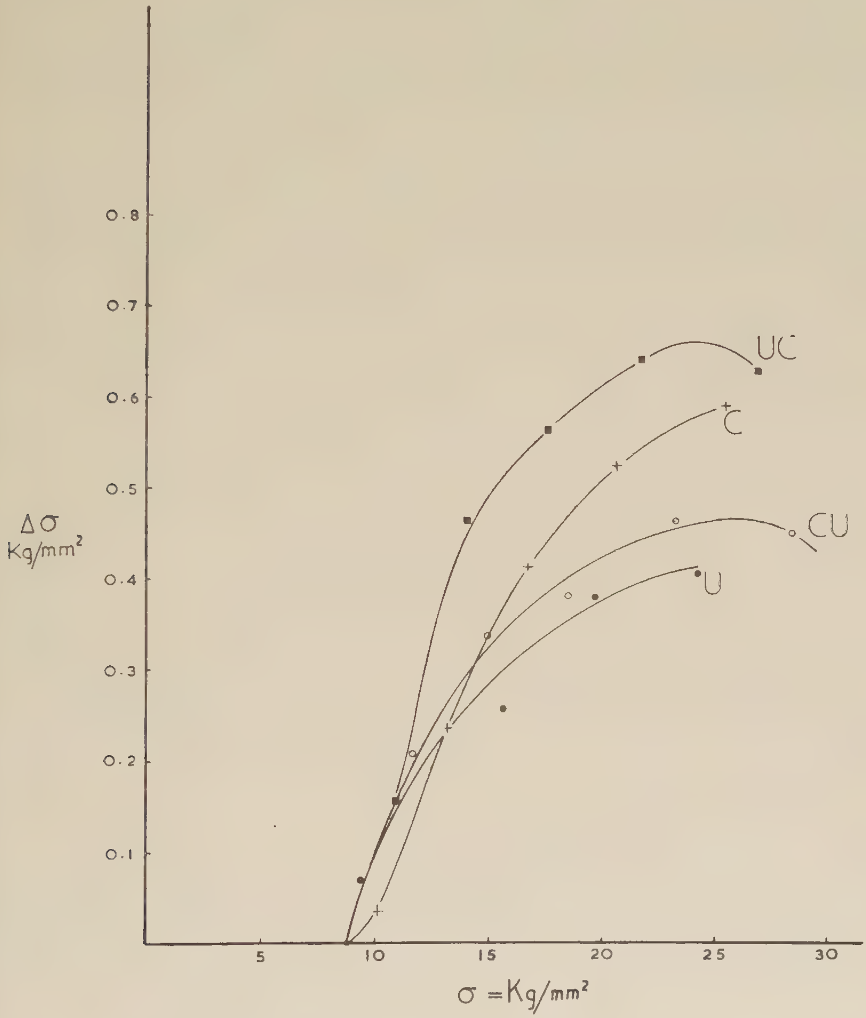

On one sample at room temperature tests were conducted for unloading, U, ageing at stress, C, and combinations of the two UC, and CU. U—●. C—+. CU—○. UC—■.

3.4. *Brass—Interaction of the Two Yield Types*

The following experiment on alpha brass was performed many times. The results for tests on one specimen tested at room temperature are shown in fig. 9, which is representative of all similar tests. Four curves are shown: the U curve is for abrupt unloadings; the C curve is for ageing at stress for 120 sec; the points of the CU curve were obtained by ageing for 120 sec, then unloading abruptly and then retesting; and the UC curve was obtained by unloading abruptly, reloading abruptly, ageing for 120 sec just before the yield was reached and then continuing the deformation. The statements which will be made about the curves are to be based upon the observations of other tests as well, where the ageing time was different from 120 sec. It may first be seen that the C curve is lower than all the others involving unloading, at the lower stresses. Next it is observed that the C curve rises above both the U and the CU curves. Finally it is of great interest that the UC curve is uppermost and almost parallel to the C curve at the higher stresses.

The observations of § 3.3 on unloading indicate that the true yield effect is time-independent and of a value slowly increasing with deformation. It is most likely due to a dislocation interaction as proposed by Haasen and Kelly (1957) and Makin (1958) with its particular characteristics changed with the nature of deformation in a polycrystalline specimen. The characteristics of the C and U curves have already been shown. For now it may be assumed that ageing (i.e. solute migration), and a dislocation reaction, are respectively responsible for these. If they occurred separately, the highest should govern the magnitude of the yield effect; the possible interactions are the ageing of newly formed sessile dislocations or the reduction in number of aged dislocations during the formation of these sessile dislocations on unloading. On this basis it may be understood that ageing after unloading and just below the yield stress would strengthen dislocations that are more immobile than those available on simple ageing at stress; UC curves are high but similar to C curves. Also on this basis if strong impediments to plastic flow have been formed before unloading, the reloading should give a higher effect than just the unloading yield effect; CU curves are higher than U curves. Because the CU curves are lower than C curves it is possible that back flow during unloading is capable of reducing the number of aged dislocations.

3.5. *Other Metals*

An incomplete set of both ageing at stress and unloading tests were performed on polycrystalline samples of Ag, Al, Cu, Ni, Pb, Pb–0·1 at. % Ag and Cu–7% Al. The important results will be briefly stated. The purities of the metals used are quoted in table 3.

3.5.1.

At 77°K all these metals exhibited a yield point produced by smooth unloading whose magnitude was dependent on the amount of unloading and did not appear to be time-dependent. Attempts to arrange the metals in some order according to the size of the yield effect under similar conditions did not prove successful because different amounts of creep were obtained during smooth unloading depending on the metal, and abrupt unloading was not used. This made any order determined by the definition of the yield effect (i.e. $\Delta\sigma_{HK}$ or $\Delta\sigma_M$) depend on this definition. In addition it is possible that different grain sizes, specimen sizes and other variables existing from metal to metal would affect the results.

In view of the observations made by Westwood and Broom (1957) specimens of the superpurity Al and the Cu were subjected to ageing under stress at 77°K. These experiments confirm their observations that a yield point effect can be produced at this low temperature. The size of the effect in copper was just on the limit of observation at the highest deformations achieved with the apparatus used. In aluminium the yield points produced were also small but larger than in the copper; it was possible to confirm that the same magnitude effect was achieved in the same times, etc., as used by Westwood and Broom. No attempt was made to determine an activation energy by tests at various temperatures. To complete the observations at 77°K it should be noted that the yield point effect produced in alpha brass at this temperature by ageing under stress (reported in § 3.1) was higher than for either the aluminium or the copper.

Table 3

Metal	Purity
Ag	99·999%
Al	99 992% (super-purity)
Al	99%
Cu	99·98% (O.F.H.C.)
Ni	99%
Pb	99·9999% (zone-refined)
Cu–7 wt % Al	(Alloyed from the purer quoted constituents)
Pb–0·1 at. % Ag	(Alloyed from the quoted constituents)

3.5.2.

At room temperature, any of the metals which did not undergo recovery during the time of smooth unloading and reloading exhibited the unloading yield effect. This group however included only the more impure aluminium, the copper, the nickel, and the aluminium–bronze alloy. Even the copper showed a diminished value of the yield effect and there was evidence of recovery occurring. The other metals which showed recovery, exhibited a reduced, smooth flow stress on reloading.

Ageing under stress was performed on specimens of each metal and no yield effect was observed in the recovering metals nor in the copper or the impure aluminium. The aluminium–bronze exhibited a yield effect similar in all the simple details to those observed in the alpha brass. The impure nickel also showed the production of a yield point which was much smaller than for either the brass or the bronze.

3.5.3.

Additional tests were performed at temperatures between 77°K and 293°K on several of the metals in order to avoid the effects of recovery.

At 194°K and 250°K both silver and copper exhibited the unloading yield effect, but not the ageing yield effect even with the occurrence of creep and the absence of recovery. It must be stated that no extremes of time were used in the ageing tests, however. Similarly, at 194°K the super-purity aluminium exhibited the unloading effect but not the ageing effect.

At 77°K, ~154°K and 194°K the zone-refined lead showed the unloading effect but no ageing effect. The lead–silver alloy exhibited an interesting yield point effect at 250°K. The yield point was transient as some recovery occurred with time at test; after 10 or 20 sec at stress a yield point could be observed; after much longer times a smooth, reduced flow stress was obtained. This seems similar to the observations of Thomas (1958) with an aluminium–zinc alloy at temperatures where recovery is an important process.

3.5.4.

In summary, it may be said that all the face-centred cubic metals tested showed an unloading yield point effect at temperatures where recovery is not an immediate process. The purer metals showed no ageing at stress yield effect except at 77°K.

§ 4. DISCUSSION

A direct conclusion from all the experiments is that the unloading yield point effect is a general phenomenon in all the face-centred cubic metals and alloys studied. In all the observations specific to this effect nothing has been found to contradict the proposed explanation that the mechanism responsible for the recoverable hardening is a dislocation–dislocation interaction. Further comment on the exact nature of this interaction cannot be made from the results presented here.

During the report of the experiments concerning 'ageing' under stress it has been implicitly assumed that the mechanism responsible for the production of the yield point is the formation of some configuration of atoms at or around dislocations, different from that in the undisturbed solid. This was done partly to facilitate the presentation but mainly because it seems the best conclusion to be drawn. At temperatures where the movement of solute or impurity atoms seems possible by a vacancy mechanism, the yield effect appears only in alloys or impure metals, not in the purer metals. The exact nature of the configuration which is formed during the segregation must depend on whether the interaction is chemical or elastic in nature. As well, it cannot be discounted that the configuration is one of a short-range order in the vicinity of a dislocation.

The treatment of the data from the process of ageing under stress was considered in a manner which assumes elastic interaction between the solute atoms and simple edge dislocations. It is also possible for chemical interaction to produce a yield point effect in alpha brass where edge dislocations should be extended into complex partial dislocations separated by a low energy stacking fault. Suzuki (1957) has presented the arguments for both processes and it seems that both are possible in the temperature range investigated. However, it is not likely that diffusion into a small layer such as a stacking fault would follow a $t^{2/3}$ law unless the interaction of solute atoms with partial dislocations provides a short-circuit path for the process. A directional, short-range order segregation at dislocations could also produce a yield point, but the kinetic treatment has not been considered.

The production of the ageing yield point is inextricably connected with the occurrence of creep. However, three facts eliminate the significance of creep as a prime factor in the ageing. First, the creep occurred in all the metals investigated by ageing under stress whether a yield point was produced or not. Secondly, it is noted that the amount of creep which was obtained, although dependent on the stress level of the test, was smaller the more rapid and the larger the ageing effect. For example, at the lower temperatures more creep was obtained than at the higher—which may be interpreted as implying that the dislocations were further from ageing at these temperatures and/or the ageing occurred more slowly. Finally to counter the possibility that there was evidence for the 'sweeping-up' of solute during the creep the experiments of § 3.4 seem pertinent. The particular test, UC, that of ageing at stress after unloading and before the yield, is most easily explained as a larger yield point produced by ageing dislocations which are initially more immobile—those formed during unloading. If these interacted dislocations are truly sessile before the yield, they should not be subject to creep and thus capable of 'sweeping-up' solute atoms.

A conclusion that the diffusion of solute atoms towards dislocations is the mechanism responsible for the creation of the configurations impeding plastic flow raises several questions concerning the explanations for all types of strain-ageing in face-centred cubic metals and other systems as well. (Brown, in this department, has recently been observing yield effects similar to those produced by ageing under stress in single crystals of NaCl, doped with Ag, K, Cd or Cu.)

One of the problems which arise comes from the following observations. Ageing without stress requires much longer times or higher temperatures to achieve a yield effect equal in magnitude to one produced by ageing at stress—this, in spite of the fact that there are more immobile dislocations, produced by unloading to age. The excess vacancy concentration produced by the deformation should exist for the same periods of time in both cases. The activation energy obtained for the process of ageing under stress is within the error for the activation energy obtained for repeated yielding, or 'repeated strain-ageing'.

One explanation has been advanced in the following manner. When strain-ageing occurs in the absence of stress, any amount of locking must have reached a value higher than the flow stress of the deformed material in order to be observed. However, during ageing under stress each dislocation is immobile (neglecting the creep), under a balance of forces between the external stress and the internal stress field. Then any amount of locking will inhibit plastic deformation in addition to the inhibition by the internal stress field. It does not seem possible to extend this reasoning or others using these experimental results and current theories, without a great amount of speculation.

A second problem concerns the magnitude of the activation energy obtained from ageing under stress. It has been regarded as the activation energy for vacancy migration in the alpha brass. Hino *et al.* (1957) have determined the tracer diffusion activation energies for a 69:31 alpha brass; they are about 1·8 ev for both zinc and copper. A comparison with the activation energies for self-diffusion, vacancy formation, and vacancy migration in copper as summarized by Broom and Ham (1957) may be made. If it is assumed that the increased diffusion rates in brass are due to a decrease in both the energy of formation and of movement of a vacancy, then on a proportionate basis $Q_m \sim 0{\cdot}6$ ev for the brass. The experimental value $Q_m = 0{\cdot}41 \pm 0{\cdot}08$ ev is not consistent with this derived value.

Cottrell (1957) has observed that the values of activation energy obtained from experiments on repeated yielding in more dilute face-centred cubic alloys are lower than those for vacancy migration in the solvent metal. However, the two sets of values for these alloys may be reconciled if the concentration of vacancies is set as $c = A\epsilon^{1{\cdot}4}$ rather than $c = 10^{-4}\epsilon$. There is then no basis for a comparison to be drawn between these results and those for a concentrated alloy.

Another problem concerns the ageing process at low temperatures (~77°K). The ageing effect certainly is not found in the absence of stress, but it may be hidden for several reasons when unloading is performed. Ageing under stress is found and, as suggested by Westwood and Broom (1957) interstitial migration and locking may be responsible. The information available at present is insufficient to adequately support this explanation.

These questions which have been presented are not all the obvious ones. Nevertheless some conclusions may be made from the experiments.

The process of ageing under stress gives rise to a yield point effect more rapidly than simple ageing. Over the range of temperature – 45°c to 50°c, the activation energy derived for the process is $0{\cdot}41 \pm 0{\cdot}08$ ev. In this range the characteristics of ageing under stress are related to those of repeated yielding for which the same activation energy is obtained. At low temperatures a yield point effect is produced by ageing under stress but the kinetics cannot be the same as those at higher temperatures.

The concentration of vacancies in a deformed metal can be described as having a dependence on the strain of the form $c = A\epsilon^m$ where $m = 1{\cdot}3\,(6)$ in the range investigated.

The process of unloading face-centred cubic polycrystalline metals gives rise to a time-independent yield point effect at all temperatures below the recovery temperature. This yield point can be altered by ageing under stress—the most simple interaction is the addition of the ageing effect to the unloading effect.

ACKNOWLEDGMENTS

This work was made possible by a fellowship from the National Research Council of Canada. Research facilities at the Department of Physical Metallurgy of the University of Birmingham were kindly provided by Professor G. V. Raynor. The author is thankful for the encouragement of Dr. R. W. Cahn and for the helpful criticisms received from the members of the Department. Dr. H. Conrad and Dr. G. Schoeck at Westinghouse Research Laboratories have also provided much stimulating discussion during preparation of the manuscript.

REFERENCES

ADAMS, M. A., 1958, *Acta Met.*, **6,** 327.
ARDLEY, G. W., and COTTRELL, A. H., 1953, *Proc. roy. Soc.* A, **219,** 328.
BROOM, T., and HAM, R. K., 1957, Symposium on Vacancies and Other Point Defects in Metals and Alloys, Institute of Metals.
COTTRELL, A. H., 1953, *Phil. Mag.*, **44,** 829 ; 1957, Symposium on Vacancies and Other Points Defects in Metals and Alloys, Institute of Metals.
COTTRELL, A. H., and BILBY, B. A., 1949, *Proc. phys. Soc. Lond.* A, **62,** 49.
HAASEN, P., and KELLY, A., 1957, *Acta Met.*, **5,** 192.
HARPER, S., 1951, *Phys. Rev.*, **83,** 709.
HINO, J., TOMIZUKA, C., and WERT, C., 1957, *Acta Met.*, **5,** 41.
MAKIN, M. J., 1957, *Nature, Lond.*, **180,** 1476 ; 1958, *Phil. Mag.*, **3,** 287.
MOTT, N. F., 1953, *Phil. Mag.*, **44,** 742.
PIERCY, G. R., CAHN, R. W., and COTTRELL, A. H., 1955, *Acta Met.*, **3,** 331.
SEITZ, F., 1952, *Advanc. Phys.*, **1,** 43.
SUZUKI, H., 1957, *Dislocations and Mechanical Properties of Crystals* (Lake Placid).
THOMAS, A. T., 1958, *Nature, Lond.*, **181,** 1728.
VAN BUEREN, H. G., 1955, *Acta Met.*, **3,** 519.
VAN BUEREN, H. G., and JONGENBURGER, P., 1955, *Nature, Lond.*, **175,** 544.
WESTWOOD, A. R. C., and BROOM, T., 1957, *Acta Met.*, **5,** 249.

Impurity Conduction in Indium-Doped Germanium†

By J. S. Blakemore
Honeywell Research Center, Hopkins, Minnesota

[Received December 15, 1958]

Abstract

Studies were made of electrical conductivity at low temperatures in germanium crystals grown with indium and antimony as majority and minority impurities respectively. The indium densities were kept small enough ($<2\times10^{16}$ cm^{-3}) to ensure that impurity conduction was controlled by the degree of compensation, which was carefully determined from Hall and resistive behaviour in the extrinsic temperature range. The impurity conduction results illustrate trapping of electrons on preferred acceptor sites at the lowest temperatures, in accordance with the model recently postulated by Mott (1956) and elaborated by Price (1957, 1958). The trapping energy ϵ_t is some 10^{-3} ev. The mobility of electrons involved in the impurity conduction process appears to be essentially temperature independent—a result at variance with the predictions of Conwell (1956). However the increase of mobility with impurity density does generally follow the lines of Conwell's model.

§ 1. Introduction

When an extrinsic semiconductor is cooled, a steady increase of the Hall coefficient is anticipated since current carriers are progressively de-excited from the principal bands to their parent impurity levels. However, the Hall coefficient may decrease again below a certain temperature, the resistivity undergoing a change in its temperature dependence at the same point. These phenomena were first observed in SiC by Busch and Labhart (1946) and in Ge by Hung and Gliessman (1950, 1954) and were attributed by them to conduction in the impurity levels. Especially in the case of germanium, subsequent investigations (e.g. Fritzsche 1955, 1958; Koenig and Gunther-Mohr 1957) have confirmed that the secondary conduction process which makes itself evident at low temperatures is a bulk effect controlled by the impurity content.

Until fairly recently, little attention was paid to distinguishing between *two* kinds of impurity conduction. The term *impurity band conduction* is more appropriate for the process effective when the impurity density is large, so that the overlap of atomic orbitals is considerable and the eigen-states of the system have essentially non-localized wave functions.

---

† Communicated by the Author.

The present paper is concerned with a quite different process which can occur in semiconductors containing relatively few impurities. The overlap of the ground-state wave functions for adjacent centres is then very small. As Conwell (1956) and Mott (1956) have remarked, the eigen-states of such a system of impurities correspond with localized levels, and multiple occupancy of the region around a monovalent centre is forbidden. This renders conduction impossible in a set of weakly interacting impurities which are all neutral—as will be the case at low temperatures with no compensation. Impurity conduction can occur only if some members of the set are ionized, since then there is an opportunity for electron transfer between neighbouring centres in differing states of ionization. This situation occurs if the semiconductor contains some compensating impurities. Current is not carried through the compensators, which remain permanently ionized, but the charge supplied by them permits electron transfer between the majority centres.

It was the purpose of our measurements to explore this impurity conduction process (in indium-doped germanium crystals containing some antimony for compensation), particularly in the light of two recent theoretical discussions. One of these concerns a point raised by Mott (1956) and elaborated by Price (1957, 1958), that the number of carriers free to take part in impurity conduction should vary with temperature. Using the language appropriate for our indium–antimony-doped germanium, it is postulated that electrons will reside on some of the indium acceptor levels as a result of the partial compensation. Not all of these electrons will be equally free to migrate, since an acceptor which happens to be located very near to a donor ion will offer a lower energy for electron occupancy. Such acceptors behave as 'trapping sites', and an electron must be thermally activated from a trap to one of the remaining 'free' acceptor sites before it can contribute towards impurity conduction.

Koenig and Gunther-Mohr (1957) and Fritzsche (1958) acknowledged familiarity with the Mott–Price model of carrier availability; but unaccountably did not attempt to compare their data with the temperature-dependent provisions of this model. As briefly reported in a preliminary account of our work (Blakemore 1958), the indium-doped germanium specimens studied here conform closely to the behaviour predicted for an electron trapping situation.

The second theoretical discussion is that of Conwell (1956) concerning mobility in a set of impurity levels. This is based on the conventional atomic orbital approach to the hydrogen molecule–ion problem. Not much data have been available so far for comparison with this model. McWhorter (1958) discusses the conductance of five germanium samples at 4·2°K, but does not distinguish between the fate of 'free' and 'trapped' electrons. Our results do not support the temperature dependence of mobility which Conwell predicts, but do indicate a mobility increasing with impurity density generally as she anticipates.

§ 2. EXPERIMENTAL PROCEDURES

The specimens used in this investigation were cut from horizontally grown zone levelled germanium crystals. Indium doping was introduced at the beginning of growth, and pellets of compensating antimony arranged to be successively engulfed by the advancing molten zone. Bridge-shaped samples were cut with axes along 100 directions, etched, and supplied with soldered contacts.

A fairly conventional helium cryostat and d.c. electrical measurement system was used for observations of the electrical conductivity σ and Hall coefficient R. A platinum resistance thermometer was used from 300°K down to about 15°K, where it was succeeded by a carbon thermometer. Conductivity measurements on most samples were possible from 300°K down to 2°K. Hall measurements were made down to the temperature at which R reached a maximum (see for example fig. 2) and beyond this point as far as possible. The limit was reached when the Hall voltage became immeasurably small compared with competing effects—this was usually at a temperature of the order of 5–8°K. In no case could R be followed into the range of comparative temperature independence expected for purely impurity conductive behaviour, and reported for more heavily doped samples by Fritzsche (1955).

§ 3. ANALYSIS OF SPECIMENS

A prime objective of this investigation was the careful establishment of the impurity densities N_a and N_d in each sample, in order to evaluate properly the behaviour under impurity conduction dominated conditions. The determinations of N_a and N_d were made principally through analyses of the Hall coefficient behaviour for temperatures at which valence band depopulation was progressing.

The Hall coefficient for p-type germanium depends in a complicated fashion on the contributions from p_1 heavy holes and p_2 light holes, as illustrated by the calculations of Beer and Willardson (1958). But dramatic simplifications occur when (*a*) the product of mobility and magnetic field is large for both kinds of hole, and (*b*) the lattice contributes most of the scattering. When both conditions are obeyed, then

$$1/eR_{12} \simeq (p_1+p_2)=p. \quad . \quad . \quad . \quad . \quad . \quad . \quad . \quad . \quad (1)$$

The first condition is satisfied below about 200°K in our specimens when Hall voltages are measured for $H=11\,000$ gauss. The temperature below which condition (*b*) is violated depends on the extent of compensation, but calculations suggest that, at any rate for the weakly compensated samples, no great error is introduced by employing (1) down to some 10–15°K.

Then when experimental Hall data are expressed in the style of fig. 1, the ordinate can be treated as a scale of total free hole density. The impurity concentrations N_a and N_d, and the acceptor ionization energy ϵ_a, are found by fitting such data to

$$p^2+p(N_d+A)=A(N_a-N_d) \qquad (2)$$

where

$$A=2\beta^{-1}(2\pi kT/h^2)^{3/2}(m_1^{3/2}+m_2^{3/2})\exp(-\epsilon_a/kT)$$
$$=1\cdot08\times10^{15}\,T^{3/2}\beta^{-1}\exp(-\epsilon_a/kT). \qquad (3)$$

Fig. 1

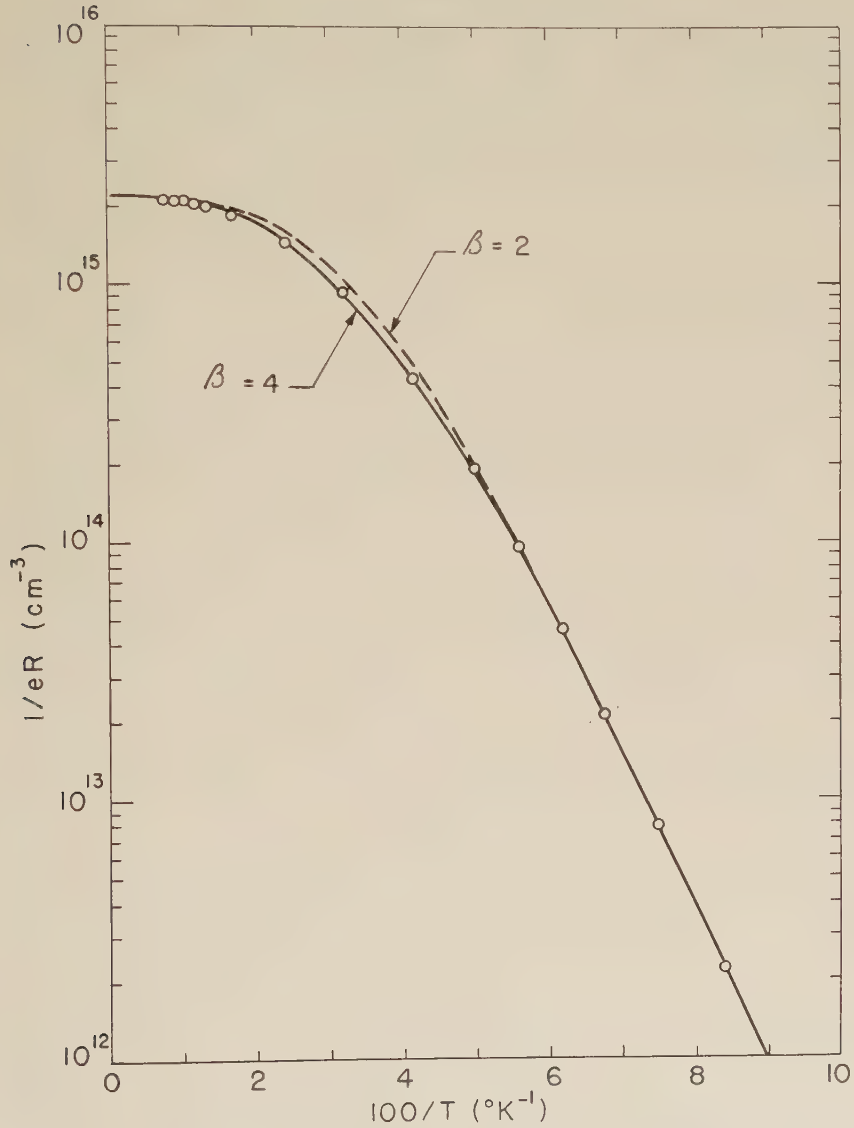

Hall data for specimen 5, expressed as $1/eR$ against reciprocal temperature in the extrinsic range of temperature. The ordinate is essentially a scale of free hole density.

The customary density of states masses for the heavy and light holes are used in expressing (3). The degeneracy of the acceptor level is $\beta=2$ on the simplest theories. However, the Hall data for our samples are better fitted by assuming a four-fold degenerate ground state for the acceptor, a situation predicted on theoretical grounds by Kohn (1957).

Table 1 lists the values of N_a, N_d, and ϵ_a which permitted the best fit to the Hall data on thirteen samples for which complete results are available. It cannot be expected that the entries in this table will be of equal reliability. Thus (N_a-N_d) can be determined with an uncertainty of less than 1%, and a similar accuracy is possible for ϵ_a in specimens where the departure of R from the form of (1) does not occur until the lowest temperatures. But the value assigned to N_d is highly sensitive to any small error in ϵ_a; then despite the array of decimal places in table 1, entries of N_d may be incorrect by as much as 3–5%.

Table 1. Parameters of Germanium Specimens

Specimen number	N_a(cm^{-3})	N_d(cm^{-3})	ϵ_a (10^{-3} ev)	Hole mobility μ_{12} at 25°K 10^3 cm^2/volt-sec	
				Calculated	Experimental
1	$3{\cdot}80\times10^{15}$	$5{\cdot}1\times10^{13}$	9·91	22·7	22·7
2	3.29×10^{15}	$1{\cdot}25\times10^{14}$	10·09	23·7	23·5
3	$2{\cdot}90\times10^{15}$	$1{\cdot}54\times10^{14}$	10·26	24·6	24·7
4	$4{\cdot}13\times10^{15}$	$3{\cdot}8\times10^{14}$	9·05	20·3	19·8
5	$2{\cdot}66\times10^{15}$	$4{\cdot}8\times10^{14}$	10·25	23·2	23·3
6	$2{\cdot}95\times10^{15}$	$7{\cdot}0\times10^{14}$	10·43	21·0	21·3
7	$5{\cdot}15\times10^{15}$	$2{\cdot}65\times10^{15}$	9·57	11·5	10·6
8	$6{\cdot}64\times10^{15}$	$4{\cdot}44\times10^{15}$	9·40	8·00	8·00
9	$7{\cdot}29\times10^{15}$	$5{\cdot}31\times10^{15}$	9·22	6·90	6·90
10	$1{\cdot}34\times10^{16}$	$9{\cdot}6\times10^{15}$	8·88	4·22	4·40
11	$1{\cdot}66\times10^{16}$	$1{\cdot}05\times10^{16}$	8·02	4·13	4·13
12	$1{\cdot}85\times10^{16}$	$1{\cdot}36\times10^{16}$	7·70	3·26	3·26
13	$1{\cdot}297\times10^{16}$	$1{\cdot}240\times10^{16}$	8·88	2·78	2·78

A secondary check on impurity densities was made by comparing hole mobilities in all samples at 25°K, this being a typical temperature at which scattering both from the lattice and from impurities should be important. The comparison was an approximate one in that the light and heavy hole bands were treated as a single system, while the scattering contributions of the lattice, neutral acceptors, ionized acceptors, and ionized donors were simply added. According to the criteria of Blatt (1957), it should be legitimate to use the same scattering cross section for ionized donors and ionized acceptors under our conditions. In practice it was necessary to use a scattering rate for all ionized centres only one-third of that expected from the Brooks (1955) expression. The neutral impurity scattering rate was exactly that given by Erginsoy (1950), when a value was assigned for the wave function radius which corresponds to the true acceptor ionization energy. With these provisos, excellent agreement was found between experimental and calculated mobilities, as shown by the last two columns of table 1. This indicates at least that the impurity densities obtained from Hall data have good internal consistency.

§ 4. Results and Discussion

The typical behaviour of a specimen is illustrated in fig. 2. The valence band is dominant at the higher temperatures, but for this sample impurity conduction becomes the controlling factor below about 10°K. The latter process involves a much smaller temperature dependence of conductance; but the dependence is by no means negligible, as illustrated by the curve for the same specimen in fig. 3 (where the scales have been suitably expanded and contracted).

4.1. *Free Carrier Density in the Impurity Conduction Process*

Reference was made in § 1 to the theoretical discussions by Mott (1956) and Price (1957, 1958) concerning trapping of electrons which would otherwise participate in impurity conduction. Basic to Price's discussions is the concept that for each compensating ionized donor there are r acceptors which are so close to the donor that they offer energetically favourable conditions for electron occupancy. In a real semiconductor, impurities are randomly distributed on lattice points, and acceptors will be influenced to varying extents by neighbouring donors; but as an approximation it is supposed that there are N_d identical groupings of trapping sites. In a rather involved version of the model, it is supposed that, when one trap contains an electron, the other sites in the grouping continue operating but with a modified trapping potential.

It is much simpler, and still instructive, to compare our results with the earlier model in which is envisaged the capture of only one electron per grouping. At any temperature T the trapping energy ϵ_t determines the number n_f of electrons on the (N_a-rN_d) 'free sites' in relation to the number on the 'trap sites'. For this model, n_f is controlled by the quadratic equation

$$[r\exp(\epsilon_t/kT)-1]n_f^2+[N_a-(r-1)N_d]n_f=N_d[N_a-rN_d]. \quad (4)$$

In a weakly compensated sample we may certainly expect that conduction will come principally from the motion of the n_f electrons in the large array of 'free' sites. But as the semiconductor becomes more heavily compensated, this 'band' will tend to become rather full and it would seem proper to consider the neutral (empty) trap sites as a seat of conduction. This could get complicated if it were not for the likelihood that in a strongly compensated sample there would be only one trap per donor, so that the number of ionized 'free' sites would be equal to the number of neutral 'trap' sites. Then for samples of either weak or strong compensation, n_f is the quantity of interest.

For a specimen in which N_a and N_d are known, it is a simple matter to check on whether the electrical behaviour can be correlated with the temperature dependence of n_f in eqn. (4). The shape of $\ln . n_f$ as a function

Fig. 2

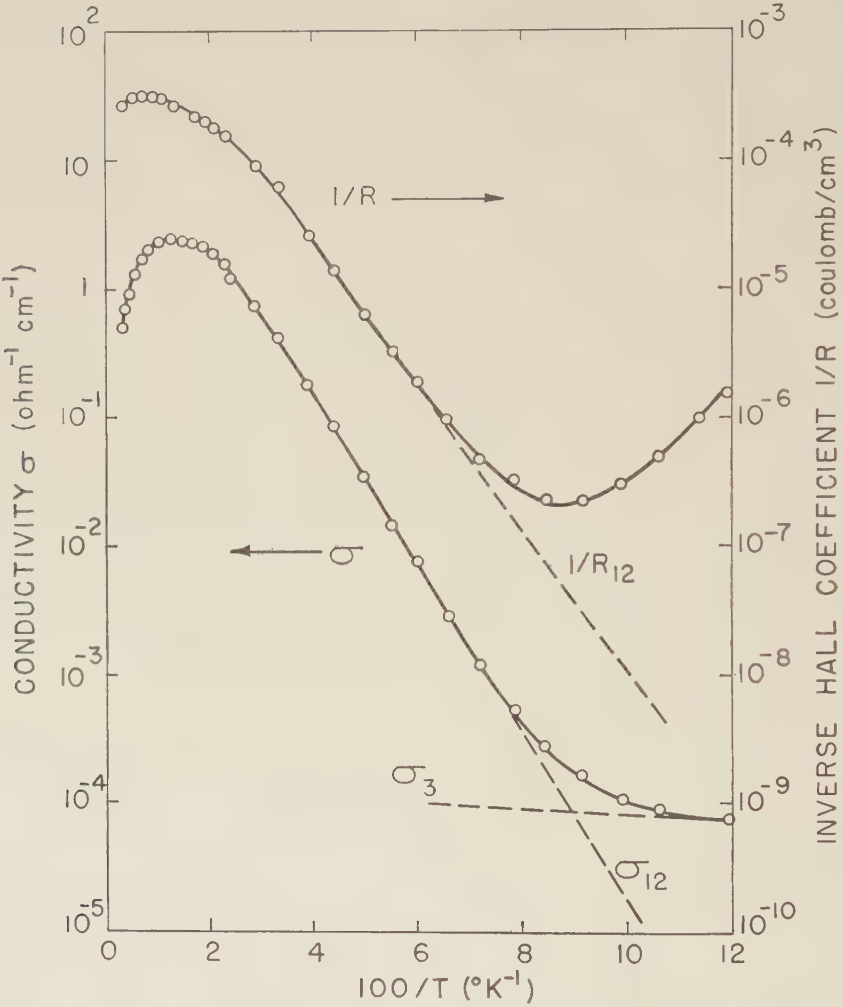

Conductivity and reciprocal Hall coefficient for specimen 9 as functions of inverse temperature. Dashed curves marked σ_{12} and $1/R_{12}$ indicate expected contributions of the valence bands at lower temperatures. σ_3 indicates the expected impurity conduction contribution at higher temperatures. The solid curves for the transition region show the result of combining the calculated contributions.

of $1/T$ has some characteristic features, and when a match of theory and experiment is attempted over a wide range of $1/T$ there is not much doubt as to whether experimental results are consistent with (4) for any values of r and ϵ_l.

Fig. 3

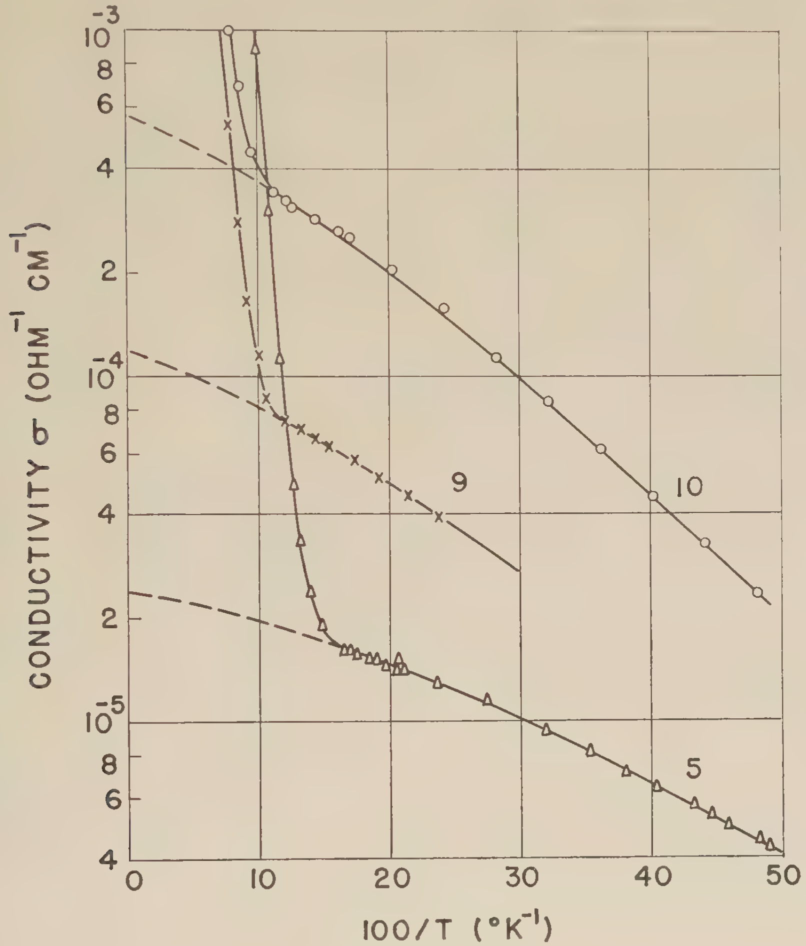

Conductivity of specimens 5, 9, and 10 as a function of inverse temperature, with scales chosen to display the impurity conduction region. The dashed curves indicate the fit of the Mott–Price model for $r=1$, with values of ϵ_r, and μ_3 as indicated in table 2.

We shall provisionally assume that the mobility μ_3 for impurity conduction does not vary with temperature. (This point is discussed in a later sub-section.) Then n_f is expected to vary with temperature in the same manner as the conductivity of this process, σ_3. The low temperature conductivity of almost all our samples can be well fitted on this basis.

Three examples of this are provided in fig. 3. In each case the fit of the conductivity presumes that $r=1$ (i.e. that there is only one trapping acceptor per donor). This may well be expected for a sample such as No. 9, which is 70% compensated. For this sample, the data can be fitted by assigning a trap energy $\epsilon_t=0{\cdot}00127$ ev, and the relative positions of the vertical scales for σ_3 and n_f then correspond to a mobility $\mu_3=0{\cdot}523$ cm^2/volt-sec.

4.2. *Transition from Valence Band to Impurity Conduction Domination*

At a temperature around 10°K the conductivity and Hall coefficient are influenced both by holes in the valence bands and by electrons in the free acceptor levels. A transition of the dominating conduction mechanism is apparent in fig. 2. In this figure a dashed curve marked σ_{12} indicates the expected conductivity of the valence bands, based on calculated hole densities and an extrapolation of hole mobility data. The curve σ_3 similarly shows the expected contribution of the impurity levels — this is the same dashed curve as that given in fig. 3 for conformity of specimen 9 with the Mott–Price model. It is encouraging for our syntheses of both mechanisms that the solid conductivity curve satisfying $(\sigma_{12}+\sigma_3)$ accords fairly well with experimental points through the transition range.

At first sight, the problem of accounting for the behaviour of the Hall coefficient through the transition region would appear to be intractable; for the theory of Hall behaviour with multiple bands and mixed scattering is complicated (Beer and Willardson 1958). Strictly speaking, allowance should be made for two valence bands, each of which is in a condition intermediate between low-field and high-field for $H=11\,000$ gauss. Nevertheless, the simplification $1/R_{12}\simeq e(p_1+p_2)=ep$ is not far from the truth, and it is the dashed curve of this which is shown in fig. 2 for specimen 9.

The carriers in the impurity levels have a mobility μ_3 which is very much smaller than the mean hole mobility μ_{12}. The Hall coefficient R_3 for the impurity conduction process is of the low-field type, but it is probably reasonable to suppose that $1/R_3\simeq en_f$, and that the total effect is

$$R\simeq\frac{p\pm n_f(\mu_3/\mu_{12})^2}{e[p+n_f(\mu_3/\mu_{12})]^2}.$$

In view of the smallness of the mobility ratio, the second term in the numerator can be ignored for most of the transition range, and we might hope to fit data for this range to

$$R\simeq\frac{p}{e[p+n_f(\mu_3/\mu_{12})]^2}. \quad \ldots\ldots\ldots \quad (5)$$

This was successfully attempted for several specimens, including specimen 9 (as illustrated in fig. 2). The solid Hall curve for the transition region in this figure is drawn to satisfy eqn. (5) for a mobility ratio $(\mu_3/\mu_{12}) = 3 \times 10^{-4}$ (this being the ratio indicated by the mobilities μ_3 and μ_{12} deduced from the separate conductive behaviour at lower and higher temperature). It can be seen that the solid curve so calculated is in good agreement with the experimental points.

Fig. 4

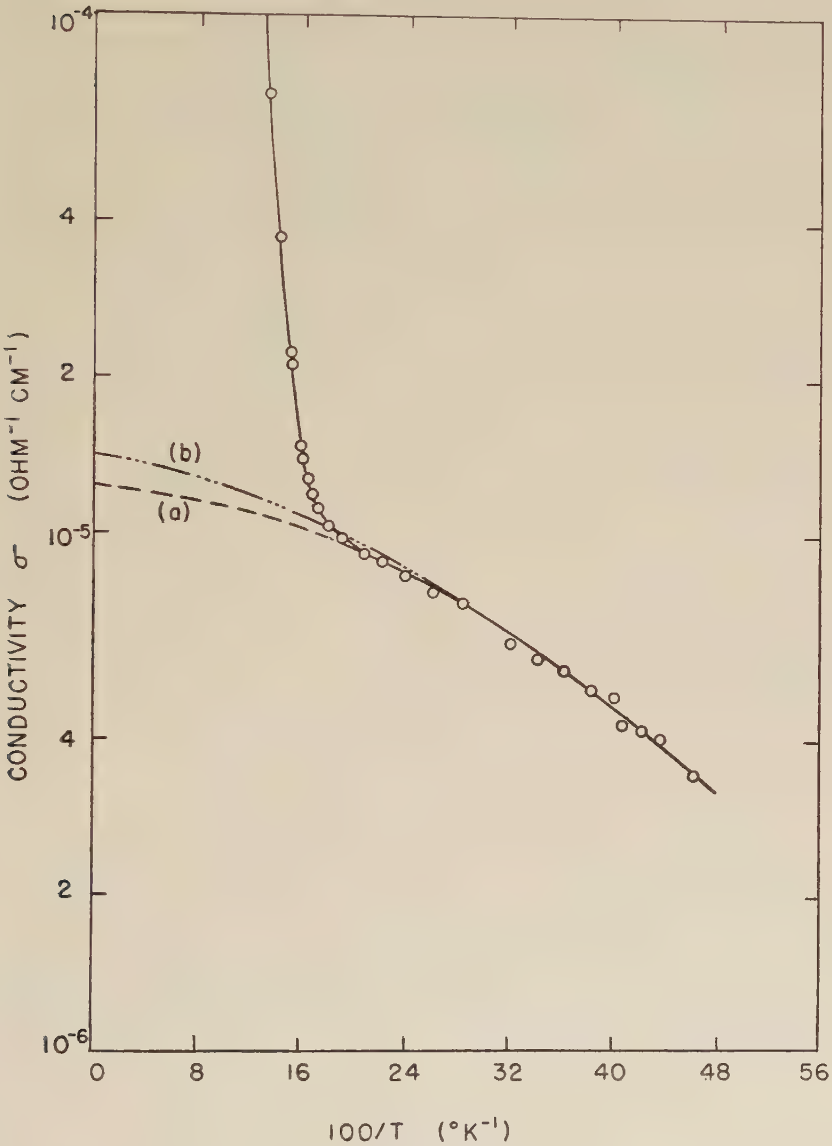

Attempts to fit impurity conduction results on specimen 3.
(*a*) For $r=1$, $\epsilon_t = 0{\cdot}00098$ ev. (*b*) For $r=2$, $\epsilon_t = 0{\cdot}00092$ ev.

4.3. *Trapping States and Trapping Energy*

In analysing impurity conduction on the heavily compensated specimen 9 it was supposed that there would be only one trapping acceptor per donor ($r=1$). For weakly compensated samples it is obviously possible that there could be one or more traps per donor, and attempts must be made to compare experimental results with the requirements of models for $r=1$, 2, 3, etc. An example is shown in fig. 4, where the conductivity of specimen 3 (which is 5% compensated) is matched (*a*) for $r=1$, and (*b*) for $r=2$. It is evident that the choice $r=2$ does not permit such a good fit of the data, and of course the use of $r>2$ would provide a curve even less in sympathy with the results.

Fig. 5

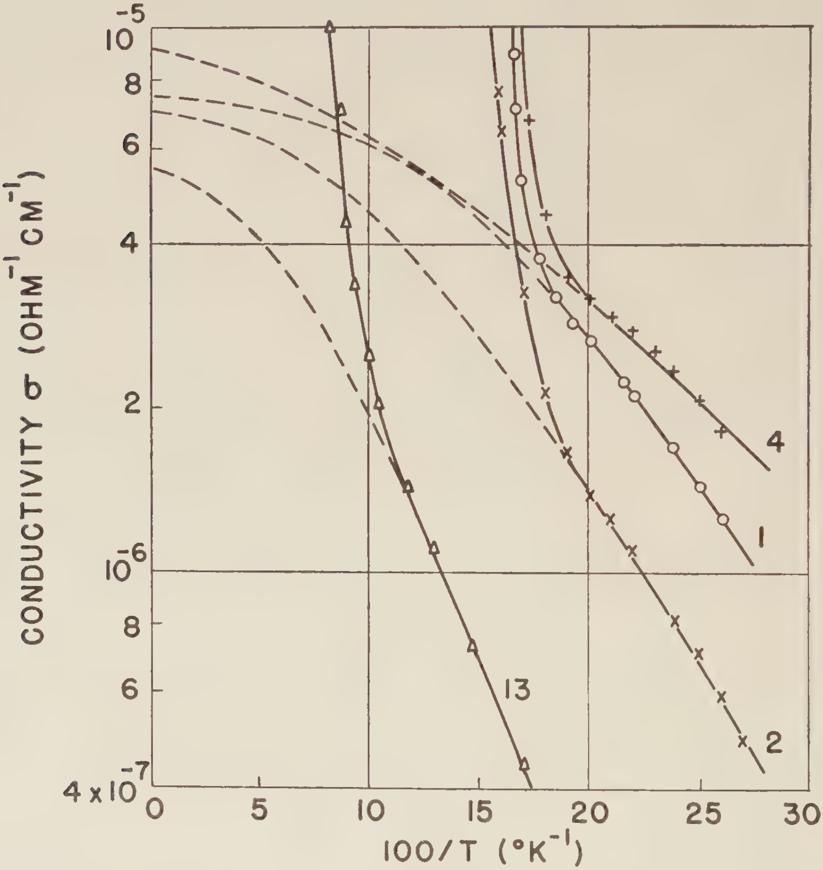

Impurity conduction results for four samples where a fit to the Mott–Price model requires a large trapping energy. The dashed curves are for $r=1$, and for values of ϵ_t and μ_3 as indicated in table 2.

Rather surprisingly, this is the case for almost all our samples. The exceptions are four samples (one very highly compensated, three lightly compensated) for which ϵ_t is abnormally high; the data do not extend over a range wide enough to establish a definite value for r. These four samples are illustrated by fig. 5, the dashed curves showing the fit for $r = 1$. An equally good fit is possible in any of these cases with $r = 2$ or $r = 3$ (making trifling changes in ϵ_t). Nevertheless, it is true to say that for all our specimens $r = 1$ gives *at least as good* a fit as any other value. Accordingly, table 2 presents the values of μ_3 and ϵ_t deduced by fitting each sample for $r = 1$. There is a tendency for ϵ_t to become larger as the germanium is more heavily doped (see fig. 6). This is to be expected, since Coulomb forces should be more important as inter-impurity distances decrease.

Table 2. Impurity Conduction Properties of Germanium Specimens. (Deduced on the basis that $r = 1$ and that μ_3 is not a function of temperature)

Specimen number	N_a (cm^{-3})	$(N_a - N_d)$ (cm^{-3})	Impurity conduction mobility μ_3 (cm^2/volt-sec)	Trapping energy ϵ_t (10^{-3} ev)
1	$3{\cdot}80 \times 10^{15}$	$3{\cdot}75 \times 10^{15}$	0·910	2·54
2	3·29	3·16	0·360	2·69
3	2·90	2·75	0·538	0·98
4	4·13	3·75	0·106	1·89
5	2·66	2·18	0·388	0·91
6	2·95	2·25	0·130	1·12
7	5·15	2·50	0·394	1·14
8	6·64	2·20	0·430	1·31
9	7·29	1·98	0·523	1·27
10	$1{\cdot}34 \times 10^{16}$	3·8	1·28	1·41
11	1·66	3·1	4·30	1·35
12	1·85	4·9	3·72	1·54
13	1·297	$5{\cdot}65 \times 10^{14}$	0·063	4·10

Triangles are used in fig. 6 (and fig. 8) to mark the four specimens yielding anomalously high values of ϵ_t. Anomalous behaviour is really not too surprising for specimen 13, since this is 95% compensated, and any microscopic spatial fluctuations of N_a and N_d will have enormously amplified results. But for weakly compensated samples it is not easy to see why, for instance, specimen 2 has a trapping energy almost three times as large as specimen 3. For the moment this remains a mystery.

4.4. *Mobility*

Conduction in impurity levels is envisaged as the ability of a hole to transfer itself from one acceptor to a neighbouring ionized acceptor.

This ability is controlled by the small but perceptible overlap of impurity wave functions. It is a convenient simplification to assume that the bound hole on an indium impurity has a hydrogen-like wave function, characterized by an ionization energy ϵ_a and a radius r_0. These quantities are then related by

$$\epsilon_a = e^2/2Kr_0 \qquad (6)$$

where K is the dielectric constant.

Fig. 6

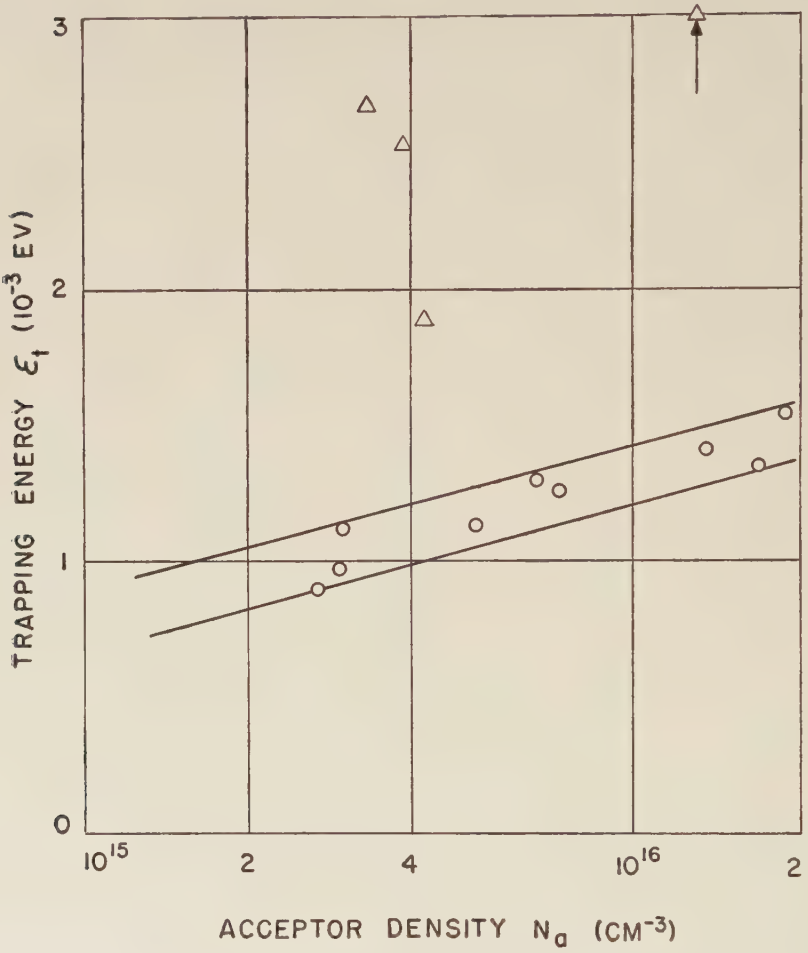

Trapping energy for 13 samples as a function of acceptor density.

Were each acceptor to be surrounded by a sphere of radius r_s, the combined volume of the spheres would equal that of the semiconductor if $r_s = (3/4\pi N_a)^{1/3}$. Now impurities are randomly distributed over the lattice sites, yet most inter-acceptor distances will be approximately $2r_s$. Evidently the overlap of atomic wave functions (and the ability to support conduction) will be critically dependent on the ratio r_s/r_0.

Conwell (1956) has discussed this problem, treating the system of two impurity ions with one carrier as essentially a hydrogen molecule-ion in a medium of dielectric constant K. In this way she was able to take over

Fig. 7

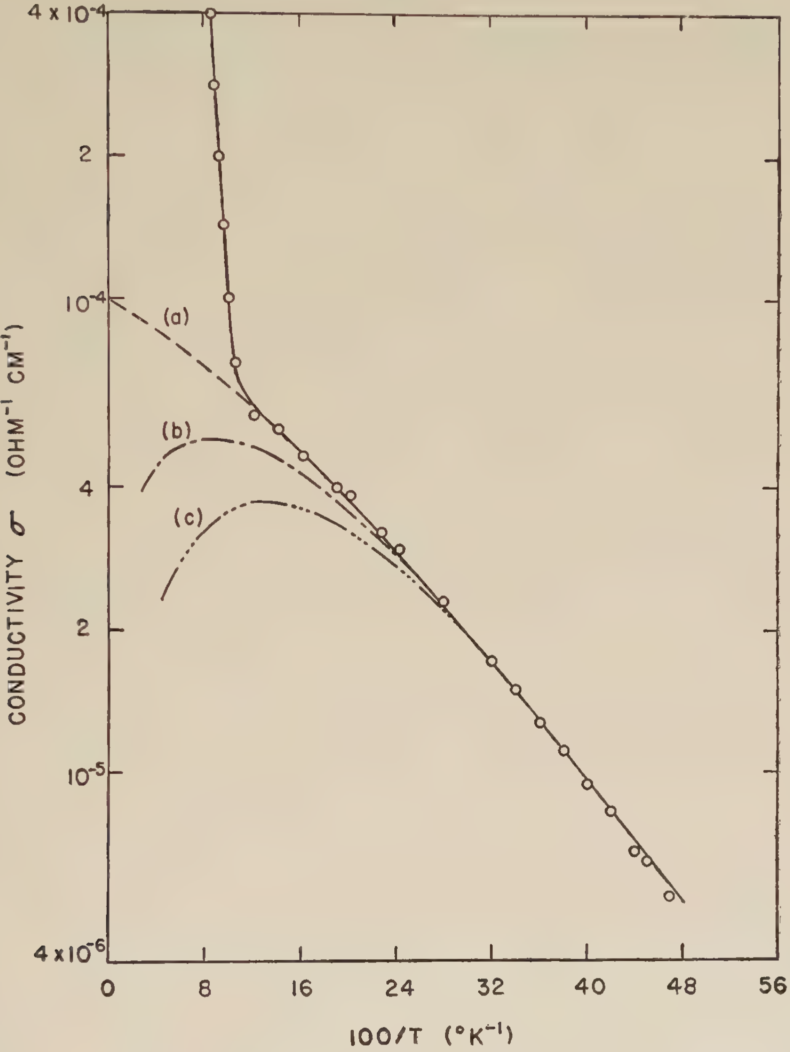

Impurity conduction results for specimen 8 fitted (*a*) assuming mobility to be temperature independent, (*b*) assuming $\mu_3 \alpha T^{-1/2}$, and (*c*) assuming $\mu_3 \alpha T^{-1}$ as expected from Conwell's model.

the result of Pauling and Wilson (1935) (based on the simple linear combination approach) for the energy difference between symmetric and antisymmetric configurations, viz.

$$\Delta E = \frac{8e^2 r_s}{3Kr_0^2} \exp(-2r_s/r_0), \quad r_s \gg r_0. \qquad . \quad . \quad . \quad . \quad (7)$$

Conwell then remarked that this energy difference should determine a frequency $\Delta E/h$ of charge oscillation between impurities. Since in three-dimensional diffusion the diffusion constant = (1/6)(jump distance)^2(jump frequency), this quantity will be

$$D_3 = 2r_s^2 \Delta E/3h. \qquad (8)$$

The diffusion constant is then not dependent on temperature; and the impurity conduction mobility μ_3 which follows from an application of the Einstein relation must vary inversely with temperature. It is more convenient to express this mobility in terms of N_a rather than of r_s, viz.

$$\mu_3 = \frac{1{\cdot}71 \times 10^{11}}{r_0^2 N_a T K} \exp\left(-\frac{1{\cdot}24}{r_0 N_a^{1/3}}\right) \text{cm}^2/\text{volt sec.} \qquad (9)$$

Now such a temperature-dependent mobility is inconsistent with our experimental results, as typified by the data for specimen 8 in fig. 7. Here we suppose that n_f will vary with temperature in conformity with the Mott–Price model (for $r = 1$). The data can be very well fitted by optimizing values for a trapping energy ϵ_t and a temperature-independent mobility μ_3, as demonstrated by curve (*a*). But the fit is much less favourable for curve (*c*), where it has been supposed that μ_3 varies as $1/T$, and optimum values sought for the parameters ϵ_t and $(\mu_3 T)$. Even the supposition of μ_3 proportional to $T^{-1/2}$, as in curve (*b*), is distinctly less satisfactory than that of a constant mobility.

In comparing mobilities of the various specimens, there is inevitably a great deal of scatter superimposed on any trend, since microscopic fluctuations of impurity density exert a powerful influence. Nevertheless, μ_3 does increase with impurity density; the most significant trend occurring when μ_3 is plotted as a function of $(N_a - N_d)$, the 'free site' density. This plot is shown in fig. 8. The solid curve in this figure follows

$$\mu_3 = \frac{8{\cdot}3 \times 10^{21}}{(N_a - N_d)} \exp\left[-\left(\frac{1{\cdot}08 \times 10^{19}}{N_a - N_d}\right)^{1/3}\right] \text{cm}^2/\text{volt sec} \qquad (10)$$

which is appropriate on Conwell's model (eqn. (9)) at 4°K in a semiconductor for which $K = 16$ and $r_0 = 5{\cdot}6 \times 10^{-7}$ cm. This value for r_0 is rather larger than might be expected (it corresponds with $\epsilon_a = 0{\cdot}008$ ev on the basis of eqn. (6)); but μ_3 is a very sensitive function of r_s/r_0, and little adjustment of r_0 is possible.

Some kind of jump mechanism for conductivity called for by the trend of μ_3 with $(N_a - N_d)$ in fig. 8. But the check of experimental points against the consequences of Conwell's model is not conclusive. Measurements for samples with higher and lower impurity densities would assist on this point.

The data for specimen 13 are markedly at variance with that for other samples, and again this is not very surprising.

4.5. *Dependence of Conductivity on Electric Field*

Considerable interest is currently shown in the variations of low-temperature conductivity with electric field strength (e.g. Koenig and Gunther-Mohr 1957). It was not a primary concern of this investigation to study these variations, but rather to examine the ohmic behaviour characteristic of small electric fields. Breakdown itself occurs at a field of several volts per centimetre, but minor departures from Ohm's law are apparent with fields as small as 0·25 volt/cm. For all of our specimens, precautions were taken to remain within the ohmic region.

Fig. 8

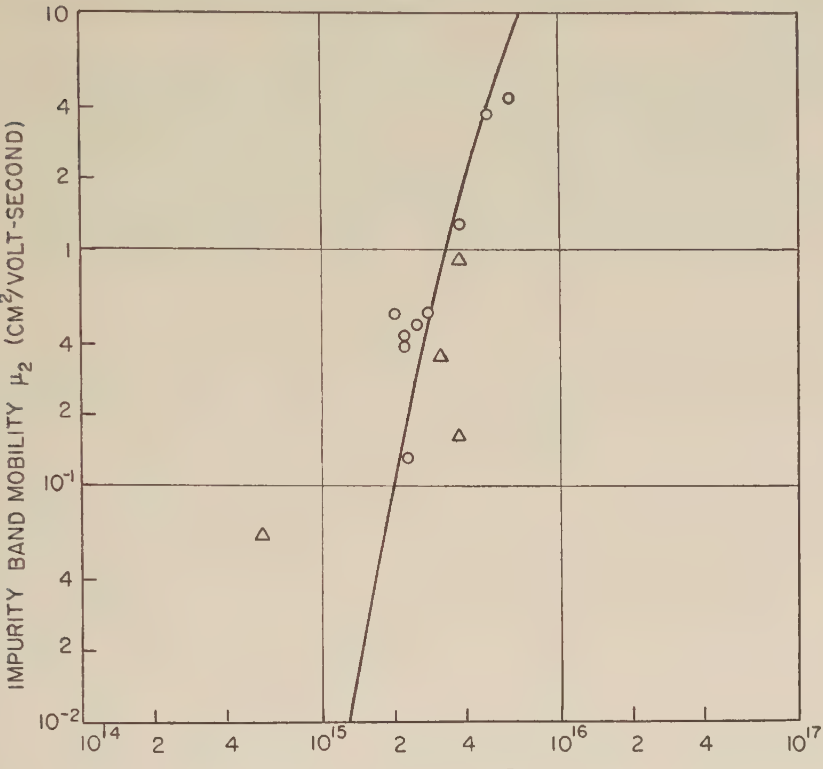

Mobility μ_3 for 13 samples as a function of $(N_a - N_d)$. Triangles indicate the samples for which ϵ_t was abnormally large. The curve follows Conwell's model (eqn. (9)) for $T = 4°\text{K}$, $K = 16$, and $r_0 = 5{\cdot}6 \times 10^{-7}$ cm (eqn. (10)).

Acknowledgments

It is a pleasure to thank J. Myers for assistance in the measurements and C. D. Motchenbacher for his design and construction work on the cryostat and its associated equipment. The cooperation of R. E. Buck in growing germanium crystals for this programme is gratefully acknowledged. The interpretation of this work has benefited greatly from numerous discussions with D. Long.

REFERENCES

BEER, A. C., and WILLARDSON, R. K., 1958, *Phys. Rev.*, **110,** 1286.

BLAKEMORE, J. S., 1958, *Bull. Amer. phys. Soc.*, **3,** 328.

BLATT, F. J., 1957, *J. Phys. Chem. Solids*, **1,** 262.

BROOKS, H., 1955, *Advances in Electronics and Electron Physics* (New York: Academic Press), **7,** 85.

BUSCH, G., and LABHART, H., 1946, *Helv. phys. acta*, **19,** 463.

CONWELL, E. M., 1956, *Phys. Rev.*, **103,** 51.

ERGINSOY, C., 1950, *Phys. Rev.*, **79,** 1013.

FRITZSCHE, H., 1955, *Phys. Rev.*, **99,** 406; 1958, *J. Phys. Chem. Solids*, **6,** 69.

HUNG, C. S., and GLIESSMAN, J. R., 1950, *Phys. Rev.*, **79,** 726; 1954, *Ibid.*, **96,** 1226.

KOENIG, S. H., and GUNTHER-MOHR, G. R., 1957, *J. Phys. Chem. Solids*, **2,** 268.

KOHN, W., 1957, *Solid State Physics* (New York: Academic Press), **5,** 257.

MCWHORTER, A. L., 1958, *Lincoln Laboratory* (*M.I.T.*) *Solid State Quarterly Report* (April–June).

MOTT, N. F., 1956, *Canad. J. Phys.*, **34,** 1356.

PAULING, L., and WILSON, E. B., 1935, *Introduction to Quantum Mechanics* (New York: McGraw Hill).

PRICE, P. J., 1957, *J. Phys. Chem. Solids*, **2,** 282; 1958, *I.B.M. J.*, **2,** 123.

The Martensite Transformation in Thin Foils of Iron–Nitrogen Alloys†

By W. Pitsch
Max-Planck-Institut für Eisenforschung, Düsseldorf, Germany

[Received November 10, 1958]

Abstract

The martensite transformation in thin foils of an iron–nitrogen alloy has been investigated. Under these particular experimental conditions the martensite consists of very thin fibre crystals which are twin orientated. The orientation relationship is $[1\bar{1}0]_\gamma \| [\bar{1}\bar{1}1]_{\alpha'}$ and $[001]_\gamma \| [1\bar{1}0]_{\alpha'}$. This is different from all orientation relationships found in bulk materials. The difference is explained by the fact that in thin foils the transformation mechanism is less hampered by the surrounding parent lattice than in bulk materials. A simple transformation mechanism is deduced consisting of a pure distortion and a half twin shear.

§ 1. Introduction

The experimental work on martensite transformations is usually done at bulk materials. Under such circumstances those regions of the matrix which have already transformed are still in contact with other regions not yet transformed. Therefore the crystallographic transformation mechanism is restricted by the condition that in the interface, where the transformation product grows into the parent phase, not more than small distortions or rotations are allowed. Furthermore the pronounced volume change which occurs during the transformation, produces constraining stresses and lattice deformations.

These facts have been taken into account by all recent analyses of the crystallography of martensite transformations, an extended review of which has been given recently by Bilby and Christian (1955). Therefore all those analyses probably do not determine the ideal transformation mechanism but a modified one (Geisler 1953), which is particularly valid for bulk materials.

In order to check this view, the martensite transformation is investigated in the present paper under conditions where little or no constraints operate. It was expected to determine the ideal crystallographic transformation mechanism and to learn how it is influenced by the constraints operating in bulk materials.

§ 2. Experimental

The particular experimental conditions mentioned above can be realized in thin foils with a thickness of some 100 Å, for there is no constraining parent lattice above and underneath those foils. Thin foils of iron were prepared by vacuum evaporation on to collodion substrates at room temperature (for details see Pitsch 1957). After dissolving away the collodion the iron foils were mounted on a grid and heat treated at temperatures between 600 and 700°C in a furnace under various atmospheres. The foils were subsequently withdrawn into the water-cooled end of the furnace tube and allowed to cool rapidly to room temperature. The specimens were examined by direct transmission in the Siemens Elmiskop I operating at 80 kv. The crystal structure and orientation of the areas examined were determined by electron diffraction.

---

† Communicated by the Author.

If an atmosphere of purified hydrogen was used the quenched foils were pure α-iron (fig. 1, Pl. 69). If a gas mixture of hydrogen and ammonia was used the foils could be nitrided to form iron–nitrogen alloys with a nitrogen content determined by the nitriding temperature, the gas ratio and the rate of gas flow (Lehrer 1930). For example, after nitriding at 700°C with about 7·5 vol. % NH_3 the quenched foils were face centred cubic with a lattice constant of $a = 3{\cdot}62$ Å. This structure corresponds to nitrogen–austenite with 2·15 wt % N (Jack 1951). An electron micrograph of this foil is shown in fig. 2, (Pl. 69).

After nitriding at 670°C with less than 7·5 vol. % NH_3 the diffraction pattern consisted of weak spots of retained austenite and lines of a body centred tetragonal structure with $a = 2{\cdot}85$ Å and $c = 3{\cdot}00$ Å. This structure corresponds to nitrogen–martensite with 1·5 wt % N (Jack 1951). Figure 3 (Pl. 69) shows an electron micrograph of this foil. There are fine parallel striations, which are often arranged in two groups perpendicular to each other (*a*). Otherwise the pattern of the foil may be called a dotted pattern (*b*).

The present paper presents the structure analyses of the areas with fine striations and deals with the martensite transformation in these areas.

§ 3. Results

Areas of about 1 μ in diameter were selected and the electron diffraction of these areas investigated. Figure 4 (Pl. 70) shows the diffraction pattern of the area (*a*) in fig. 3. It consists mainly of diffuse layer lines, which are running perpendicular to the striations in fig. 3. This means, that the striations in fig. 3 are representing very thin fibre crystals, markedly thinner than 100 Å. By measuring the distance of the layer lines the atomic distance along the fibre axis was computed to 2·51 Å. This corresponds exactly to the distance of iron atoms along the $\langle 111 \rangle_{\alpha'}$ direction of a martensite lattice with $a = 2{\cdot}85$ Å and $c = 3{\cdot}00$ Å and means, that the fibres are martensite fibres which are grown with $\langle 111 \rangle_{\alpha'}$ in fibre axis.

The analysis of the spots on the layer lines has been done by using the two schemes, which are drawn into fig. 4 in order to make the arrangement of the spots more clear. The analysis is presented in fig. 5. It shows that the fibres are orientated like twins of a body centred tetragonal lattice. The twin plane $(11\bar{2})_{\alpha'}$ is stretched by the direction of simple shear $[111]_{\alpha'}$, in this particular case consequently by the fibre axis, and by the direction $[110]_{\alpha'}$. In both twin orientations $[1\bar{1}0]_{\alpha'}$ runs normal to the plane of the foil. By this the crystallographic structure of one group of martensite fibres is analysed as shown in fig. 6 (*a*).

In the area (*a*) in fig. 3 there are two groups of fibres perpendicular to each other. Therefore in fig. 4 there are also parts of a second diffraction diagram, which is perpendicular to the already analysed one. Otherwise the two diagrams are in full agreement with each other. By this the structure of the two groups of martensite fibres is determined as shown in fig. 6 (*b*). The two groups of fibres are independent from each other and do not have one common lattice, for there are no two $\langle 111 \rangle_{\alpha'}$ directions, which are perpendicular to each other.

Fig. 5

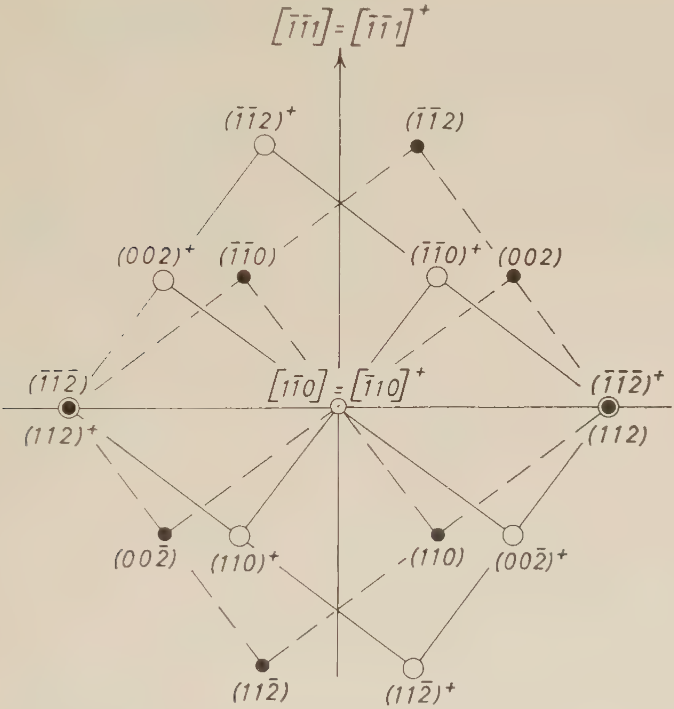

Computed diffraction diagram of two martensite twins orientated as described by the indices in angular brackets. One twin orientation is marked by little crosses. The spots are inscribed with the reflecting lattice planes.

In order to determine the orientation relationship of the transformation besides the martensite structure the original structure of the austenite must be known. This structure is not determined directly, but it can be concluded easily by the assumption that the close-packed arrays of atoms in the austenite and in the martensite are parallel:

$$\langle 110 \rangle_{\gamma} \| \langle 111 \rangle_{\alpha'} . \quad . \quad . \quad . \quad . \quad . \quad . \quad . \quad . \quad (1)$$

This assumption is confirmed: (1) theoretically by the fact that otherwise there are no two lattice directions with such a striking coherence of the atomic arrangement; (2) this parallelity has already been determined in earlier investigations with bulk materials of the analogous iron–carbon alloys (e.g. Kurdjumow and Sachs 1930, other references see Bilby and Christian 1955); (3) by this assumption it will be possible to develop a simple transformation mechanism, which explains entirely the determined martensite structure.

Fig. 6

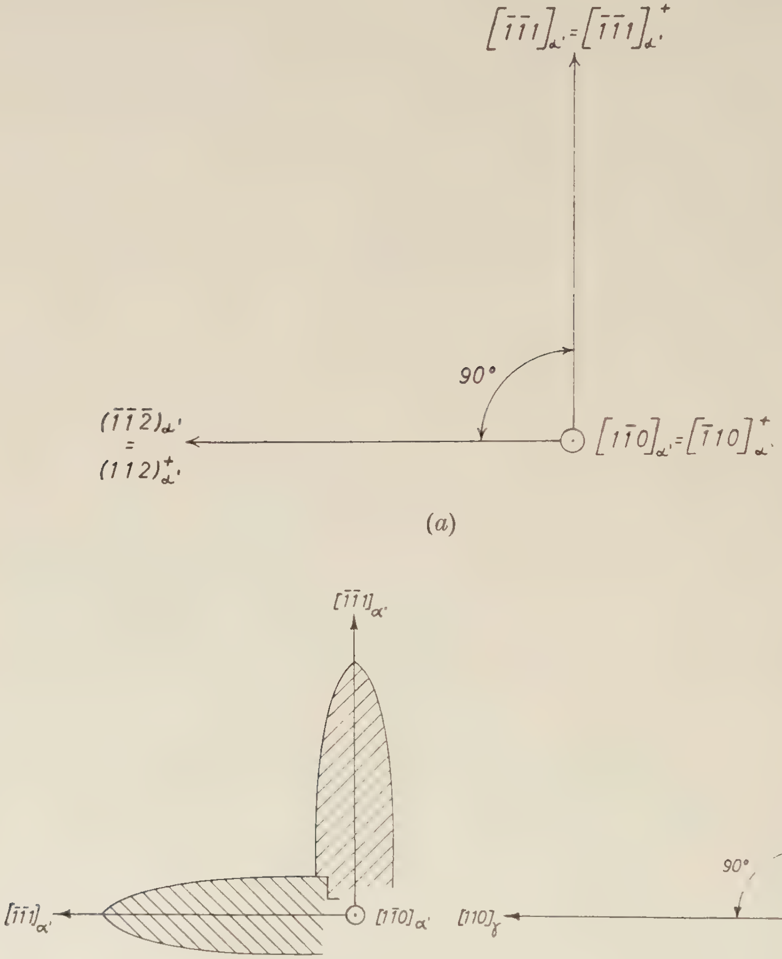
$[\bar{1}\bar{1}1]_{\alpha'} = [\bar{1}\bar{1}1]^{+}_{\alpha'}$
90°
$(\bar{1}\bar{1}\bar{2})_{\alpha'} = (112)^{+}_{\alpha'}$
$[1\bar{1}0]_{\alpha'} = [\bar{1}10]^{+}_{\alpha'}$
$[\bar{1}\bar{1}1]_{\alpha'}$
$[\bar{1}\bar{1}1]_{\alpha'}$
$[1\bar{1}0]_{\alpha'}$
$[1\bar{1}0]_{\gamma}$
90°
$[110]_{\gamma}$
$[001]_{\gamma}$

(*a*)

(*b*) (*c*)

(*a*) The twinned structure of one group of martensite fibres in area (*a*) of fig. 3. (*b*) The crystal structure of the two groups of martensite fibres in area (*a*) of fig. 3. (*c*) The orientation of the transformed austenite lattice in area (*a*) of fig. 3.

Now, if the assumption (1) is correct the austenite, which has been transformed into the martensite of fig. 6 (*b*), must have been orientated as shown in fig. 6 (*c*). Comparing fig. 6 (*a*) and fig. 6 (*c*) the orientation relationship of this transformation is determined exactly as:

$$\left.\begin{array}{ll} & [1\bar{1}0]_{\gamma} \| [\bar{1}\bar{1}1]_{\alpha'}, \\ & [001]_{\gamma} \| [1\bar{1}0]_{\alpha'}, \\ \text{and} & (110)_{\gamma} \| (\bar{1}\bar{1}\bar{2})_{\alpha'}. \end{array}\right\} \quad . \; . \; . \; . \; . \; . \; . \quad (2)$$

This orientation relationship is different from all those, which have been determined in earlier investigations using bulk specimens of iron alloys.

§ 4. Discussion

For there are no comparable results on bulk specimens of Fe–N alloys, the orientation relationship (2) must be compared with those determined in the analogous Fe–C alloys. Here it has always been found (e.g. Kurdjumow and Sachs 1930, other references see Bilby and Christian 1955), as well as in Fe–Ni alloys (e.g. Nishiyama 1934/35, other references see Bilby and Christian 1955), that the close-packed planes $\{111\}_{\gamma}$ and $\{110\}_{\alpha'}$ are parallel to each other, which conflicts with the relationship (2). The difference can be explained by analysing the particular experimental conditions of this transformation (see also Pitsch 1959).

It is possible to describe the transformation of the austenite lattice of fig. 6 (*c*) into the martensite lattice of fig. 6 (*a*) by combining two processes: a pure distortion with the principal axes $[110]_{\gamma}$, $[001]_{\gamma}$ and $[110]_{\gamma}$ (for the definition of these terms see e.g. Wechsler *et al.* 1953) and a half twin shear. The pure distortion consists of the following atomic movements†:

(*a*) $[1\bar{1}0]_{\gamma}$ transforms into $[\bar{1}11]_{\alpha'}$ by a 1·5% contraction of the atomic distances.

(*b*) $[001]_{\gamma}$ transforms into $[1\bar{1}0]_{\alpha'}$ by a 12% expansion of the atomic distances. The 12% expansion would produce strong lattice deformations in bulk material. But in this case $[001]_{\gamma}$ is normal to the plane of the foil. That means that the expansion can take place easier than in bulk specimens.

(*c*) The plane distance of $(110)_{\gamma}$ must decrease by 6% in order to change into the plane distance of $(\bar{1}\bar{1}\bar{2})_{\alpha'}$.

The austenite lattice which has been deformed by this pure distortion corresponds exactly to a martensite lattice, which has undergone half twinning. This is explained in fig. 7. The iron atoms of two twin orientations in martensite are drawn as small black and large white spheres. The sizes of the spheres do not correspond to the real size of the iron atoms. The plane $(\bar{1}1\bar{2})_{\alpha'}$ is the plane of twinning and $[\bar{1}11]_{\alpha'}$ the direction of twin shear. The iron atoms of the former austenite lattice, having moved in the described manner, are now located on the crosses in fig. 7.

---

† The following computations have been done by using an austenitic lattice constant of 3·60 Å, which corresponds to an austenite with 1·5 wt %N at room temperature (Jack 1951).

In order to establish the final martensite structure, those iron atoms have still to do a half twin shear either in $[\bar{1}\bar{1}1]_{\alpha'}$ or in $[11\bar{1}]_{\alpha'}$ direction. After those shear processes the final martensite structure will be just as shown in fig. 6 (*a*).

Fig. 7

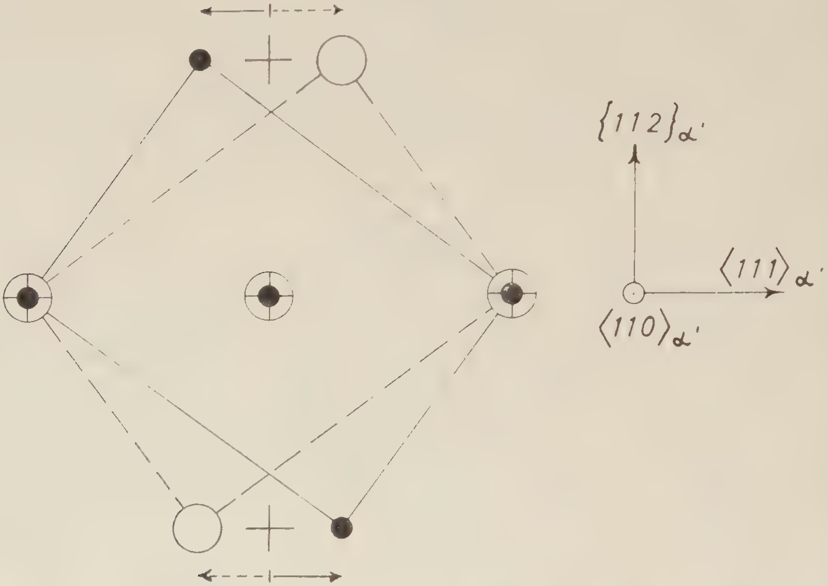
$\{112\}_{\alpha'}$
$\langle 111\rangle_{\alpha'}$
$\langle 110\rangle_{\alpha'}$

Two twinned martensite lattices (small black and large white circles) and the former austenite lattice altered by the pure distortion described in this paper (crosses).

It is reasonable to assume that the atomic movements of the pure distortion and of the half twin shear occur simultaneously. Otherwise, if the austenite lattice is deformed only by the pure distortion described in (*a*) to (*c*) the atomic distance along the former $(110)_{\gamma}$ direction would become smaller than the close-packed direction (fig. 7).

By this analysis the atomic movements during the investigated martensite transformation are found to happen mainly in the following manner: the close-packed arrays of iron atoms in the austenite lattice alter their mutual distances without altering the position of the $(110)_{\gamma}$ planes and simultaneously those former $(110)_{\gamma}$ planes shear in either the positive or the negative direction of the close-packed arrays of atoms. The amount of the shear is equal to a half twin shear of the final martensite lattice. A model how this possibly could take place, is shown, for example, in fig. 8. The arrows indicate the movements of the atoms during the shear process, starting at positions which the atoms would have reached after the pure distortion already would have happened. The martensite fibres, which originate from such atomic movements are martensite twins, which would cause just the diffraction patterns of fig. 4. But other similar models are possible, too.

Fig. 8

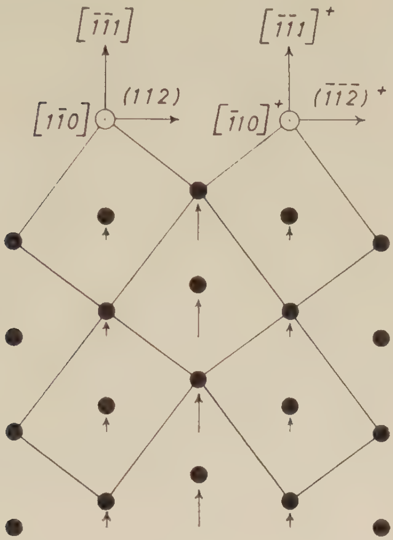

A model how the austenite possibly could be transformed into a twinned martensite structure by a pure distortion and a half twin shear. In order to make the process more clear, the atomic movements only of the half twin shear are indicated by arrows. The arrows start at positions, which the atoms would have reached, if the pure distortion already would have happened. In reality the two processes probably take place simultaneously.

Fig. 9

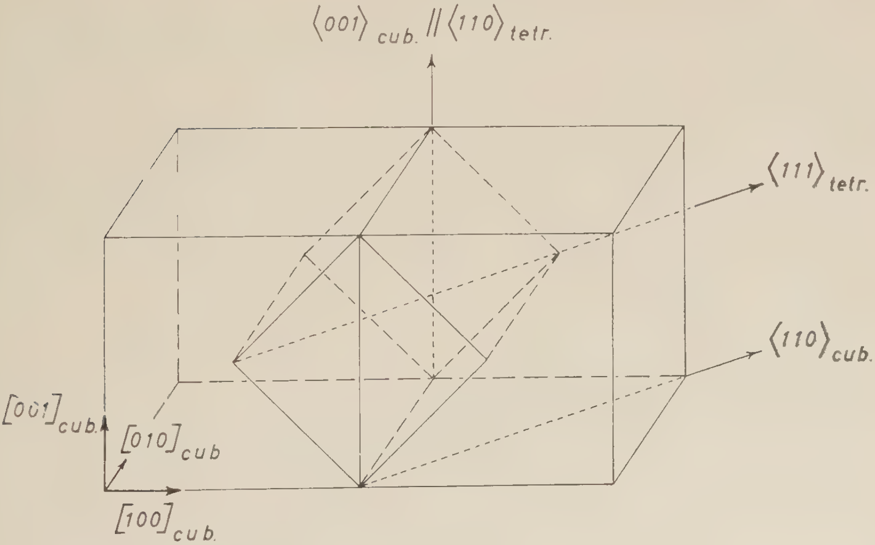
$\langle 001 \rangle_{cub.} \parallel \langle 110 \rangle_{tetr.}$
$\langle 111 \rangle_{tetr.}$
$\langle 110 \rangle_{cub.}$
$[001]_{cub.}$
$[010]_{cub}$
$[100]_{cub.}$

The austenite lattice described either as a face centred cubic or as a body centred tetragonal lattice.

The orientation relationship (2) is already present when the austenite lattice is described either as a face centred cubic or as a body centred tetragonal lattice (fig. 9). And furthermore, if the iron atoms move as it is described by the pure distortion and the simultaneously occurring half twin shear, this relationship is maintained throughout the whole transformation process.

Formally the transformation could be described also as the pure distortion early suggested by Bain (1924) plus a rigid rotation around $[001]_\gamma$. In this case the twinned structure of the martensite fibres could be explained by the assumption that in alternating regions the compression of the Bain distortion happens either along $[010]_\gamma$ or along $[100]_\gamma$ (fig. 9). This mechanism would be similar to that of the analysis of Wechsler *et al.* (1953), where this mechanism is used in order to establish an interface between the martensite and the surrounding austenite, where the average distortion is zero. But in this investigation there is no interface, which constrains the transformation and therefore the analysis of Wechsler *et al.* is not applied. The described pure distortion and half twin shear mechanism is thought to be more reasonable to describe the real atomic movements occurring in this transformation.

Twins in martensite structures have already been assumed in theoretical analyses to be the inhomogeneous part of martensite transformations (e.g. Wechsler *et al.* 1953, Bowles and Mackenzie 1954). Direct evidence that twinning can occur during martensite transformations in iron alloys is shown in this paper. There is nothing to be said about the habit planes for they did not arise in the thin foils investigated in this paper. The areas in fig. 3, which have been called dotted areas (*b*), correspond to martensite fibres, which are more parallel to the normal of the foil.

ACKNOWLEDGMENT

The author wishes to thank Miss H. Ibach for her assistance in preparing the specimens.

REFERENCES

BAIN, E. C., 1924, *Trans. Amer. Inst. min. (metall.) Engrs*, **70**, 25.

BILBY, B. A., and CHRISTIAN, J. W., 1955, Symposium on the Mechanism of Phase Transformations in Metals. Organized by the Metal Physics Committee of the Institute of Metals in London, Metals Monograph and Report Series No. 18, 121.

BOWLES, J. S., and MACKENZIE, J. K., 1954, *Acta Met.*, **2**, 224.

GIESLER, A. H., 1953, *Acta Met.*, **1**, 260.

JACK, K. H., 1951, *Proc. roy. Soc.* A, **208**, 200.

KURDJUMOW, G., and SACHS, G., 1930, *Z. Phys.*, **64**, 325.

LEHRER, E., 1930, *Z. Elektrochem.*, **36**, 383.

NISHIYAMA, Z., 1934/35, *Sci. Rep. Res. Inst. Tohoku Univ.*, **23**, 637.

PITSCH, W., 1957, *Arch. Eisenhüttenw.*, **28**, 745 ; 1959, *Ibid.* (to be published).

WECHSLER, M. S., LIEBERMANN, D. S., and READ, T. A., 1953, *Trans. Amer. Inst. min. (metall.) Engrs*, **197**, 1503.

Strong Hydromagnetic Disturbances in a Collision-free Plasma†

By J. W. Dungey
Department of Mathematics, King's College, Newcastle

[Received October 31, 1958]

Abstract

An attempt is made to extend the exact pulse solutions found by Adlam and Allen (1958) at zero temperature to finite temperatures and the heating of the plasma is studied. A linear treatment shows that the increase in the temperature is small except for very strong pulses. An approximate treatment of the gas pressure is found to be invalid for strong pulses at the experimental values of the initial temperature. Discussion of the ions which start with large thermal velocities shows that some of them are likely to gain energy, but that their effect on the field may be important at the experimental values.

§ 1. Introduction

In a pinched discharge, designed to produce a hot plasma, it is believed that a hydromagnetic shock travels into the plasma in front of the current-bearing layer. It is hoped that the shock heats the plasma considerably more than an equal adiabatic compression would, as is the case for a shock in an ordinary gas. In an ordinary gas shocks are controlled by collisions, but in the plasmas of current interest the collision frequency is much smaller than the gyration period of the ions in the magnetic field. It is therefore of interest to consider the theoretical possibilities, when collisions are completely neglected. There are then important differences between the plasma and an ordinary gas. The velocity distribution behind a shock need not be Maxwellian; in fact, if it were, Liouville's theorem shows that the temperature variation must be adiabatic. It is therefore convenient to use an effective kinetic temperature for each kind of particle defined by the mean energy of their random motion; this effective temperature is significant for thermonuclear reactions. If the velocity distribution is not Maxwellian, Liouville's theorem also shows that it is most unlikely to be isotropic. This implies that there must be oscillations behind a shock, associated with the rotation of the velocity distribution by the magnetic field, and the decay of the oscillations is probably dependent on collisions. The solution to this problem may therefore differ considerably from the familiar kind of shock.

---

† Communicated by the Author. Work partly done during a visit to A.W.R.E., Aldermaston.

The general problem involves the calculation of the orbits of the particles simultaneously with the self-consistent magnetic and electric fields. This is difficult if the orbits contain loops. The presence of loops in an orbit depends on the frame of reference, but this is prescribed by the method to be used: the frame moving with the shock is used, because the solution is then independent of time. A useful beginning has been made by the discovery (Adlam and Allen 1958) of an exact solution of the non-linear equations for the case of zero temperature, with the additional approximation that the difference between the number densities of the ions and electrons is neglected, this approximation being justified by the numerical values. This solution represents a symmetrical pulse and it appears to be a suitable foundation on which to build further approximations. In order to study heating it is necessary to put in a finite temperature. In practice the ratio β of the gas pressure in front of the pulse to the magnetic pressure is of order 0·1. In this paper the effects of the pulse on the temperature and of the temperature on the pulse are considered in turn, but first Adlam and Allen's solution must be briefly recapitulated with a slightly different notation.

In the frame moving with the pulse all quantities are independent of y, z and t. The magnetic field H is directed in the z-direction and the electric field E is perpendicular to it; E_y is independent of x. In this frame the orbits have no loops, so that the velocities of the electrons and positive ions are single-valued; they are $(U, V_e, 0)$ and $(U, V_p, 0)$; their masses are m_e and m_p and both their number densities are N. Let $F = 4\pi(m_p + m_e)NU$; the rate of flow of mass is $F/4\pi$, so that F is independent of x. The equations are

$$m_e U\, dU/dx = -e(E_x + V_e H/c), \qquad (1)$$

$$m_p U\, dU/dx = e(E_x + V_p H/c), \qquad (2)$$

$$m_e U\, dV_e/dx = -e(E_y - UH/c), \qquad (3)$$

$$m_p V_p = -m_e V_e, \qquad (4)$$

$$\frac{dH}{dx} = \frac{eF}{m_p c}\frac{V_e}{U}, \qquad (5)$$

and from (1), (2) and (4)

$$U\, dU/dx = -eH\, V_e/m_p c. \qquad (6)$$

An integral obtained from (5) and (6) is

$$FU + \tfrac{1}{2}H^2 = FU_0 + \tfrac{1}{2}H_0^2, \qquad (7)$$

where the suffix zero denotes limiting values in front of the pulse. It is convenient to take the centre of the pulse as $x = 0$, and, to make U_0 positive, the gas in front of the pulse must be in the region of negative x, so that the suffix zero refers to $x \to -\infty$.

The pulse is obtained when

$$H_0^2 < FU_0 < 4H_0^2, \qquad (8)$$

which shows that U_0 is a little larger than Alfven's wave velocity.

Integration of (3) and (5) with the help of (7) gives

$$m_e F^2 V_e^2 = m_p (H - H_0)^2 \{FU_0 - \tfrac{1}{4}(H + H_0)^2\} \quad . \quad . \quad . \quad (9)$$

and Adlam and Allen obtain an explicit expression for x as a function of H, but this is rather complicated and is not needed here. It is important to know that the width of the pulse is of order $d = (m_e c^2/4\pi Ne^2)^{1/2}$ and that the disturbance dies out exponentially on each side of the pulse with a scale of order d. It is here assumed that the pulse is not very weak, and this requires that FU_0 is appreciably larger than H_0^2. The time scale of the pulse d/U_0 is of the order of the geometric mean of the gyroperiods for the electrons and ions, and it is important to notice that this is ~ 60 times bigger than the gyroperiod for the electrons and ~ 60 times smaller than the gyroperiod of the ions. The limit on the strength of the pulse imposed by the right-hand side of (8) should also be noted. Since N and hence U cannot be negative, (7) and (8) show that H can never exceed $3H_0$. In the limiting case the plasma comes to rest at the peak of the pulse and N becomes infinite.

The order of magnitude of the maximum value of V_e obtained from (9) is $(m_p/m_e)^{1/2} U_0$ except for weak pulses.

§ 2. First-order Approximation for the Temperature

The aim here is to investigate the modification of Adlam and Allen's pulses appropriate to the case where the temperature in front is low but finite. The natural first step is to work to first order in the thermal velocities (or $T^{1/2}$). The velocity components of a particle will be denoted by $U+u$ and $V+v$, where U and V are the unperturbed values and the treatment will be linear in u and v. Then, assuming the field to be unaltered to first order in u and v, the values of u and v for a particular particle at one value of x are linearly related to their values at another value of x. The distribution of u and v for the particles in front of the pulse is now chosen to be isotropic, so that the mean values of u and v are zero. Then, because of the linearity, their mean values are zero everywhere; hence the perturbation in the density is of second order and so are the perturbations in the charge and current densities and hence also the perturbations in the electric and magnetic fields, as was assumed.

The linearized equations will now be given for positive ions, no suffix being used on u and v. Linearizing (2) as it stands and (3) after division by U gives

$$\frac{d}{dx}(Uu) = \frac{eH}{m_p c} v \quad . \quad . \quad . \quad . \quad . \quad . \quad . \quad . \quad (10)$$

and

$$\frac{dv}{dx} = -\frac{eE_y}{m_p U^2} u. \quad . \quad . \quad . \quad . \quad . \quad . \quad . \quad (11)$$

Sufficiently far from the pulse the solutions of these equations oscillate with wavelength $2\pi U_0 m_p c/eH_0$, but the present problem does not necessitate the complete solution of the equations.

It is convenient to use the suffix zero to refer to a specific point $x=-D$, where D is large enough for U and H to be taken as U_0 and H_0; a specific point is needed to define the phase of the oscillation in u and v. The suffix 1 is used to indicate values at the peak of the pulse, $x=0$, and the suffix 2 for values at $x=+D$.

Equations (10) and (11) determine linear relations between (u_0, v_0), (u_1, v_1) and (u_2, v_2) and use can now be made of the symmetry of the pulse. Let the relation between (u_0, v_0) and (u_1, v_1) be written in matrix form

$$\begin{pmatrix} U_0 u_0 \\ v_0 \end{pmatrix} = \begin{pmatrix} p & q \\ r & s \end{pmatrix} \begin{pmatrix} U_1 u_1 \\ v_1 \end{pmatrix}. \quad . \quad . \quad . \quad . \quad (12)$$

Now the relation between (u_2, v_2) and (u_1, v_1) is determined by the same differential eqns. (10) and (11) and, since H and U are even functions of x, the change in the sign of x is equivalent to changing the sign of v and leaving u the same; hence

$$\begin{pmatrix} U_0 u_2 \\ v_2 \end{pmatrix} = \begin{pmatrix} p & -q \\ -r & s \end{pmatrix} \begin{pmatrix} U_1 u_1 \\ v_1 \end{pmatrix}. \quad . \quad . \quad . \quad . \quad . \quad . \quad (13)$$

The relation between (u_2, v_2) and (u_0, v_0) is then

$$\begin{pmatrix} U_0 u_2 \\ v_2 \end{pmatrix} = (ps-rq)^{-1} \begin{pmatrix} ps+rq & -2pq \\ -2rs & ps+rq \end{pmatrix} \begin{pmatrix} U_0 u_0 \\ v_0 \end{pmatrix}. \quad . \quad . \quad (14)$$

The ratio α of the effective temperature behind the pulse to that in front may now be expressed in terms of p, q, r and s by putting $u_0=\cos\theta$, $v_0=\sin\theta$, and averaging $u_2{}^2+v_2{}^2$ over θ. This gives

$$\alpha = 1+2\left(\frac{rsU_0+pq/U_0}{ps-rq}\right)^2 \quad . \quad . \quad . \quad . \quad . \quad . \quad . \quad (15)$$

which shows that a decrease in temperature is impossible.

The quantities p, q, r and s must next be related to eqns. (10) and (11) and for this purpose it is convenient to introduce two particular solutions of these equations: u', v' satisfying the conditions $u_1{}'=1$, $v_1{}'=0$ and u'', v'' satisfying the conditions $u_1{}''=0$, $v_1{}''=1$. Then

$$p=U_0 u_0{}'/U_1, \quad q=U_0 u_0{}'', \quad r=v_0{}'/U, \quad \text{and} \quad s=v_0{}''.$$

Hence

$$\alpha = 1+2\left(\frac{u_0{}'u_0{}''+v_0{}'v_0{}''}{u_0{}'v_0{}''-u_0{}''v_0{}'}\right)^2. \quad . \quad . \quad . \quad . \quad (16)$$

Now from (10) and (11) $$\frac{d}{dx}\left[U\left(u'v''-u''v'\right)\right]=0$$

whence

$$u_0{}'v_0{}''-u_0{}''v_0{}'=U_1/U_0. \quad . \quad . \quad . \quad . \quad . \quad . \quad . \quad (17)$$

Also using (7)

$$\frac{d}{dx}\left(U^2 u' u'' + \frac{U^3 H}{E_y c} v' v''\right) = \frac{v'v''}{E_y c}\frac{d}{dx}(U^3 H) = \frac{v'v''}{E_y c} U^2\left(U-\frac{3H^2}{F}\right)\frac{dH}{dx} \qquad (18)$$

whence
$$u_0' u_0'' + v_0' v_0'' = (FE_y c\, U^2)^{-1} \int_{H_1}^{H_0} v' v''\, U^2 (FU - 3H^2)\, dH. \qquad (19)$$

This quantity is easy to estimate if the pulse is neither very strong nor very weak. If the pulse is not too strong, U is never very small, and the solution of (10) and (11) oscillates with a wavelength $\sim 2\pi U_0 m_p c/eH_0$. If the pulse is not too weak, its width is much less than this wavelength. Then we may put in the integral in (19)

$$v' \sim -eE_y/m_p \int_0^x U^{-2}\, dx \text{ and } v'' \sim 1.$$

Here only the order of magnitude is required and, taking the order of magnitude of $FU - 3H^2$ as H_0^2 and using the width of the pulse d, the order of magnitude of the right-hand side of (19) is $(m_e/m_p)^{1/2}$. It can be shown that this is still true for strong pulses, and then (16) with (17) give

$$\alpha - 1 \sim \frac{m_e}{m_p}\left(\frac{N_1}{N_0}\right)^2. \quad . \quad . \quad . \quad . \quad . \quad . \quad . \quad . \qquad (20)$$

This shows that the increase in effective temperature due to a single pulse is small unless the pulse is strong enough to compress the plasma by a large factor at the peak. Such a compression must also increase the gas pressure by a large factor, and the approximation can therefore be valid only for very low values of β. An approximate treatment of the gas pressure is given in the next section.

§ 3. THE GAS PRESSURE

The last section showed that, except for strong pulses, the effective temperature behind the pulse is only slightly greater than that in front, but the gas pressure may nevertheless vary considerably inside the pulse. In this section reversible variations of gas pressure are considered, which may affect the form of the pulse, but leave it symmetrical and do not contribute directly to the heating. To justify the approximations used it is helpful to picture eqns. (1)–(4) with any initial velocity as a motion in velocity space with x playing the part of time. The motion of the ions is a rotation about the instantaneous centre $(cE_y/H, -cE_x/H)$ with ‘angular velocity’ $(U m_p c)^{-1} eH$ inversely proportional to U. When $U \sim U_0$ this ‘angular velocity’ is slow relative to the width of the pulse, whereas for electrons it is fast. Consequently the approximations appropriate for electrons and ions are different. Because the velocity distribution of the electrons is rotating fast it remains nearly isotropic about its instantaneous mean. The velocity distribution of the positive ions does not remain isotropic. The distribution is affected most by E_x $(E_x \sim V_e H/c \sim (m_p/m_e)^{1/2} E_y)$, which tends to stretch the distribution parallel to the U-axis. It may also be noted that the mean thermal velocity of the ions is less than U_0 for $\beta < 1$, while that of the electrons is $(m_p/m_e)^{1/2}$ times larger.

The hydrodynamic equations must now be considered, mean velocities being denoted by a bar. The partial pressures must be treated as tensors, and for each kind of particle are defined by

$$p_{xx}=m\int_{-\infty}^{\infty}\int_{-\infty}^{\infty}(U-\bar{U})^2 f\,dU\,dV,$$

$$p_{xy}=m\int_{-\infty}^{\infty}\int_{-\infty}^{\infty}(U-\bar{U})(V-\bar{V})f\,dU\,dV$$

where f is the velocity distribution function. The hydrodynamic equations for the ions are

$$m_p\bar{U}\,d\bar{U}/dx=e(E_x+\bar{V}_p H/c)-N^{-1}dp_{pxx}/dx \qquad . \quad . \quad . \qquad (21)$$

and

$$m_p\bar{U}\,d\bar{V}_p/dx=e(E_y-\bar{U}H/c)-N^{-1}dp_{pxy}/dx \qquad . \quad . \quad . \qquad (22)$$

and the equations for the electrons are similar. There is still a stress integral, which is now

$$F\bar{U}+\tfrac{1}{2}H^2+4\pi(p_{pxx}+p_{exx})=FU_0+\tfrac{1}{2}H_0^2(1+\beta) \qquad . \quad . \qquad (23)$$

if the limiting values of p_{pxx} and p_{exx} outside the pulse are both $\beta H_0^2/16\pi$.

The approximations discussed previously are now used for the variation of p_{pxx} and p_{exx} through the pulse. Taking the electron velocity distribution to remain isotropic, the variation of p_{exx} is adiabatic: $p_{exx}\propto N^2$. This may alternatively be seen by considering a circle of constant f in the velocity plane; the area of such a circle must be proportional to N. In case of the ions the most important influence is E_x, which elongates their distribution in the U-direction as well as reducing $\bar{U}$. Their spread in the V-direction varies much less and so their spread in the U-direction is approximately proportional to N, giving $p_{pxx}\propto N^3$. Then (23) becomes

$$F\bar{U}+\tfrac{1}{2}H^2+\tfrac{1}{4}\beta H_0^2((U_0/\bar{U})^2+(U_0/\bar{U})^3)=FU_0+\tfrac{1}{2}H_0^2(1+\beta). \qquad (24)$$

An important feature is that, if (24) is used to express H as a function of $\bar{U}$, H has a maximum at a positive value of $\bar{U}$.

The current density must now be discussed. The contribution of p_{pxy} to $\bar{V}_p$ is seen from (22) to be $-p_{pxy}/(N_0U_0m_p)$. Since p_{pxy} must result from the rotation of the elongated velocity distribution in velocity space through an angle of order $(m_e/m_p)^{1/2}$, $p_{pxy}\sim(m_e/m_p)^{1/2}p_{pxx}$. The contribution to $\bar{V}_p$ is then of order $(m_e/m_p)^{1/2}\beta U_0^4/\bar{U}^3$ or $\beta(m_e/m_p)(U_0/\bar{U})^3$ times the order of magnitude of $\bar{V}_e$. This will be neglected and then $\bar{V}_p$ is still much less than $\bar{V}_e$ and (5) can be used. Because the electron velocity distribution is nearly isotropic, p_{exy} is also neglected and from (3) and (5):

$$\bar{V}_e\,d\bar{V}_e/dH=-(m_p/Fm_e)(cE_y-\bar{U}H). \qquad . \quad . \quad . \qquad (25)$$

Using (24), integration gives

$$\begin{aligned}\bar{V}_e^2=(m_p/Fm_e)(2cE_y(H_0-H)&+F(U_0^2-\bar{U}^2)\\&+\tfrac{1}{4}\beta H_0^2U_0(7-4(U_0/\bar{U})-3(U_0/\bar{U})^2)). \qquad . \quad . \qquad (26)\end{aligned}$$

Equations (5), (24) and (26) have solutions representing symmetrical pulses, but there are values of β and FU_0/H_0^2, such that H reaches its maximum value determined by (24) before $\bar{V}_e$ and hence dH/dx reach zero.

This imposes a condition analogous to the right-hand side of (8), which was needed to make V_e vanish before U. But there is now an analogy between (24) and certain anomalies in aerodynamics, which are resolved by inserting shocks. It would not do to insert a shock here, since the structure of a shock was our original problem, but the occurrence of this phenomenon indicates the breakdown of our approximations and suggests that $\bar{U}$ should vary rapidly.

The most useful result of this section appears to be the condition for the solutions to exist. The critical condition is for V_e to vanish when H has its maximum value according to (24). Let the value of $U_0/\bar{U}$ for this maximum be δ. From (24)

$$4FU_0/H_0^2=\beta(2\delta^3+3\delta^4). \quad . \quad . \quad . \quad . \quad . \quad . \quad (27)$$

Taking this together with (24) and the vanishing of the right-hand side of (26) eventually yields

$$\beta=48(\delta+1)(\delta-1)^{-1}(3\delta^2+8\delta+7)^{-2}. \quad . \quad . \quad . \quad . \quad (28)$$

For $\delta=2$, $\beta\simeq 0{\cdot}12$, and for larger values of δ, β decreases rapidly. Thus for the experimental values of β, this type of solution does not exist for pulses involving compression ratios greater than about 2.

§ 4. HEATING BY REBOUNDS

The heating discussed in § 2 must result in elliptical distortion of the velocity distribution, because only elliptical distortions can be described by the linear equations. The approximations made in § 3 also assumed an elliptical type of distortion, and so our whole discussion has been confined to this lowest order kind of distortion.

The conclusions were that for very low values of β, very strong pulses were needed to give strong heating, and that the treatment was inadequate for strong pulses and larger values of β, an estimate of the critical condition being given by (28). Consequently a more accurate description of the distribution function is required, and the next step may be to look at some of the possible orbits for the ions in a field like Adlam and Allen's. An attack of this kind has been made by Gardner *et al.* (1958). It has already been pointed out that the ions are affected mainly by E_x, while they are in the pulse, and these authors regard the pulse as a potential barrier, and point out that those ions which are unable to cross the barrier first time rebound from it and so gain energy. This effect is illustrated in the figure, which shows the velocity, in the original rest-frame of the gas, with which the ions meet the barrier again for certain values of their velocity when they were reflected. The effect is quite different from those discussed in §§ 2 and 3.

There must be a mapping relating the velocity of a particle behind the pulse to its velocity in front. The construction of this mapping is complicated by the possibilities of particles rebounding more than once and of their hitting the barrier from behind. The barrier may be idealized so that particles with U^2 less than some critical value are reflected specularly and the rest are unaffected. In this case the figure suffices to show that a closed curve in the space of the velocity in front may map on to two or more unclosed curves in the velocity space behind. The break between the curves is due to the discontinuous property of the idealized barrier. In reality the connection must be maintained by those particles which hover for an appreciable time on the peak of the barrier and are consequently affected by E_y, but these particles are few. It seems that rebounds may provide an important heating mechanism, though it has not been assessed quantitatively. It is possible that after a series of pulses the velocity distribution would acquire a fine scale structure in velocity space. Since the effect of collisions can be regarded as causing diffusion in velocity space, they could remove a variation of fine enough scale (without changing the effective temperature), so that the distribution could become isotropic, with the gas in a nearly uniform state different to its original state. Because the lowest energy particles do not rebound, the distribution would depart from Maxwellian form by an excess of low and high energies with a deficiency between.

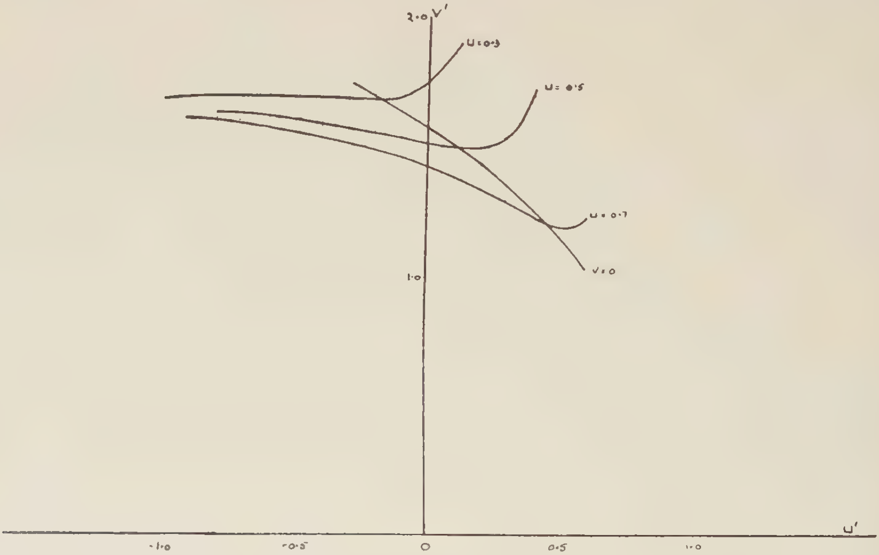

Velocity (U', V') of second impact of an ion with the barrier after first impact with velocity (U, V). Velocity of barrier = (1, 0).

The difficulty of calculating the self-consistent field with looped orbits appears again in connection with rebounding ions. They disturb the charge and current density in front of the pulse and the question arises whether they are sufficiently numerous to change the field appreciably. If the original velocity distribution is Maxwellian the number of ions with sufficient energy to rebound to a distance x across the field is proportional to $\exp[-x^2(eH/c)^2/kTm_p]$. Consequently their importance is likely to depend on the ratio of $(kTm_p)^{1/2}c/(eH)$ to the scale length d of the pulse. This ratio is $(\beta m_p/m_e)^{1/2}$. So the effect is probably important for values of β substantially greater than m_e/m_p. It must be concluded that all the approaches presented here are invalid for strong disturbances at $\beta \sim 0{\cdot}1$.

REFERENCES

ADLAM, J. H., and ALLEN, J. E., 1958, *Phil. Mag.*, **3**, 448.

GARDNER, C. S., GOERTZEL, H., GRAD, H., MORAWETZ, C. S., ROSE, M. H., and RUBIN, H., 1958, Second Geneva Conference on the Peaceful Uses of Atomic Energy, paper 15/P/374.

A Domain Theory of Magnetic Grains in Rocks†

By F. D. Stacey
Department of Geophysics, Australian National University,
Canberra, Australia

[Received November 17, 1958]

Abstract

The activation theory of domain wall movements cannot explain the observed coercive forces of magnetite powders if the individual grains are considered to be divided into lamellar domains with alternately opposite directions of magnetization. Experimental data are shown to be consistent with a 'rod model' in which the grains are divided into domains of square cross section extending right across the grains. This model leads to a coercive force proportional to the $-\frac{3}{4}$ power of grain diameter, in agreement with observations on powdered magnetite. An approximate calculation of the energies of the two models indicates that the rod model has the lower energy if magnetostrictive strain is more important than magnetic anisotropy in determining domain structure. It appears probable that this is the case in magnetite, and therefore that the rod model gives a better picture of the domain structure of magnetic grains in rocks.

§ 1. Introduction

Because no adequate theoretical description of multidomain magnetic grains has been available, theories of the magnetic properties of rocks have generally used the model of single domain grains (Néel 1955), although it is recognized that the principal magnetic constituents in rocks occur as multidomain grains (Nagata 1953, Néel 1955). Recently it has been shown (Stacey 1958) that a simple theory of thermo-remanent magnetization (TRM) of multidomains is in quantitative agreement with observed artificial TRM's in rocks but no model for the domain structure was suggested and no fundamental explanation was given for the magnetic characteristics of coercive force and blocking temperature. The present paper is intended to fill these gaps in the theory of multidomain grains.

When the magnetic moment of a grain is small, the volume is divided into a number of regions of saturated magnetization or domains, the vector sum of whose moments is the net moment of the grain. As long as the grain is far from saturated, changes in this moment occur mainly by movements of the domain walls or boundaries, so that certain domains grow at the expense of their neighbours. Such movements are opposed by natural potential barriers, whose heights are modified by magnetic fields. On activation theory thermal agitation assists domain walls to cross these barriers, and the calculations in the following sections are based on this principle. It is already established through the work of Street and Woolley (1949, 1950) and Néel (1955) and has also been discussed by Stacey (1959). Although it is basically sound, certain details are open to question for reasons considered in § 2, where it is concluded that the principle is valid for highly coercive materials including most rocks but may require modification to apply to magnetically soft materials.

---

† Communicated by the Author.

The use of this principle to determine the coercive force of a grain in which the domains are thin lamellae with alternating directions of magnetization leads to a quite unsatisfactory result in § 3. This suggests the calculation of § 4, in which it is shown that, in a simple case, the subdivision of a grain into domains of roughly square cross section extending the whole width of the grain results in a lower energy than the lamellar structure. This 'rod' model also overcomes the difficulty encountered in § 2 with the lamellar model, and is used in § 5 to relate the coercive force of a grain to its size and to temperature.

§ 2. THE ACTIVATION THEORY OF DOMAIN WALL MOVEMENTS

The probability that a domain wall will acquire in time dt sufficient energy to overcome a potential barrier of height E is

$$dP = C\exp(-E/kT)\,dt, \qquad \ldots\ldots \quad (1)$$

where k is Boltzmann's constant and T the absolute temperature. A value of the factor C has been calculated (Stacey 1959) but this may be of little value if the probability that a movement will occur differs greatly from the probability that sufficient energy becomes available. The difficulty arises on account of the fact that C is a very high frequency, but wall movements may be relatively sluggish. To cross a barrier a domain wall must be impelled by the thermal agitation field, consistently in one direction for the time, τ', it takes to move through the half-width of the barrier (i.e. to 'climb up' the barrier). If τ' is much greater than $1/C$, most of the excursions of the thermal agitation field which reach sufficient energy may be of too short duration to take effect as wall movements.

Unfortunately the magnitude of τ' is unknown but to obtain an upper limit we may use the values of domain wall velocity v measured under special conditions in a nickel–iron alloy by Sixtus and Tonks (1935), who found

$$v \sim 2\times 10^4 (H-H_0), \qquad \ldots\ldots\ldots \quad (2)$$

H being the field exerted on the wall in oersteds, H_0 the critical field below which no large scale movements are observed and v is in cm sec^{-1}. Bozorth (1951, p. 496) suggested that the principal limitation on this velocity was that imposed by eddy currents. If so, the velocities must be much higher in magnetite and other magnetic minerals, which, if not good insulators, are certainly poor conductors. However it is evident from the existence of a critical field H_0 that there is another important effect, probably connected with the potential barriers. Therefore it is useful to consider the possibility that domain wall velocities are comparable in insulators and metals, and to examine the conditions under which they will cause a modification of eqn. (1).

The excursion of the thermal fluctuating field which causes a domain wall movement must have a magnitude comparable with the coercive force, H_c. The number of such excursions, having energy E or greater, occurring in one second is $C\exp(-E/kT)$ but the probability that the field has this energy at any instant is $\exp(-E/kT)$, so that the average duration of the excursions is $1/C$. Assuming that, once a movement begins, it proceeds with a velocity

$$v = 2\times10^4 H_c$$

and must continue for a distance ω, the half-width of a potential barrier, under the influence of the thermal field, this field must operate for a time

$$\tau' = \frac{\omega}{2\times10^4 H_c}. \qquad (3)$$

Then eqn. (1) breaks down if $\tau' > 1/C$, i.e. if

$$H_c < \frac{\omega C}{2\times10^4}. \qquad (4)$$

Taking Stacey's (1959) value $C \sim 6\times10^{12}\,\mathrm{sec}^{-1}$, at room temperature, and as an approximate value $\omega \sim 5\times10^{-8}$ cm, roughly the distance between planes of Fe atoms in magnetite, for reasons considered in § 3, we find the critical value of H_c below which eqn. (1) is not valid to be ~ 15 oersteds. This must be regarded as an upper limit, and as H_c exceeds this value in most rocks which are of interest, it appears that eqn. (1) is valid. However, for the purpose of comparing the theory of § 4 with experimental data, values of H_c down to 3·7 oersteds are used, so that the modification which must be made to eqn. (1) if eqn. (4) applies will be considered.

The probability that the thermal fluctuating field will have a particular direction and energy E or greater at any instant is $\exp(-E/kT)$, and at a time $1/C$ later the field will be practically independent of its first value, and again have a probability $\exp(-E/kT)$ of having energy E, the total probability of its remaining above E being of the order $\exp(-2E/kT)$. Thus the probability that an excursion of the field with energy E will last for a time $\tau' > 1/C$ is of the order $\exp(-\tau' CE/kT)$ and the probability that such a pulse will occur in time dt is

$$dP' = C\exp(-\tau' CE/kT)\,dt, \qquad (5)$$

where τ' is given by eqn. (3). Equation (5) is only an approximation, as no rigorously derived equation for the distribution function of the interval between successive occasions when a random fluctuating function has a particular value is available (Rice 1944, 1945). The calculations of § 3 and § 5 indicate that the dependence of coercive force on grain size is the same for eqns. (1) and (5) but that the dependence on temperature differs. It may further be noted that if the domain wall velocities observed by Sixtus and Tonks (1935) were limited by potential barriers, so that each barrier acted as a delay in the movement, then the jumps between barriers must be more rapid than the results indicate, and eqn. (1) is valid in any case.

§ 3. THE LAMELLAR DOMAIN MODEL

In the presence of a field the effective height of a barrier is reduced for wall movements in one direction and increased for the opposite direction. This effect arises from the field energy which is released by (or put into) a wall when it 'climbs up' the barrier. In the case of a 180° wall of area A in a material of saturation magnetization I_s, moving through a barrier of half-width ω under the influence of a field H, this energy is $(2HI_sA\omega\sin\theta)$, where θ is the angle between H and the normal to the wall. Then the probability that such a movement will occur in a time dt is

$$dP = C\exp[-(E-2HI_sA\omega\sin\theta)/kT]\,dt. \qquad (6)$$

If H is the coercive force H_c, as measured in an experiment which takes a time τ (τ is of the order $1/2\pi f$ for an a.c. measurement at frequency f), the probability becomes unity in a period τ, whence

$$E-2H_cI_sA\omega\sin\theta = kT\ln(C\tau). \qquad (7)$$

The fact that C is very large explains why H_c is almost independent of τ, even at high temperatures at which the right-hand side of eqn. (7) becomes important.

At the blocking temperature T_B, $H_c=0$, so that, neglecting the dependence of C upon T, we have

$$E_B = kT_B\ln(c\tau), \qquad (8)$$

E_B being the value of E at temperature T_B. Since E is proportional to the square of spontaneous magnetization I_s (Stacey 1959), which increases by a factor ~ 3 between T_B and room temperature T_R (Stacey 1958), we have for the value of E at T_R:

$$E_R \sim 9E_B. \qquad (9)$$

Since also $T_B \sim 3T_R$, we have

$$E_R \sim 27kT_R\ln(C\tau). \qquad (10)$$

Thus to a good approximation at low temperatures the right side of eqn. (7) is negligible and

$$E = 2H_cI_sA\omega\sin\theta. \qquad (11)$$

Again considering rocks with high blocking temperatures to which eqn. (10) applies, using the result of Stacey (1959) $C \sim 6\times10^{12}\,\mathrm{sec}^{-1}$ and putting $\tau = 1$ sec, which is arbitrary but does not greatly affect the calculation, we find

$$E \sim 800kT. \qquad (12)$$

In order that the potential barriers in a grain should be able to resist the process of self-demagnetization of even an infinitesimal moment over geological time it is necessary that

$$E > 60kT, \qquad (13)$$

so that we may take eqns. (12) and (13) to define the range of values of E which are of interest. Such large energies cannot be explained by the magnetic interaction of spontaneous magnetization with single crystal defects and it is necessary to suppose that each wall is impeded by a large number of elementary barriers simultaneously. These barriers must be distributed through each grain so that the number which are encountered by a wall at any position during its progress through a grain fluctuates randomly about a mean value. In § 5 it is assumed that this fluctuation is Gaussian. The random superposition of many barriers indicates that the peaks in the energy of a moving wall only have widths comparable with the separation of planes of Fe atoms in the lattice of the material concerned, so that $\omega \sim 5 \times 10^{-8}$ cm as assumed in § 2, although the half-width of each elementary barrier must be of the same order as half the domain wall thickness, which is much greater.

Kittel (1949) showed that for a grain which is not too small, a division into lamellar domains extending right across the grain, so that each domain wall has an area equal to the cross-sectional area of the grain, results in a lower energy than the single domain state of the same grain. It has since been assumed (Néel 1955) that this was a proof that the domains in small grains are lamellae, but it will be shown here that this assumption is not justified. The coercive force of such a model is readily calculated using eqn. (11), or, as here, experimental values of coercive force (Gottschalk 1935) may be used to estimate ω from eqn. (11). Taking $E = 800kT$, $I_s = 500$ e.m.u., $H_c = 100$ oersteds for a grain diameter of 5×10^{-4} cm, we find $\omega \sim 2{\cdot}5 \times 10^{-9}$ cm, which is both obviously too small and an apparently inescapable conclusion of the lamellar model, so that the model must be re-examined in the manner of § 4.

It may first be noted that Kittel's (1948, 1949) calculation of the coercive force of small grains in terms of the nucleation of domains antiparallel to the prevailing direction is inapplicable. The observation of coercive force necessarily implies zero moment and therefore that the domain structure is already complete. When grains are in this state changes in their magnetic moments are results of modifications in domain structure, which do not involve the nucleation of new domains. The inadequacy of the nucleation theory of coercive force was noted in the later review (Kittel and Galt 1956) in which coercive force was recognized to be a measure of the barriers opposing domain wall movements.

§ 4. MAGNETIC ENERGY OF DOMAIN STRUCTURE IN SMALL GRAINS

The calculation in this section is based on the principles of domain theory, fully described in the review articles by Kittel (1949) and Kittel and Galt (1956) whose analyses are assumed except where minor disagreements are specifically noted. The basic principle is that the domain structure is self-determined to give the minimum energy, which is a balance between several contributions. As noted by Kittel (1949) the general problem of calculating domain structure would be far too difficult to tackle and the useful procedure is to make approximations consistent with a preconceived physical picture of the structure considered.

For simplicity we consider a grain which is a cube of side d, in which the easy directions of magnetization are parallel to the cube edges. Then neither the main domains nor the closure domains, which are magnetized in these directions, give contributions to anisotropy energy. It is further assumed that the system of closure domains is complete so that there is no magnetostatic energy due to surfaces of magnetic polarity, and that the grain is in a demagnetized state in zero external field. Under these conditions the only contributions to the magnetic energy which have to be considered are those of magnetostrictive strain and domain walls. The conditions of balance between these two will be determined for the lamellar and rod models.

If the domains are lamellae, all parallel to one pair of cube faces, and separated by W ($\gg 1$) equally spaced 180° domain walls, which have an energy B per cm^2, then the total wall energy is

$$E_w = BWd^2. \qquad (14)$$

Since the domains are thin, the area of 90° walls between the lamellae and the closure domains is negligible. The magnetostrictive strain energy results from the distortion of the two sheets of closure domains on opposite sides of the cube, relative to the bulk of the grain. These domains are magnetized parallel to one cube edge in which direction their unconstrained length differs from the unmagnetized length by a fraction λ_s, the saturation magnetostriction. In the same direction the lamellar domains have changed by a fraction $(-\lambda_s/2)$ so that the relative change is $(3\lambda_s/2)$. In the perpendicular direction within the planes of the cube faces both lamellar and closure domains change by $(-\lambda_s/2)$ and no strain results. Considering the closure domains as two strained skins whose total volume is so small that it cannot materially distort the body of the grain, we see that the strain energy is proportional to the total volume of the closure domains $(d^3/2W)$ and to the square of the magnetostrictive difference between lamellar and closure domains in the direction of strain. We write the magnetostrictive strain energy as

$$E_s = D(d^3/2W)(3\lambda_s/2)^2, \qquad (15)$$

where D is a constant involving the elastic constants, but considered to be arbitrary for the present purpose.

The number of domain walls is self-adjusted so that the total energy $(E_w + E_s)$ is a minimum, i.e.

$$\frac{d}{dW}(E_w + E_s) = 0.$$

When this differentiation is carried out we find

$$W^2 = \frac{9}{8}\frac{D\lambda_s^2}{B}.d, \qquad (16)$$

whence

$$E_w + E_s = ((9/2)BD\lambda_s^2)^{1/2} d^{5/2}. \qquad (17)$$

This energy can be compared with the similar calculation for the rod model. In this case we consider W equally spaced walls to cross the grain in each of two sets of mutually perpendicular planes, so that the total wall energy is

$$E_w' = 2BWd^2. \qquad (18)$$

The closure domains are pyramids whose square bases are outlined by the diagonals of the squares formed by the projection of the main domain walls on to the cube faces. The height of the pyramids is $(d/2W)$ and the total volume of the closure domains is $(d^3/3W)$. Each closure domain is magnetized in a direction perpendicular to its most immediate neighbours, so that in each direction the closure domains have magnetostrictions λ_s and $(-\lambda_s/2)$ alternately, while the rod domains have magnetostrictions $(-\lambda_s/2)$ in both directions. When the sheets of closure domains are considered to be strained skins as before they have an overall magnetostriction of $(\lambda_s/4)$ in each direction, relative to $(-\lambda_s/2)$ for the body of the grain, giving a difference of $(3\lambda_s/4)$ in each direction. The total magnetostrictive strain energy is thus

$$E_s' = 2D(d^3/3W)(3\lambda_s/4)^2. \qquad (19)$$

Differentiating the total energy with respect to W and equating to zero, as before, we find

$$W^2 = \frac{3}{16}\frac{D\lambda_s^2}{B}.d, \qquad (20)$$

$$E_w' + E_s' = (3BD\lambda_s^2)^{1/2}.d^{5/2}. \qquad (21)$$

Comparing eqns. (17) and (21) it is seen that the 'rod' model gives the lower energy; although an exact calculation of the magnetostrictive strain energy has not been made, the difference is sufficient to show that it is quite reasonable for the rod model to have the lower energy. It must here be noted that the corresponding calculation of the balance between domain wall energy and magnetic anisotropy energy, with magnetostrictive strain considered to be negligible, favours the lamellar structure. It is no simple matter to estimate which calculation gives the closer approximation for any particular material, especially as in the general problem of a grain of irregular shape, having easy directions of magnetization uncorrelated with the shape, the structure must be irregular and domain closure incomplete allowing magnetostatic energy to compete with anisotropy and magnetostrictive strain.

However, if the crystal structure is cubic and not uniaxial we can in principle arrange the directions of magnetization in the closure domains to be reasonably close to easy directions, in which case their magnetostrictive strain is more important than their anisotropy energy. This may be particularly important in an irregular grain because a system of rod domains is more flexible in adapting itself to the surface of the grain than is the lamellar structure.

While it cannot be claimed that the occurrence of rod-shaped domains in small grains has been proved, this structure appears at least to be entirely reasonable. The particular reason for considering the rod model is the fact that the domain walls have much smaller areas than in the lamellar model so that it is not necessary to postulate unreasonably sharp potential barriers in order to explain the observed coercive forces. It will also be shown in § 5 that the rod model gives a more satisfactory dependence of coercive force on grain size.

§ 5. COERCIVE FORCE OF THE ROD MODEL

The probability that a domain wall movement will occur is given by eqn. (6), where the area of the domain walls is now

$$A = d^2/W.$$

Since W is given by eqn. (20), we have

$$A \propto d^{3/2}. \qquad (22)$$

For reasons discussed in § 3, the potential barriers which a wall encounters are not considered to be single independent barriers, but random combinations of large numbers of elementary barriers, such that the energy of a wall is a random function of its position. Taking the mean energy to be zero on an arbitrary scale we may expect the probability that a particular wall, of area A, will have an energy between E and $(E+dE)$ in any position to be given by

$$\frac{2}{\sqrt{(\pi)}\epsilon} \exp(-E^2/\epsilon^2)\, dE,$$

where the standard deviation, ϵ, is a measure of the heights of the barriers opposing wall movements. The same probability applies to a second similar area of wall adjoining the first, so that when the two are combined into a single wall of area $2A$, we again have a Gaussian distribution for the energy of the wall in any position, but its standard deviation is $\sqrt{(2)}\epsilon$. Further sections of wall can be added on the same principle, so that the heights of the barriers which a wall of area A encounters are given by

$$E \propto A^{1/2}. \qquad (23)$$

As in § 3, the coercive force is given by eqn. (11) where E is given by eqn. (23) and A by eqn. (22); so that at room temperature,

$$H_c \propto d^{-3/4}. \qquad (24)$$

This conclusion of the present theory is the one most susceptible to experimental check. In the figure Gottschalk's (1935) data on the coercive forces of magnetite grains are plotted against the $-\frac{3}{4}$ power of the mean grain diameter for comparison with the theoretical straight line. The agreement appears to be as good as the data will allow.

We may also examine the variation of H_c with T for grains of uniform size. We first examine the variation of W with R in terms of the constants of eqn. (20). Kittel (1949) calculated the energy of a 180° wall separating saturated domains to be proportional to $K^{1/2}$, K being the anisotropy energy. Since this calculation arises from a balance between exchange and anisotropy energies we can generalize Kittel's expression to take account of unsaturated domains, the energy of a wall being proportional to the square root of the product of anisotropy and exchange energies, the latter being proportional to I_s^2. Thus

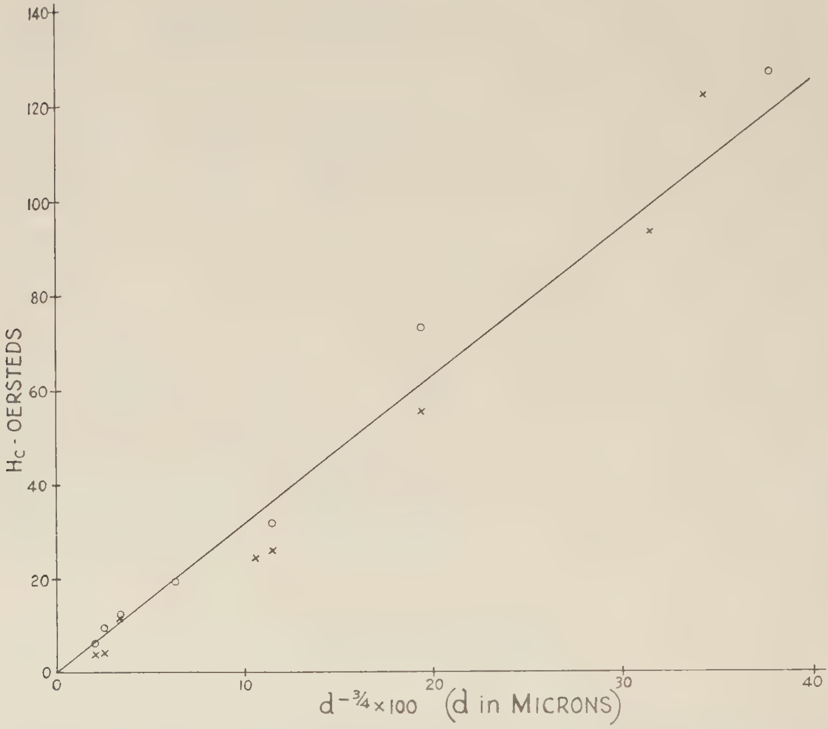

Coercive force, H_c, of magnetite grains as a function of mean grain diameter d. Gottschalk's (1935) data compared with theoretical straight line.
⨀ Natural magnetite. × Artificial magnetite.

$$B \propto K^{1/2} I_s, \quad . \quad . \quad . \quad . \quad . \quad . \quad . \quad . \quad . \quad (25)$$

the other factors in Kittel's (1949), eqn. (3.2.7) being independent of temperature. Bozorth (1951, p. 569) gives an empirical relation for the temperature-dependence of K, which he observed to give a good fit to the experimental data on nickel, the most intensively measured ferromagnetic:

$$K = K_0 \exp(-\alpha T^2), \quad . \quad . \quad . \quad . \quad . \quad . \quad (26)$$

K_0 and α being constants. If eqn. (26) is valid also for minerals then from eqns. (25) and (26) we have

$$B \propto I_s \exp[-(\alpha/2)T^2]. \quad \ldots \ldots \quad (27)$$

D in eqn. (20) only varies with T as the elastic modulus, which is assumed to be constant, but we have

$$\lambda_s \propto I_s^2 \quad \ldots \ldots \quad (28)$$

according to Döring (1936), so that inserting eqns. (27) and (28) into eqn. (20) we find

$$W \propto \lambda_s B^{-1/2} \propto I_s^{3/2} \exp[(\alpha/4)T^2]. \quad \ldots \ldots \quad (29)$$

The heights E of the potential barriers are proportional to I_s^2 (Stacey 1959) and $A^{1/2}$ (eqn. (23)) so that we may put

$$E = E_0 I_s^2 A^{1/2}$$

into eqn. (7) giving

$$H_c = \frac{E_0}{\omega} I_s A^{-1/2} - \frac{k}{\omega} \ln(C\tau) \,.\, T I_s^{-1} A^{-1}. \quad \ldots \ldots \quad (30)$$

Since the area of each domain wall is given by $A \propto W^{-1}$ and W is given by eqn. (29),

$$H_c = R I_s^{1/2} \exp[(\alpha/8)T^2] - S T I_s^{1/2} \exp[(\alpha/4)T^2],$$

where R and S are temperature-independent constants. We may also use the condition that at the blocking temperature T_B, $H_c = 0$ and $I_s = I_B$, to eliminate R:

$$H_c = S I_s^{1/2} \exp[(\alpha/8)T^2] \left\{ \left(\frac{I_s}{I_B}\right)^{5/4} T_B \exp[(\alpha/8)T_B^2] - T \exp[(\alpha/8)T^2] \right\}. \quad \ldots \quad (31)$$

At low temperatures the second term in eqn. (31) is negligible, so that H_c decreases more slowly with T than does $I_s^{7/4}$. This conflicts with observations by Akimoto (quoted by Nagata 1953, p. 47) who found a very sharp initial decrease with T in the coercive force of a magnetically hard rock. However a reliable check on eqn. (31) will require data on grains of uniform size, as in Gottschalk's (1935) experiments. It may also be necessary to take account of thermal history and the possibility of phase separations, as discussed in § 6.

§ 6. Discussion

In the experiments of Gottschalk (1935) the finer grains of magnetite were produced by crushing larger ones. That the dependence of H_c on grain size shows no discontinuity at the point where measurements were on crushed rather than the original grains indicates that whatever the potential barriers responsible for impeding domain wall movements are, they are not significantly altered by the process of crushing. This may have been due to the fact that the grains were initially in a fully work-hardened state, and that lower coercive forces might well have been observed had all the specimens been annealed before the measurements were made, or else that magnetite is so brittle that very little plastic deformation can occur and therefore no hardening is possible.

It is remarkable that the coercive forces of both the artificial and natural magnetite grains used by Gottschalk (1935) fit the same line in the figure so well. Unless they have by chance exactly the same impurity content it is apparent that in magnetite coercive force is not very dependent upon composition.

This question is related to a further difficulty in comparing theory with the observed temperature-dependence of the coercive force of a rock. The objection that potential barriers, effective at low temperatures are annealed out before the high temperature measurements are made is overcome if measurements are made first at the highest temperature. However, this still leaves the possibility that the number and character of the barriers is a reversible function of temperature, owing perhaps to a process of phase separation which is known to be common in natural magnetic minerals. (Kawai *et al.* 1956).

An important advantage of using coercive force as a characteristic of the magnetic properties of material is that its measurement follows saturation in a high field which has wiped out any memory of previous magnetic history at the same temperature. Thus all specimens are known to be in the same magnetic state. This is important in estimating the variation of coercive force with grain size as it is possible that when a grain is broken up into a number of smaller ones (as in Gottschalk's (1935) experiments) the parts preserve in metastable equilibrium some of the domain structure of the original. After saturation this is destroyed and when the grains are demagnetized they form their own domain structure. The problem of explaining the nucleation of domains anti-parallel to the direction of a saturated grain remains but this is not connected with coercive force. Kittel (1949) considered the problem of nucleation but his suggestions have been criticized (Néel 1955) as not conforming to observations. Possibly the potential barriers themselves act as centres for the nucleation.

The foregoing domain theory of small grains is based upon activation theory, which, it was shown in § 2, is not entirely understood. One of the difficulties is that we have no precise picture of the fluctuating magnetic field which is the manifestation of thermal agitation responsible for disturbing ferromagnetic domains. Therefore the properties of this field and its interaction with potential barriers remain reasonable assumptions rather than deductions, although the validity of eqn. (1) itself cannot be criticized on this ground (Stacey 1959). The success of spin-wave theory, particularly in explaining saturation magnetization at low temperatures (Dyson 1956), suggests that the fluctuating field is in fact spin waves. This would explain the directness of their interaction with domain walls, which are very similar to spin waves (Kittel 1949).

While particular attention has been given to the problem of magnetism in rocks the arguments in this paper may be applied with very little modification to a dispersed powder of any ferromagnetic material with a cubic crystal structure. In uniaxial crystals it is probable that magnetic anisotropy will be more important than magnetostrictive strain and therefore that the rod-type domain structure is less likely to form.

ACKNOWLEDGMENT

The author's understanding of the domain geometry used in this paper was greatly clarified by discussions with Dr. M. S. Paterson.

REFERENCES

BOZORTH, R. M., 1951, *Ferromagnetism* (New York: D. Van Nostrand Co. Inc.).
DÖRING, W., 1936, *Z. Phys.*, **103,** 560.
DYSON, F. J., 1956, *Phys. Rev.*, **102,** 1230.
GOTTSCHALK, V., 1935, *Physics*, **6,** 127.
KAWAI, N., KUME, S., and SASAJIMA, S., 1956, *Proc. imp. Acad. Japan*, **32,** 459.
KITTEL, C., 1948, *Phys. Rev.*, **73,** 810; 1949, *Rev. mod. Phys.*, **21,** 541.
KITTEL, C., and GALT, J. K., 1956, *Solid State Physics*, **3** (New York: Academic Press Inc.), p. 437.
NAGATA, T., 1953, *Rock Magnetism* (Tokyo: Maruzen Co. Ltd.).
NÉEL, L., 1955, *Advanc. Phys.*, **4,** 191.
RICE, S. O., 1944, *Bell Syst. tech. J.*, **23,** 282; 1945, *Ibid.*, **24,** 46.
SIXTUS, K. J., and TONKS, L., 1935, *Phys. Rev.*, **48,** 425.
STACEY, F. D., 1958, *Phil. Mag.*, **3,** 1391; 1959, *Proc. phys. Soc. Lond.*, **73,** 136.
STREET, R., and WOOLLEY, J. C., 1949, *Proc. phys. Soc. Lond.* A, **62,** 562; 1950, *Ibid.* B, **63,** 509.

Observations of Dislocations and Precipitates in Aluminium Alloys[†]

By G. THOMAS
Metallurgy Department, Cambridge University

[Received November 29, 1958]

ABSTRACT

Electron transmission micrographs of quenched aluminium alloys show that the specimens contain many complex dislocations and large dislocation loops with diameters up to 2000 Å. These dislocations could not be moved by heating the foils in the electron beam and their immobility is thought to be due to substitutional atmospheres of solute atoms which form at, and lock, the dislocations by vacancy-aided diffusion. This has been confirmed by ageing the foils, which causes precipitation to occur on the dislocations. These precipitates also lock the dislocations by a pinning action because stresses of the order of $\mu/50$ are required to free the dislocations. The observations are discussed in relation to the hardening effect of quenching and of precipitation after ageing.

The movement of glissile dislocations in quenched alloys is typical of a material of high stacking fault energy, i.e. there are no partial dislocations and cross slip is frequently observed.

§ 1. INTRODUCTION

HIRSCH *et al.* (1956), Whelan *et al.* (1957), Bollmann (1956), and Tomlinson (1958) have shown that dislocations are revealed in thin metal foils by contrast effects resulting from the Bragg diffraction mechanism. Hirsch *et al.* (1958) have also shown that dislocation loops are formed in quenched metals as a result of the collapse of discs of vacancies and that there are fewer loops near grain boundaries and dislocation lines. This has been interpreted by supposing that grain boundaries and dislocation lines act as sinks for vacancies. Westwood and Broom (1957) have associated strain–ageing in aluminium–magnesium alloys with the migration of magnesium atoms aided by vacancies produced during prior strain. Since both magnesium and zinc are mobile in aluminium, then, if vacancies migrate to sinks, these sinks should become sites for precipitation in alloys of these metals, because the solute atoms should also move with the vacancies. Electron microscope experiments were therefore carried out in the present work in an attempt to observe precipitates at grain boundaries and dislocations in quenched and aged alloys. The alloys used were based on the ternary aluminium–zinc–magnesium system, the ageing characteristics of which are now known in detail (Thomas and Nutting 1959).

[†] Communicated by the Author.

§ 2. EXPERIMENTAL

The alloys examined were high purity ternary aluminium—7·5%, zinc—2·5% magnesium and a quaternary alloy containing 0·5% copper in addition to magnesium and zinc. These were supplied in sheets by James Booth and Co. Ltd., and after annealing were rolled to 0·1 mm section. These were then heat treated, i.e. quenched or quenched and aged. Thin metal foils were prepared from quenched alloys by electropolishing at 0°c in ethyl alcohol–perchloric acid (4 : 1) at 14 volts and 0·4 amps and from aged alloys by a technique previously described by Nicholson *et al.* (1958). The foils were examined in a Siemens and Halske Elmiskop 1 electron microscope operating at 80 kv. Electron micrographs were taken at instrumental magnifications of 20 000–80 000 working with a fine focus beam of high intensity.

The normal procedure for solution heat-treatment of the alloy consisted of 4 hours at 470°c followed by water quenching. Some specimens were more severely treated by heating just below the solidus temperature (550°c) and then quenching directly from the furnace into iced brine. Ageing was done in oil baths at 120°c and 160°c.

§ 3. RESULTS AND DISCUSSION

3.1. *Quenched Alloys*

Figures 1 and 2† are micrographs obtained from foils quenched into iced brine. They show contrast effects in the form of loops 100–2000 Å diameter and complex lines. These contrast effects are changed when the specimen is tilted in the electron beam and dark field experiments prove conclusively that the contrast results from Bragg diffraction, as expected from dislocation lines. The dislocation loops A are much larger than the loops observed in quenched aluminium (Hirsch *et al.* 1958). They are also fewer in number and do not have regular crystallographic forms. In copper-bearing alloys the dislocations sometimes occur as spirals or helices, as shown in fig. 3. The mechanism of formation of large dislocation loops and spirals is not known but one possibility is that vacancies condensing on screw dislocations can cause the dislocations to adopt cork-screw forms (Cottrell 1957). More experiments are being carried out to investigate the origin of these quenching defects more thoroughly.

Small dislocation loops about 200 Å diameter have been found only in a few areas of quenched foils. These correspond more closely to the loops found in pure aluminium by Hirsch *et al.* (1958), and are alway seen in regions away from grain boundaries and dislocation lines, so that it is probable that they are formed as a result of the collapse of vacancy discs. An example is shown in fig. 4. In this micrograph the average number of loops is about 10^{11} cm^{-3}; assuming the loops to be collapsed discs of vacancies the corresponding concentration of vacancies is about 10^{-6}. However, since areas of the type shown in fig. 4 are not often observed, only a small fraction of the available vacancies condense to loops. Presumably, most of the vacancies collect at dislocations and grain boundaries. No stacking faults have been observed in quenched foils so that the loops must be whole dislocations.

---

† All figures are shown as plates.

The dislocation lines in quenched foils are complex in form, as shown at C in figs. 1 and 2. It is probable that the networks C form as a result of the intersection of large loops and dislocation lines. The misorientation across foils containing such network has been calculated from the splitting of the Kikuchi lines obtained on diffraction patterns and is about 0·1 deg.

No precipitates have been observed in quenched foils.

3.2. *Movement of Dislocations*

Dislocations can be made to move in foils if the intensity of the electron beam is increased. In quenched alloys, an area has to be heated for 20–30 min before dislocations are seen to move. This movement usually begins near the edges of the foil, e.g. fig. 5, or at grain boundaries. Dislocations of the type shown in figs. 1–4 are locked too firmly to be moved by the stresses induced in the foil by heating. The dislocations behave as expected in metals of high stacking fault energy, i.e. no partials or stacking faults are seen and cross-slip frequently occurs as shown in fig. 6. In this micrograph the dislocations A may be acting as obstacles which cause cross slip at BB.

Figure 7 shows long dislocations in a foil of [112] orientation. These lie in the $[1\bar{1}0]$ directions and the segments at A, in the $[\bar{1}01]$ directions are glissile in $[1\bar{1}0]$. Annihilation of one of these segments may be occurring at B.

3.3. *Ageing of Quenched Foils*

Ageing for one week at room temperature does not produce precipitation in the alloy and dislocation loops and networks remain visible, as shown in fig. 8. The micrographs obtained after this ageing treatment are similar to those obtained in quenched foils. If however the ageing temperature is raised precipitates are observed in the matrix, on the dislocations and at grain boundaries. The precipitates in the latter sites are always larger than elsewhere in the matrix, indicating a higher rate of diffusion in these regions. Figure 9 shows precipitates lying at a low angle grain boundary at B, and on large dislocation loops at A. The precipitates in the matrix are spherical G.P. zones rich in magnesium and zinc atoms and about 50 Å diameter, whilst those in the dislocations are about 150 Å in diameter. The G.P. zones are more clearly seen in fig. 10 at B, and precipitates are also visible on the large loops at A. The dislocations at C may be spirals.

When ageing is prolonged, precipitates are observed at networks of dislocations, e.g. fig. 11, in which an extended hexagonal network can be seen near a grain boundary. The points A indicate dislocation nodes. Precipitation at the grain boundaries and on dislocations, with depletion of solute in adjacent regions, is shown in fig. 12. The precipitates visible in this micrograph are of the intermediate $MgZn_2$ phase which forms along $\{111\}$ matrix planes.

It is not possible to move dislocations in foils aged into the maximum hardening range (1–2 days at 120°c, 1–20 hours at 160°c). The fully hardened state in these alloys is that with the densest distribution of precipitates in the matrix, at a separation of about 100Å (Thomas and Nutting 1959). Since these precipitates do not show any strain contours such as those found in aluminium–copper alloys (Nicholson and Nutting 1958) there can be no long-range elastic strains associated with precipitation. We can estimate the stresses required to move dislocations through foils containing such precipitates. Dislocations can either loop around precipitates or cut through them. The stress required to loop dislocations is given by

$$\sigma_1 = \frac{\mu \mathbf{b}}{l}$$

where μ is the shear modulus, $\mathbf{b}$ the Burgers vector of the dislocation and l the separation between precipitates. Taking μ as $2{\cdot}5 \times 10^{11}$ dyne/cm^2 and $\mathbf{b}$ as $2{\cdot}8 \times 10^{-8}$ cm, then, for a particle separation of $l = 10^{-6}$ cm, the stress σ_1 is $\mu/50$ or 70 kg/mm^2. Kelly and Fine (1957) have concluded that the stress required to shear dislocations through precipitates is given by

$$\sigma_2 = \frac{\Delta E n^{1/3}}{\mathbf{b}^2 l}$$

where ΔE is the energy difference between a solute atom in the matrix and one in the precipitate, and n the number of atoms in the precipitate. ΔE can be calculated from the heat of reversion of the alloy, e.g. for copper and silver in aluminium ΔE is 0·077 ev/atom and 0·047 ev/atom respectively. Unfortunately ΔE is not known for aluminium–zinc–magnesium alloys, but if a value of 0·04 ev/atom is assumed for ΔE then in alloys where the precipitate diameter is 100Å and l is 10^{-6} cm, σ_2 is 20 kg/mm^2. The observed shear yield strengths of the alloys approach 19 kg/mm^2 which is consistent with the estimated value of σ_2. We thus expect that dislocations will cut through precipitates rather than loop around them. Whelan *et al.* (1957) have estimated that the stress induced in foils by heating them in the electron beam is about $\mu/1000$. This explains why it has not been possible to observe the movement of dislocations in aged alloys, where stresses of up to $\mu/50$ are required.

Dislocation lines containing precipitates are also stable when foils are heated in the electron beam. The explanation is again that insufficient stresses to cause movement can be induced by this method. In fig. 13 precipitates are spaced about 100Å along the dislocation lines. For the dislocations to move, they must bow out between their pinning precipitates, which necessitates a stress of $\mu\mathbf{b}/l$. Taking $\mu = 2{\cdot}5 \times 10^{11}$ dyne/cm^2, $\mathbf{b} = 2{\cdot}8 \times 10^{-8}$ cm and $l = 10^{-6}$ cm, this stress is again $\mu/50$ or 70 kg/mm^2. This means that dislocations are effectively locked by precipitates along them.

3.4. *The Mechanism of Precipitation on Dislocations*

The evidence obtained by examining a large number of micrographs is that

(*a*) dislocation loops are not observed near dislocation lines and grain boundaries,

(*b*) precipitates formed on dislocations and grain boundaries are much larger than those formed in the matrix,

(*c*) there is a depletion of solute in regions next to precipitates on dislocations and grain boundaries.

These observations indicate that both vacancies and solute atoms diffuse to dislocations and grain boundaries during quenching from the solution temperature, so producing excess concentrations at these places. Some remaining vacancies aggregate and collapse in discs to form small dislocation loops. The diffusion of solute atoms to the sinks will be assisted by the diffusion of vacancies, and since both magnesium and zinc are very mobile in aluminium it is reasonable to suppose that there will be a high concentration of these elements in the sinks prior to ageing. Similarly, solute atoms will be concentrated in the dislocation loops. It is probable that the core of a dislocation will then consist almost entirely of solute atoms which form as a 'substantial atmosphere' thereby reducing the elastic energy of the dislocation.

From the complex nature of the dislocations it is reasonable to suppose they contain many jogs, e.g. as a result of climb or by interaction with other dislocations. These jogs could be the nucleating sites for precipitation and once precipitates form they can grow by atoms migrating along the core of the dislocation. Because of the high vacancy flux near the dislocations and grain boundaries, precipitates formed at these places can grow to a larger size than those in the matrix. Finally, the dislocation will be freed of solute atoms except where it is pinned by precipitates. Even in this condition dislocations are effectively locked, because, as shown in § 3.3, stresses of the order of $\mu/50$ are required to free them completely.

The fact that precipitates also form on the dislocation loops suggests that solute atoms accompany the vacancies even when they collapse and form loops. This accounts for the stability of the loops both to deformation and to ageing.

3.5. *Hardening in Quenched Alloys*

Hirsch *et al.* (1958) have discussed the factors contributing to quench hardening in pure aluminium. They have drawn attention to the possibilities of forming Frank–Read sources of short length by the intersection of large loops as predicted by Kuhlmann-Wilsdorf (1958) and of the difficulties of moving 'joggy' dislocations (Cottrell 1957). In alloys there is the additional hardening effect of solute atoms which can pin the defects. Also, before dislocations can move and interact with precipitates in these alloys they must be freed from their own precipitates and large stresses are required to do this. All these effects account for the very high yield strengths of aluminium–zinc–magnesium type alloys.

ACKNOWLEDGMENTS

My thanks are due to Professor A. H. Cottrell, F.R.S., and Dr. J. Nutting for their continued interest and encouragement. I am also indebted to them and to Dr. J. M. Whelan and Dr. P. B. Hirsch for valuable discussions and suggestions.

REFERENCES

BOLLMANN, W., 1956, *Phys. Rev.*, **103**, 1588.
COTTRELL, A. H., 1957, *Monogr. Ser. Inst. Metals*, No. 23, p. 1.
HIRSCH, P. B., HORNE, R. W., and WHELAN, M. J., 1956, *Phil. Mag.*, **1**, 677.
HIRSCH, P. B., SILCOX, J., SMALLMAN, R. E., and WESTMACOTT, K. H., 1958, *Phil. Mag.*, **3**, 897.
KELLY, A., and FINE, M. E., 1957, *Acta Met.*, **5**, 365.
KUHLMANN–WILSDORF, D., 1958, *Phil. Mag.*, **3**, 125.
NICHOLSON, R. B., THOMAS, G., and NUTTING, J., 1958, *Brit. J. appl. Phys.*, **9**, 25.
NICHOLSON, R. B., and NUTTING, J., 1958, *Phil. Mag.*, **3**, 531.
THOMAS, G., and NUTTING, J., 1959 (to be published).
TOMLINSON, H., 1958, *Phil. Mag.*, **3**, 867.
WESTWOOD, A. R. C., and BROOM, T., 1957, *Acta Met.*, **5**, 77, 249.
WHELAN, M. J., HIRSCH, P. B., HORNE, R. W., and BOLLMANN, W., 1957, *Proc. roy. Soc.* A, **240**, 524.

The Resistance Minimum in Dilute Alloys of Tin in Copper†

By W. B. PEARSON, D. M. RIMEK and I. M. TEMPLETON
Division of Pure Physics, National Research Council, Ottawa, Canada

[Received December 12, 1958]

ABSTRACT

Previous experimental work on the resistance minimum caused by tin in dilute solid solution in polycrystalline copper led to the expectation that there might be no minimum in similar alloys which were single crystals. We find that this is the case and that the minimum can be produced by making the monocrystalline alloys polycrystalline. It is suggested that the resistance minimum occurs as a result of segregation of the tin atoms on the grain boundaries of the polycrystalline alloys. For dilute alloys of iron in copper there was, as expected, practically no difference in the resistance minimum observed in polycrystalline and in monocrystalline alloys.

§ 1. INTRODUCTION

EXPERIMENTS made several years ago (MacDonald and Pearson 1955 a, b) established that the presence of certain specific chemical impurities in dilute solid solution in polycrystalline samples of copper gave rise to a minimum in the electrical resistivity at low temperatures. Thus for instance Mn, Fe and Co and the B group solutes Ga, In, Si, Ge, Sn, Pb and Bi produced such a resistance minimum. It was subsequently shown (White 1955, Dugdale and MacDonald 1957) that at the lowest temperatures (1°K and below) the resistivity of dilute Cu–Fe and Cu–Sn alloys flattens off and ultimately becomes independent of temperature, in contrast to the behaviour of Mn in copper found by Gerritsen and Linde (1952) which causes the resistivity to rise from the minimum to a maximum and then to decline again at the lowest temperatures.

It was also established (MacDonald and Pearson 1955 a, b, Pearson 1955 a, b) that the form of the resistance minimum and the accompanying variation of absolute thermoelectric power engendered by the transition metal iron, was fundamentally different from that caused by the B group solutes Ga, In, Ge and Sn (explicitly excluding B group solutes Pb and Bi). The nature of this difference is illustrated in fig. 1 taken from Pearson 1955 a. Notably the relative (or percentage) size of the resistance minimum caused by the four B group solutes rises to a maximum value in very dilute solid solutions (about 0·005 at. % solute) and then declines sharply, showing a cusp in the curve of relative size of minimum versus alloy

---

† Communicated by the Authors.

Fig. 1

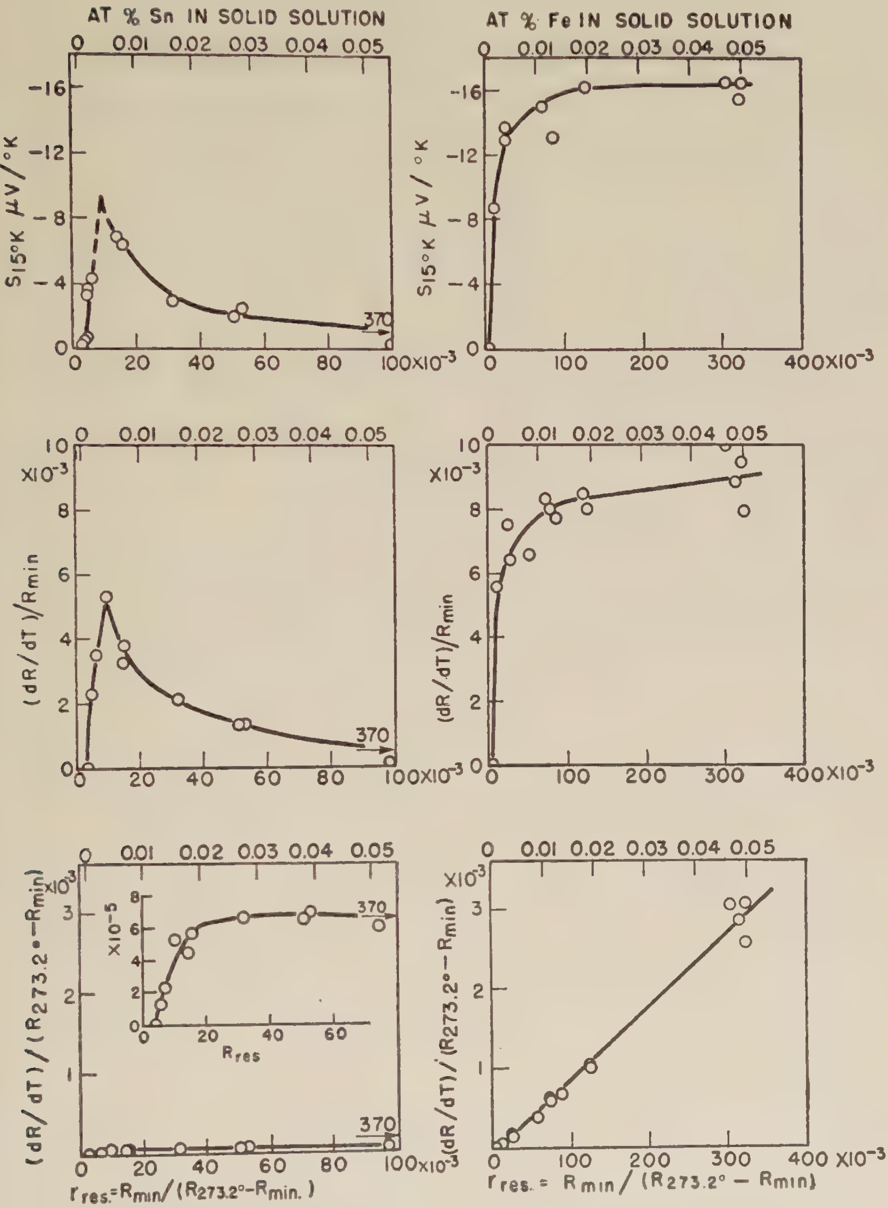

Comparison of the behaviour of dilute Cu–Sn and Cu–Fe alloys. (After Pearson 1955 a.)

Top: Variation of absolute thermoelectric power at 15°K with composition or residual resistance ratio $R_{\mathrm{min}}/(R_{273\cdot 2°\mathrm{K}} - R_{\mathrm{min}})$.

Middle: Variation of a measure of the relative size of the resistance minimum with composition.

Bottom: Variation of a measure of the absolute size of the resistance minimum with composition.

composition or residual resistivity. The absolute size[†] of the resistance minimum (in ohm cm) increases to a maximum value at a slightly higher solute concentration and then remains constant in more concentrated alloys. In contrast the relative size of resistance minimum caused by *iron* shows no 'cusp-like' behaviour as a function of composition and the absolute size of the minimum continues to rise with solute concentration in the range of solid solution up to at least 0·05 at. % Fe.

Furthermore the temperature at which the resistance minimum occurs increases to an upper limit of about 14°K in alloys of these B group solutes, whereas in alloys of iron the temperature of the minimum continues to increase reaching the remarkably high value of 27°K in an alloy containing 0·05 at. % Fe.

The behaviour of the absolute thermoelectric power of the alloys at 15°K[‡] is also markedly different as a function of composition; for the B group solutes Ga, In, Ge and Sn, $S_{15^\circ K}$ shows with concentration a cusp-like behaviour similar to that of the relative size of the resistance minimum, whereas that of iron does not (fig. 1).

The correspondence of the relative size of the resistive anomaly and the thermoelectric power at 15°K caused by the four B group solutes is demonstrated in fig. 2 where $S_{15^\circ K}$ is plotted against the relative size of the resistance minimum, and a straight line results.

It was noted by MacDonald and Pearson (1955 a) that in mechanical measurements made by Smart and Smith (1943) on very pure dilute Cu–Sn alloys, an anomaly also appeared at a solute concentration close to that of the maximum effect in the electrical anomalies (fig. 3). Thus the rate of change of the softening temperature (an arbitrary parameter describing the softening after certain cold-work) passes through a cusp at a concentration of some 0·0015 at. % solute. It was suggested that this fairly close correspondence of mechanical and electrical anomalies as a function of solute concentration, together with the saturation effects observed at higher concentrations, must be caused by some particular distribution of solute atoms in the solvent. That is to say, that the solute atoms achieve a lower free energy (the net reduction in energy more than compensating for the entropy increase of random solution) by going to particular favourable sites in the polycrystalline material, these sites being limited in number (Pearson 1954).

Since the solute and solvent atoms are of different size it was assumed that they took up positions in the interstices of misfit along the grain

---

[†] Various parameters may be adopted to describe the relative or absolute size of the resistance minimum, but they lead to similar results. The two parameters which we have used most frequently are: (1) the increase of resistivity between $T_{\min}$ and 4·2°K, or (2) the rate of change of resistivity (ohm cm/deg K) at temperatures below $T_{\min}$ where the resistivity is rising approximately linearly with decreasing temperature.

[‡] The value of the absolute thermoelectric power at 15°K is a suitable parameter to adopt for purposes of comparison, since in dilute alloys S is approximately temperature-independent in this region.

Fig. 2

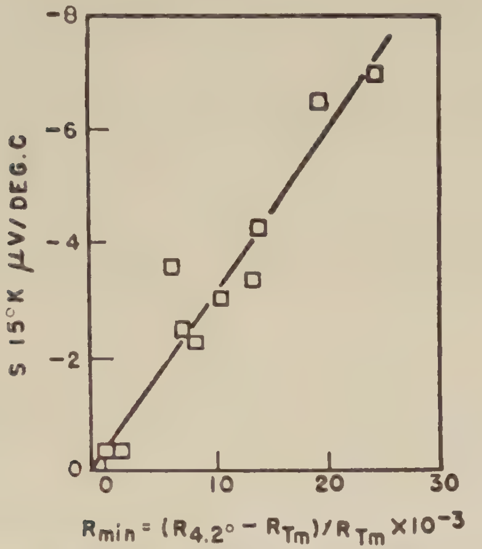

Plot of a measure of the relative size of the resistance minimum against the absolute thermoelectric power at 15°K for dilute Cu–Sn alloys. (This is virtually a plot of the data shown in fig. 1 top left and middle left diagrams, eliminating the common parameter of composition from each.) (After MacDonald and Pearson 1955 b.)

Fig. 3

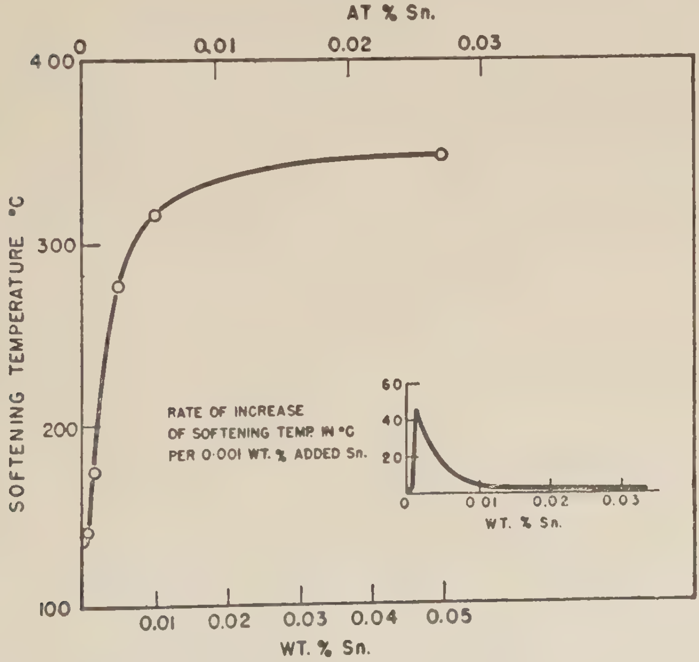

Variation of ‘ softening temperature ’ with composition in dilute Cu–Sn alloys (after Smart and Smith 1943).

boundaries, particularly as the expected number of such positions bears a reasonable relationship to the concentration of solute at which the size of the resistance minimum saturates. Such a preferential distribution of solute atoms might then somehow be responsible for the occurrence of the resistance minimum and for the saturation with increasing solute concentration in its magnitude. While no attempt was made then to suggest a *mechanism* of the phenomenon, it was at least qualitatively easier to understand how the tin atoms in close proximity to one another might give rise to the resistance minimum, as compared with a separation from each other by some 25 atomic diameters when in overall random solid solution. However, in the case of iron as solute, it was believed from the experimental evidence that the resistance minimum arose from other effects perhaps involving the *d* electrons, and that these effects were relatively large, so swamping any influence of grain boundary segregation.

Blewitt *et al.* (1954), from measurements on very pure single crystals which showed no resistance minimum until *after* they were rendered polycrystalline by straining and annealing, attributed the occurrence of the resistance minimum to the presence of *grain boundaries alone.* This argument was criticized by Cohen and Barrett (1954) on the issue of the grain boundary pressures that would result from the electron scattering. Principally, however, the interpretation of Blewitt *et al.* is refuted by the experimental fact that polycrystalline samples of pure copper can be obtained which show no sign of a resistance minimum.

The logical inference from our interpretation that the presence of B group solutes Ga, In, Ge and Sn at the grain boundaries is a necessary condition for them to give a resistance minimum, is then that *no* resistance minimum should be observed in annealed single crystals of copper containing small amounts of these solutes in solid solution. On the other hand, similar single crystals of Cu containing *iron* in solid solution should show a resistance minimum not greatly different from that of the polycrystalline materials.

We have now carried out such measurements on appropriate single crystals in order to test our earlier conclusions.

§ 2. Experimental Methods

Two series of single crystals of copper were grown by the Bridgman technique using graphite moulds. The initial copper of high purity was supplied by the American Smelting and Refining Co. Ltd. One series of crystals contained iron in concentrations from 0·0025 to 0·02 at. % Fe. The other contained tin in concentrations from 0·0025 to 0·1 at. % Sn. All crystals examined had continuous crystalline paths down their lengths. Occasionally in the more concentrated alloys there were additional grains appearing on the *sides* of the rods. The development in our laboratory of new techniques for measuring very small potentials at low temperatures (Templeton 1955) has enabled us to measure very much thicker monocrystalline rods of copper than was possible at the time of our earlier work and it is largely this factor which has made this investigation possible. The actual presence of the intended solute in the single crystals was checked by spectroscopic analysis.

In carrying out the experiments described in the next section the consequences of contamination of the specimens by iron are very severe, since about 0·002 at. % Fe can give effects as large as those found in tin alloys. About 1 mm depth was therefore etched off the surface of the crystals between each annealing operation in order to guard against the possibility of this contamination.

§ 3. Experimental Findings

The behaviour of the monocrystalline specimens of copper containing iron in dilute solid solution was, as expected, very similar to that of the polycrystalline samples which we had examined previously. This is illustrated in figs. 4 and 5 which show the relative size of the resistance minimum and the temperature of the minimum as a function of solute

Fig. 4

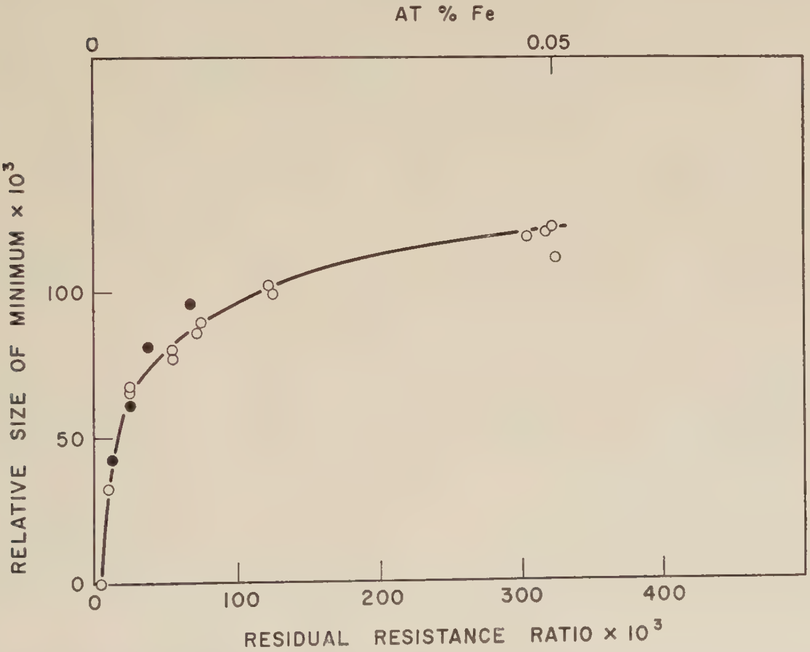

A measure of the relative size of the resistance minimum in dilute Cu–Fe alloys plotted against the residual resistance ratio or composition.

○ Data from polycrystalline alloys.
● Data from monocrystalline alloys.

Fig. 5

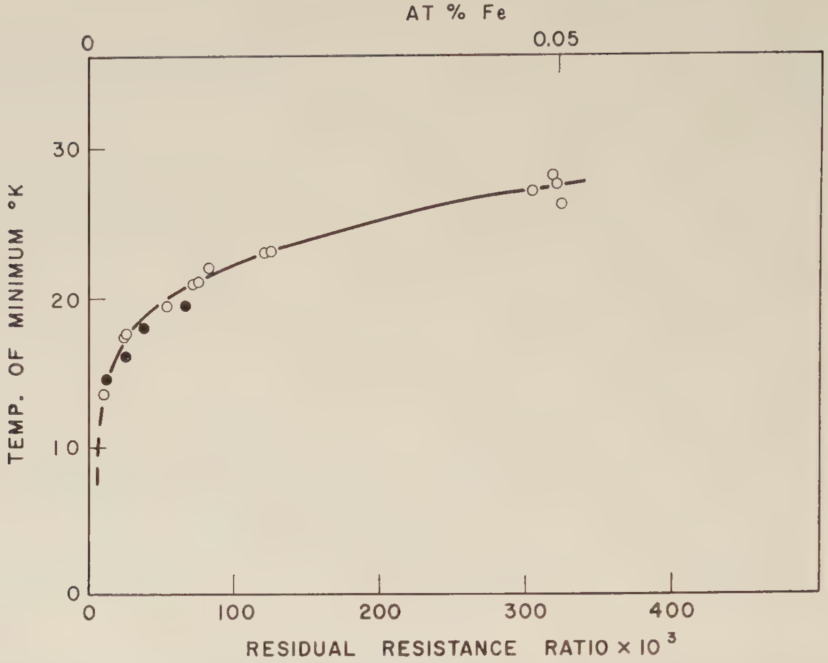

Temperature of the resistance minimum plotted against residual resistance ratio or composition of dilute Cu–Fe alloys.

○ Data from polycrystalline alloys.
● Data from monocrystalline alloys.

Fig. 6

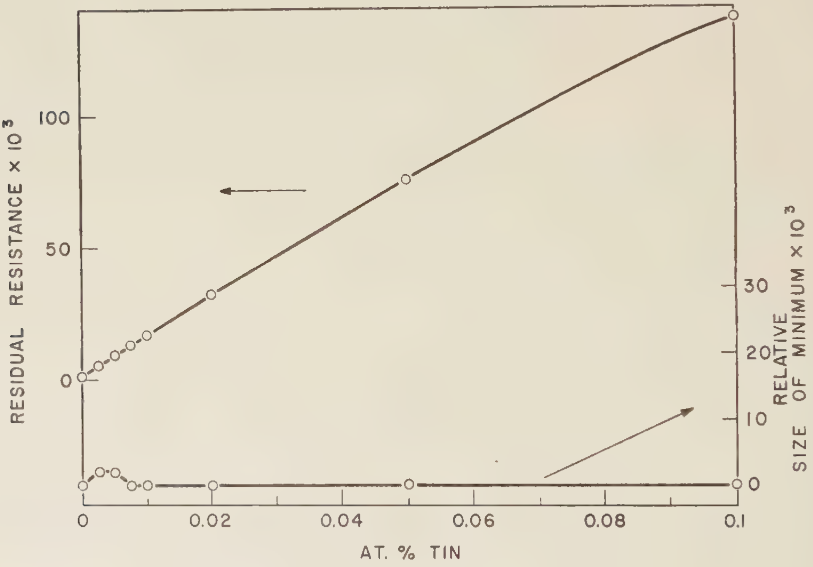

Data from singlycrystalline Cu–Sn alloys.

Top: Residual resistance ratio, $R_{\mathrm{min}}/(R_{273\cdot 2^{\circ}\mathrm{K}}-R_{\mathrm{min}})$, plotted against the composition of the alloys.

Bottom: A measure of the relative size of the resistance minimum $(R_{4\cdot 2^{\circ}\mathrm{K}}-R_{\mathrm{min}})/R_{\mathrm{min}}$, plotted against the composition of the alloys.

concentration or residual resistivity of the alloys. This was, however, by no means the case for the single crystals of copper containing tin in solid solution. As shown in fig. 6, there was only a slight suggestion of a minimum in the most dilute alloys in the concentration range corresponding to the cusp in the curve of percentage size of minimum versus composition for polycrystalline alloys (fig. 1), and the size of the resistance increase was no bigger than the experimental error in the measurements of these samples†. Figure 6 therefore suggests strongly that the resistance minimum does not occur in single crystals of copper containing tin in solid solution. That the crystals did indeed contain tin was confirmed by spectroscopic analysis, and that it entered into solid solution in a uniform manner is shown also in fig. 6 where the residual resistivity of the crystals is plotted as a function of the intended tin content. The scattering cross section for tin obtained from these experiments is in sensible agreement with that obtained in our previous work on polycrystalline alloys.

Copper + 0·0075 at. % Tin

Treatment	Residual resistance ratio $\times 10^3$	Size of minimum	
		Relative $\times 10^3$	Absolute $\times 10^4$
(*a*) Single crystal ann. 500°C	13·8	0	0
(*b*) Cold-worked ann. 500°C	13·9	3·5	0·5
(*c*) Cold-worked ann. 1055°C	21·1	34	6·9
(*d*) Ann. 500°C	14·9	38	5·5
Polycrystal (from previous work)	13·5	30	3

Our hypothesis leads us to expect that if these single crystals were strained and annealed to make them polycrystalline, they should show a resistance minimum of about the same size as had been observed previously for polycrystalline specimens. The results of a series of such experiments on the alloy containing 0·0075 at. % Sn—located near the cusp of fig. 1—are summarized in the table. On straining and annealing for a few hours at 500°C we do not expect that all the tin could reach the grain boundaries which are formed, since a 'random-walk' calculation using the known diffusion constant of tin in copper (Rhines and Mehl 1938), and neglecting the unknown driving force towards grain boundaries suggests that it would take about 30 days annealing at 500°C for all of the tin atoms to reach the grain boundaries if the grain diameter were 0·01 mm. After the actual annealing time of 14 hrs it is reasonable to suppose that up to some 20% of the tin atoms might be at the grain boundaries. This agrees with the observation that a resistance minimum was found after straining and annealing at 500°C, but that its relative size was only about $3{\cdot}5 \times 10^{-3}$ (see table, step (*b*)). When the crystals were re-strained and annealed at 1055°C, all of the tin atoms should have had ample time to reach the boundaries of the larger grains and the observed relative size of the resistance minimum of 34×10^{-3} (see table, step (*c*)) corresponds very well to what might be expected for a polycrystalline alloy containing this amount of tin. However, it is noted that by this heat treatment the residual resistance ratio has also been increased from 14×10^{-3} to 21×10^{-3}, so that it is not certain from this experiment alone that chemical contamination of a specimen has not occurred. This increase of residual resistivity of specimens after annealing at high temperatures is a feature which we have observed generally. It may be due to the presence of physical defects remaining on cooling the alloy (cf. the experiments of Bauerle *et al.* (1956) on gold). If chemical contamination of the alloy has not occurred on annealing at 1055°C, then (1) the residual resistivity should return to its original value and (2) the resistance minimum should not decrease in absolute size, if the specimen is re-annealed at 500°C without further straining. That this is indeed the case is shown in the table, step (*d*), from which it can be concluded that appreciable chemical contamination of the alloy did not occur when it was annealed at 1055°C. The resistance minimum has thus been produced by making the monocrystalline specimen polycrystalline and annealing at such a temperature that the tin atoms could migrate to the grain boundaries—or possibly to other physical defects.

---

† It should also be emphasized that the actual size of the effect which is possibly observed here is small compared to the size of the resistance minimum that can be obtained in polycrystalline alloys of Sn in copper of the same solute concentration.

One further test was carried out on several specimens. If after step (*d*) in the table the specimens were again strained and annealed for 14 hrs at 500°C, new grain boundaries would be formed and as in step (*b*) the tin would not all be able to migrate to the grain boundaries because of the low temperature of the anneal. Such a treatment should therefore lead to a reduction in the size of the resistance minimum and this was found to be the case. Similar straining and annealing experiments carried out on single crystals of other compositions gave results in general agreement with those described in detail above, and in agreement with the established relationship between size of resistance minimum and composition in polycrystalline Cu–Sn alloys.

§ 4. Conclusion

Correlation between the mechanical properties and electrical resistivity and thermoelectric anomalies in dilute solid solutions of the B group metals Ga, In, Ge and Sn in polycrystalline copper led us to suggest that it might be the presence of these impurity atoms *at the grain boundaries* which caused the resistance minimum. This now appears to be rather probable since a series of single crystals of copper containing tin showed practically no resistance minimum in the range of composition in which the minimum is found in polycrystalline material. The minimum was, however, produced in these same crystals by making them polycrystalline and annealing them for a sufficient time to allow migration of the solute to the grain boundaries. No detailed mechanism has yet been suggested for an anomalous electron scattering process, capable of causing a resistance minimum at low temperatures, due specifically to the segregation of tin atoms on grain boundaries.

Little difference was found in the behaviour of the resistivity-temperature dependence of dilute monocrystalline and polycrystalline alloys of copper containing iron.

Acknowledgments

We wish to thank Dr. D. K. C. MacDonald and Dr. T. H. K. Barron for valuable discussions of this work.

References

Bauerle, J. E., Klabunde, C. E., and Koehler, J. S., 1956, *Phys. Rev.*, **102,** 1182.
Blewitt, J. H., Coltman, R. R., and Redman, J. K., 1954, *Phys. Rev.*, **93,** 891.
Cohen, M. H., and Barrett, C. S., 1954, *Phys. Rev.*, **95,** 1094.
Dugdale, J. S., and MacDonald, D. K. C., 1957, *Canad. J. Phys.*, **35,** 271.
Gerritsen, A. N., and Linde, J. O., 1952, *Physica*, **18,** 877.
MacDonald, D. K. C., and Pearson, W. B., 1955 a, *Acta Met.*, **3,** 392; 1955 b, *Ibid.*, **3,** 403.
Pearson, W. B., 1954, *Phil. Mag.*, **45,** 1087; 1955 a, *Ibid.*, **46,** 911; 1955 b, *Ibid.*, **46,** 920.
Rhines, F. N., and Mehl, R. F., 1938, *Trans. Amer. Inst. min. (metall.) Engrs*, **128,** 185.
Smart, J. S., and Smith, A. A., 1943, *Trans. Amer. Inst. min. (metall.) Engrs*, **152,** 103.
Templeton, I. M., 1955, *J. sci. Instrum.*, **32,** 314.
White, G. K., 1955, *Canad. J. Phys.*, **33,** 119.

Experiments on the Resistance Minimum
The Effects of Certain Solutes in Copper, Silver and Gold†

By W. B. PEARSON
Division of Pure Physics, National Research Council, Ottawa, Canada

[Received December 8, 1958]

ABSTRACT

In an attempt to increase the knowledge of what chemical impurity atoms give rise to a resistance minimum in copper, silver and gold as solvents, we have examined dilute polycrystalline solid solutions of Ni, Cu, and Sn in Au, Sn in Ag, and Mg in Cu, which were of some interest. It appears that none of these particular solutes causes a resistance minimum in the solvents specified. This finding is discussed in relation to previous work.

§ 1. INTRODUCTION

ALTHOUGH no satisfactory *comprehensive* theory exists for the occurrence of the minimum in the resistance of certain metals at low temperatures (which was first observed by de Hass *et al.* 1933), it has been established experimentally that it can be specifically caused by the presence of certain metals in solid solution. The effectiveness of certain B group solutes in causing a resistance minimum‡ in copper (MacDonald 1952, MacDonald and Pearson 1955 a, b) is a particularly puzzling feature which is unlikely to be understood until more detailed experimental information has been accumulated.

This note briefly describes the results of experiments which examine three topics: (1) Experiments by MacDonald and Templeton (1951) on gold alloys containing small quantities of dissolved copper and nickel, indicated that these metals each caused a resistance minimum in gold (fig. 1). As it seems on the whole improbable that the homovalent impurity copper, in particular, would give rise to a resistance minimum, these alloys

---

† Communicated by the Author.

‡ We should perhaps define the term 'resistance minimum' as it is used in the present paper and in previous papers by the author. In solvents such as Cu. Ag, Au and Mg, it refers to a minimum in the resistivity which occurs at some temperature above 4·2°K. It does not refer to a rise of resistance which may be found below 2°K (cf. Mendoza and Thomas 1951), although the one may pass into the other. Solutes to which we have specifically attributed the property of causing a resistance minimum in a given solvent generally cause a minimum of three or more per cent of the residual resistivity at some concentration in the alloy range. If minima are observed whose size is always randomly below 0·5% in a series of dilute alloys of increasing concentration, then it is quite likely that it is caused by very small concentrations of an unintended impurity rather than by the solute specifically introduced.

have been re-examined. (2) Pearson *et al.* (1959) have reported that tin causes a resistance minimum in dilute polycrystalline alloys of copper but not in single crystals, and have attributed this behaviour to segregation of the tin atoms to the grain boundaries in the very dilute polycrystalline alloys. It is therefore interesting to know whether tin causes a resistance minimum in polycrystalline silver and gold alloys since the radius ratio $r_{\text{solute}}/r_{\text{solvent}}$ is appreciably smaller in the silver and gold alloys.

Fig. 1

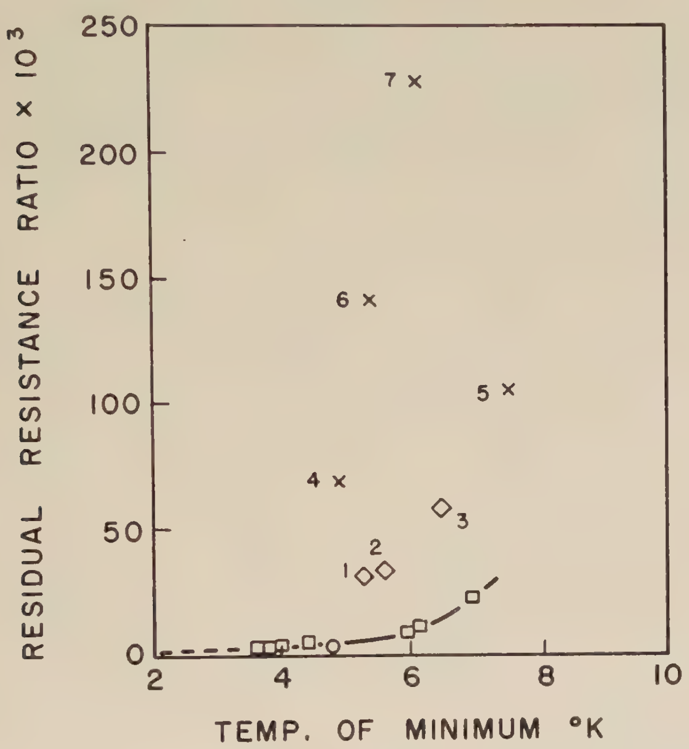

Temperature of resistance minimum of gold and its alloys plotted against the residual resistance ratio, $R_{\text{min}}/R_{273\cdot2^\circ\text{K}}$. (After MacDonald and Templeton 1951.)

□ Data of de Haas and v.d. Berg for gold.
○ Data of MacDonald and Templeton for ‘ spec pure ’ gold.
◇ Data of MacDonald and Templeton for a gold–copper alloy containing 0·05% Cu.

1. Annealed at ~850°c.
2. Annealed at ~400°c.
3. Unannealed.

× Data of MacDonald and Templeton for Au–Ni alloys.

4. 0·05% Ni annealed at ~850°c.
5. 0·05% Ni unannealed.
6. 0·2% Ni annealed at ~850°c.
7. 0·2% Ni annealed at ~400°c.

(3) The question has sometimes been asked whether a solvent metal which can show a resistance minimum itself, causes a resistance minimum when it is present as solute in another solvent. This question has been studied by examining alloys of magnesium dissolved in copper, and copper dissolved in gold.

§ 2. EXPERIMENTAL RESULTS

It is clear today that in order to determine whether a particular solute causes a resistance minimum in a given solvent it is essential to establish that the pure solvent, *melted and processed in exactly the same manner as the alloys*, does *not* show a resistance minimum. The results of our experiments are summarized in table 1 and some typical resistivity temperature curves are illustrated in fig. 2. The increasing resistivity of the alloys with increasing nominal solute concentration, together with the results of spectroscopical analyses, indicate that the added solutes were indeed present in the alloys and entered into solid solution.

Table 1

Solvent	Solute	Nominal Composition at. % solute	$\frac{R_{\min}}{(R_{273^\circ K}-R_{\min})}\times 10^3$	$\frac{(R_{2\cdot7^\circ K}-R_{\min})}{R_{\min}}\times 10^2$
Pure Au	—	—	2·26	~0
Pure Au	—	—	2·59	0†
Au	Sn	0·01	18·3	0
		0·02	31·4	0
		0·035	52·6	0
Au	Cu	0·056	14·25	0
		0·25	50·9	0
		0·31	63·6	0
Au	Ni	0·042	19·9	0
		0·168	64·5	0
Au with minimum resulting from processing			10·4	0·8†
Pure Ag	—	—	3·96	0·7
Ag	Sn	0·006	19·7	0·1
		0·009	23·1	0·35
		0·018	62·4	0·15
		0·046	132·5	0
		0·112	384	0·15
Ag with typical minimum			3·92	4·5
Cu	—	—	5·0	1·8†
Cu	Mg	0·13	22·9	~0·05†
		0·26	64·4	0·1†

† $\frac{(R_{4\cdot2^\circ K}-R_{\min})}{R_{\min}}\times 10^2$

Neither nickel, nor copper, nor tin causes a resistance minimum in polycrystalline gold. When the pure gold itself showed *no* resistance minimum, its alloys with Ni, Cu or Sn did *not* show a resistance minimum. If, however, similar alloys were prepared from pure gold that showed a small resistance minimum (as in the sixth curve of fig. 2), they also showed a resistance minimum. We were unable to melt and process pure silver that was entirely free of a resistance minimum. Curve 4 of fig. 2 shows the

Fig. 2

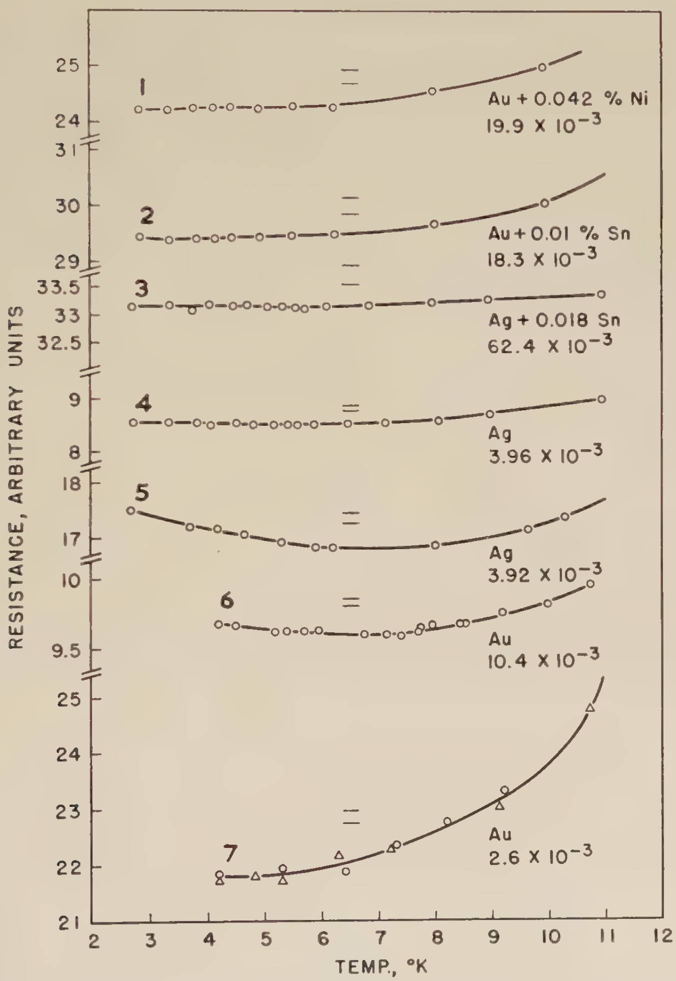

Resistivity of samples of pure gold and silver and various alloys plotted as a function of temperature. Compositions in at. % and residual resistance ratios, $R_{\min}/(R_{273^\circ\mathrm{K}}-R_{\min})$, of the specimens are given on the diagram. The separation of the parallel bars represents 1% of the residual resistivity. Curves 5 and 6 are included to show the extent of the resistance minimum which may occur in ' pure ' samples of silver and gold.

best behaviour which we were able to obtain. Curve 5 shows the relatively large resistance minimum found in very pure silver obtained from one source. This silver was not used in the preparation of the alloys reported. Since the Ag–Sn alloys reported only showed a much smaller percentage minimum than the pure silver, if any at all (table 1), it seems safe to conclude that tin does not cause a resistance minimum in polycrystalline silver. Similar reasoning leads to the conclusion that magnesium does not cause a resistance minimum in polycrystalline copper.

§ 3. Discussion

We differ from the report of MacDonald and Templeton (1951) that copper and nickel give rise to a resistance minimum in gold and the new results are in accord with our earlier findings for copper, that the homovalent impurities, silver and gold, do not give rise to a resistance minimum. The observation that neither copper dissolved in gold, nor magnesium, silver or gold dissolved in copper causes a resistance minimum in dilute polycrystalline alloys, indicates that there is no necessary connection between the occurrence of a resistance minimum in a metal and its effect when present as a solute in another solvent.

Table 2

Solvent	Solute	$r_{\text{solute}}/r_{\text{solvent}}$†	Lattice distortion per at. % solute‡	
			Δa in X units	$\Delta a/a \times 10^3$
Cu	Zn	$1{\cdot}06_5$	2·1	0·58
	Ga§	$1{\cdot}06_1$	2·7	0·75
	Ge§	$1{\cdot}04_3$	3·3	0·92
	In§	$1{\cdot}27_6$	9·3	2·88
	Sn§	$1{\cdot}20_4$	10·3	2·86
Ag	Sn	$1{\cdot}05_4$	4·2	1·03
Au	Sn	$1{\cdot}05_7$	4·1	1·01

† Pauling's (1947) R(1) values.
‡ Pearson (1957).
§ These solutes cause a similar characteristic type of resistance minimum.

Since tin appears to cause a resistance minimum in polycrystalline copper alloys, but not in silver and gold, it is interesting to compare the relative sizes of these solute and solvent atoms, because the effect in copper has been attributed to the segregation of the tin atoms to grain boundaries. Table 2 shows that the radius ratio, $r_{\text{Sn}}:r_{\text{Cu}}$, and the initial lattice distortion caused by dissolving tin in copper, are notably greater than the corresponding quantities for tin in silver and tin in gold. This difference might be responsible for a lack of appreciable segregation of tin to the grain boundaries in polycrystalline silver and gold alloys, whereas such segregation might occur in polycrystalline Cu–Sn alloys (which are suitably annealed) because of the large radius ratio. If, however, this is the case, then it is strange why gallium and germanium in polycrystalline copper give a resistance minimum having similar characteristics to that caused by tin, since the radius ratios $r_{\mathrm{Ga}}:r_{\mathrm{Cu}}$ and $r_{\mathrm{Ge}}:r_{\mathrm{Cu}}$ are about the same size as those of $r_{\mathrm{Sn}}:r_{\mathrm{Ag}}$ and $r_{\mathrm{Sn}}:r_{\mathrm{Au}}$ (table 2).

Although the general phenomenon of segregation of solute atoms to the grain boundaries in these solvents has been established through experiments by a number of investigators, some attempt must now be made using autoradiographic or other methods to determine whether this segregation only occurs for certain solutes. In this way the hypothesis that grain boundary segregation is primarily responsible for the occurrence of the resistance minimum caused by the B group solutes, Ga, In, Ge and Sn in copper could be strengthened. It seems improbable that we can at present carry out conclusive experiments to compare the size of the resistance minimum with the area of the grain boundaries in a given copper alloy, because of the somewhat random variations in resistance which are frequently found after heat treatment of wires or strips of these alloys at high temperatures. Even the crude comparisons between single crystals and polycrystals described by Pearson *et al.* (1959) were only obtained and verified after much experimental effort.

ACKNOWLEDGMENTS

I am grateful to Dr. J. C. Chaston of Johnson, Matthey and Co. Ltd., London, for discussing with me their methods of melting spectroscopically standardized pure gold, which does not show a resistance minimum, to Mrs. D. M. Rimek and Mr. W. Fisher who prepared the alloys which were examined, and also to Dr. D. K. C. MacDonald for our frequent discussions on the origins of the resistance minimum.

REFERENCES

DE HAAS, W., DE BOER, J., and VAN DER BERG, G. J., 1933, *Physica*, **1**, 1115.
MACDONALD, D. K. C., 1952, *Phys. Rev.*, **88**, 148.
MACDONALD, D. K. C., and PEARSON, W. B., 1955 a, *Acta Met.*, **3**, 392; 1955 b, *Ibid.*, **3**, 403.
MACDONALD, D. K. C., and TEMPLETON, I. M., 1951, *Phil. Mag.*, **42**, 432.
MENDOZA, E., and THOMAS, J. G., 1951, *Phil. Mag.*, **42**, 291.
PEARSON, W. B., 1957, *Canad. J. Phys.*, **35**, 358.
PEARSON, W. B., RIMEK, D. M., and TEMPLETON, I. M., 1959, *Phil. Mag.*, **4**, 612.
PAULING, L., 1947, *J. Amer. chem. Soc.*, **69**, 542.

The Atomic Diffusion of Chromium in the Titanium–Chromium System[†]

By A. J. Mortlock[‡] and D. H. Tomlin
Physics Research Laboratory, University of Reading

[Received November 21, 1958]

Abstract

Diffusion rates of chromium in the body centred cubic phase of the titanium–chromium system have been measured by an autoradiographic tracer technique using the radioactive isotope ^{51}Cr. Two alloys, Ti+10% Cr and Ti+18% Cr (by weight), in addition to two grades of Ti metal, ‘ iodide ’ and ‘ commercial ’, were used as solvents so that tracer diffusion coefficients at essentially 0, 10 and 18% Cr concentration were measured, over the temperature range 900°c to 1200°c.

The results are expressed in equations of the form $D=D_0 \exp(-Q/RT)$. The most significant feature is that the activation energy Q for tracer diffusion at zero solute concentration is very much lower than that expected for self-diffusion in pure Ti. An extension of the Johnson model of solute diffusion in face centred cubic metals to the body centred cubic lattice is proposed as an explanation of this divergence.

§ 1. Introduction

Some features of the autoradiographic method used in these studies have been described in two earlier notes (Mortlock and Tomlin 1956 a, b), together with some preliminary results. In the present paper we wish to report the completed study and discuss the results obtained.

The main reason for choosing the autoradiographic method of analysing diffusion zones was to avoid the necessity of accurate machine cutting which is essential in the more frequently adopted method of serially sectioning the specimens as a preliminary to radioactive assay by counting. On account of the difficulty of machining commercial Ti and Ti–Cr alloys, sufficiently accurate sectioning was found to be prohibitively tedious, and was used in only one experiment to give a comparison of methods (Mortlock and Tomlin 1956 b). In the course of the work it has proved that the autoradiographic method provides a number of advantages, particularly in revealing any non-uniformity or unwanted structure in the diffusion zones, and allowing multiple diffusion experiments to be carried out on an individual specimen (Mortlock and Tomlin 1956 a).

1.1. *Materials*

The high purity iodide Ti was obtained from I.C.I., Ltd., and the commercial grade metal, together with the alloys, were prepared by the

---

[†] Communicated by the Authors.

[‡] Now a member of the Metallurgy Division, Atomic Energy Research Establishment, Harwell.

Metallurgy Department, Royal Aircraft Establishment, Farnborough. Impurity analyses supplied by the manufacturers are given in table 1, which includes all elements detected in concentrations not less than 0·05% in any one of the four metals.

§ 2. Experimental Methods

2.1. *Specimens*

Specimens for the diffusion experiments were prepared from cylindrical pieces of Ti or Ti–Cr alloy, about 1 cm in diameter and 0·5 cm in length, which were annealed by vacuum heat treatment at about 1000°c for 24 hours. Each piece was ground to provide a longitudinal flat surface a few millimetres wide, and parallel to the axis, and one finely ground end face. An 8 B.A. clearance hole was drilled axially through each cylinder.

Table 1. Analyses of Experimental Materials. Impurity Concentrations in weight per cent

Element	Iodide Ti	Commercial Ti	Ti+10% Cr	Ti+18% Cr
C	<0·1	0·3	0·3	0·2
Si	<0·1	0·03	0·05	0·05
Fe	0·03	0·15	0·1	0·3
W	†	<0·02	0·06	0·01
O	†	0·21	‡	0·07
N	0·006	0·05	‡	0·002

† Not included in analysis.
‡ Not detected.

Spectrographically pure Cr which had been pile-irradiated to produce the radioactive isotope ^{51}Cr was deposited on the finely ground end faces by vacuum evaporation to a thickness estimated at 0·1 μ by an optical interference measurement. This was the thickness of a film deposited on a small glass slide placed adjacent to the metal specimen during a particular evaporation. In all further preparations the thickness of deposit was approximately controlled by visually observing the optical transmission of a glass slide similarly placed.

Sandwich type diffusion couples were made from two cylinders of a given metal by placing the coated end faces together and clamping in position, with the longitudinal flat surfaces aligned, by means of a Ti bolt and nut through the axial hole. In most cases two such sandwiches, comprising two of the metals being studied, were formed into a single specimen as shown inset in fig. 1. This provided a more direct comparison of diffusion rates for two metals than could be obtained from the separate heat treatment of two specimens.

The longitudinal flat surface of the specimen was finely ground, and then autoradiographed by direct contact with x-ray film. Tests were carried out on the possible shrinkage or expansion of the emulsions used (Ilford Industrial ‘ C ’) during normal handling and processing, and on the relationship between photographic film density and exposure time for a source of the isotope ^{51}Cr.

2.2. *Heat Treatment*

Diffusion was induced by heat treatment in a temperature controlled vacuum furnace shown diagrammatically in fig. 1. The vacuum and furnace winding tubes were originally of mullite refractory, and the winding of platinum–rhodium alloy tape. More recently pure alumina has been used for the winding tube since a reaction was found to occur between the mullite and the Pt–Rh alloy. The Pt/Pt + 13% Rh thermocouple shown in the figure at T.I. was used to control the temperature by means of a potentiometer and photoelectric circuit. A continuous record of the control thermocouple temperature was plotted on a Cambridge recorder.

Fig. 1

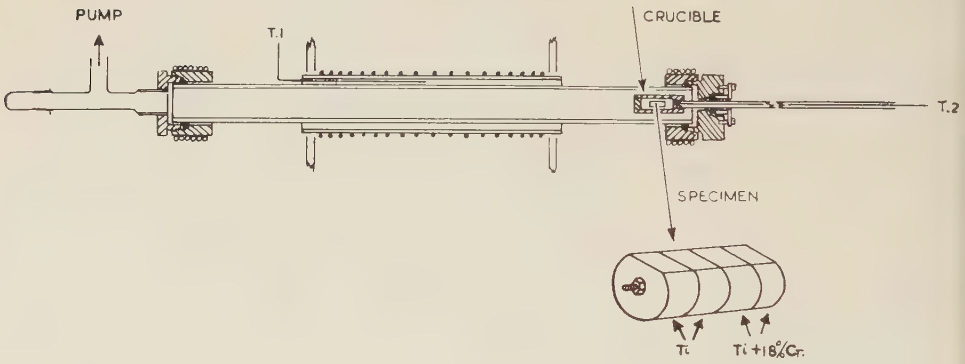

Details of the vacuum furnace and diffusion specimens.

The specimen for heat treatment was placed in a loosely stoppered Ti crucible which was in turn wrapped with molybdenum foil. This provided protection, by the gettering action of the crucible, against contamination of the specimen by residual gases, and prevented direct contact between Ti and the refractory, which react together at high temperature. A cylindrical recess at the closed end of the crucible was provided to receive the end of a mullite thermocouple sheath, again with a protective Mo foil interposed. The sheath entered the vacuum tube through a Wilson seal, and contained a second Pt/Pt + 13% Rh thermocouple, T.2, for accurate measurement of the specimen temperature. By sliding the sheath in the Wilson seal it was possible to move the crucible along the furnace. The thermocouple T.2 could be connected either to a second input of the recorder, or to a potentiometer for periodic temperature readings.

The loaded crucible was first placed at the extreme end of the vacuum tube, as shown in fig. 1, where it remained close to room temperature while the furnace was brought under control at the required treatment temperature, and then pushed into the central region of the tube. After the required time, treatment was terminated by similarly pushing the crucible to the other extreme end. Throughout the heat treatments, the furnace was continuously pumped to maintain a pressure of 10^{-5} to 10^{-4} mm Hg.

The Pt/Pt + 13% Rh thermocouples used for temperature measurement were calibrated at the National Physical Laboratory and checked periodically for drift by melting a small piece of pure gold wire welded across the thermojunctions.

2.3. *Hardness and Grain Size Measurements*

Hardness measurements were made on the specimen after heat treatment as a convenient means of detecting contamination by residual gases. Similar measurements were made on both the interior and exterior surfaces of a Ti crucible after each of a number of heat treatments, to show to what extent progressive contamination occurred, and the degree of protection afforded to the specimens.

Mean grain sizes were also measured after the initial annealing treatment and after subsequent diffusion experiments. This was possible in spite of the $\alpha \rightleftharpoons \beta$ transformation at 883°C since the β grain boundaries remained after quenching from the β-phase to room temperature, and were clearly visible as a result of thermal etching. Specimen preparation for microscopic examination was carried out by the method of Worner (1954), followed by polishing on selvyt cloth with metallographic polishing cream lubricated with a few drops of 2% aqueous HF before final etching.

2.4. *Microdensitometry*

After grinding down the longitudinal flat surface on the cylindrical specimens by about 1 mm to remove effects due to surface diffusion, autoradiographs were prepared to show the distribution of the diffused ^{51}Cr about the interfaces. Analysis of these distributions in the direction normal to the interfaces was then made by microdensitometry of the autoradiographs using a modification to a Vickers projection microscope described by Tomlin and Fayers (1955). The apparatus was adjusted to give an intrinsic resolution of about 10 μ, the total resolution then being determined by the characteristics of the X-ray film and the radiations from the tracer isotope. A measure of the total resolution was provided by observations on autoradiographs obtained before diffusion had occurred, appropriate corrections to the measured diffusion curves were then calculated.

§ 3. Results

3.1. *Hardness and Grain Size*

No significant variations in the hardness of the specimens, or of the inside surface of a crucible occurred during heat treatments, though the exterior crucible surface did show progressive hardening with use. Average measured Vickers Hardness Numbers were 95 for the iodide and 233 for the commercial Ti. Beta grain sizes in the metals as received were 2·0 and 0·05 mm respectively in the iodide and commercially pure metals, and 0·1 mm in the alloys. These increased during vacuum heat treatment, the preliminary annealing treatment at 1000°C for 24 hours was sufficient to ensure grain sizes of not less than 2 mm in the Ti specimens and 0·2 mm in the alloys.

Fig. 2

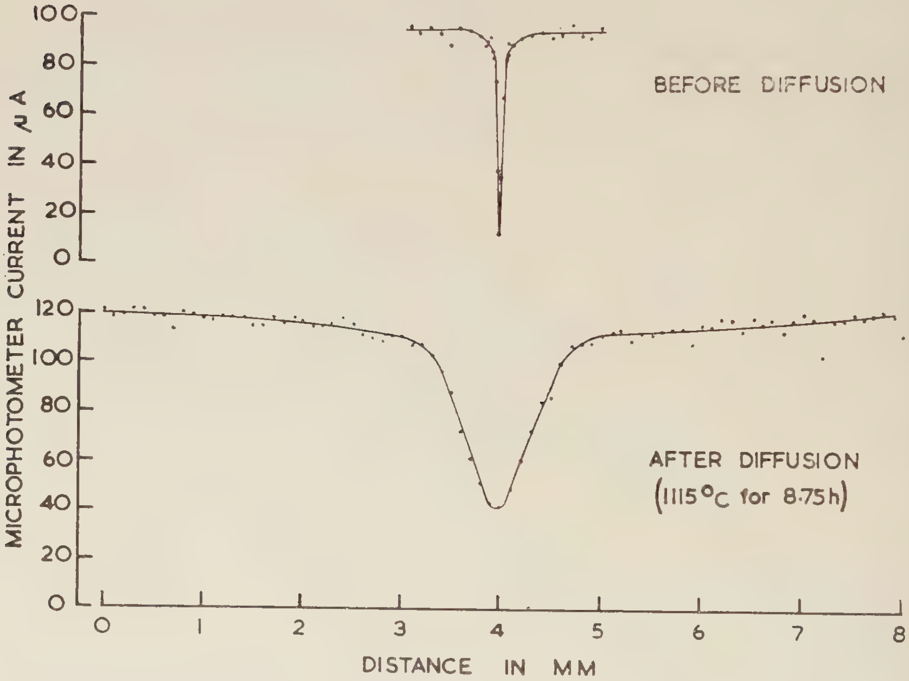

Microphotometric plots of autoradiographs from a Ti specimen before and after diffusion.

3.2. *Concentration Distributions*

Microphotometer scans obtained from autoradiographs of an iodide Ti sandwich before and after a diffusion treatment at 1115°C for 8·75 hours are shown in fig. 2. The density distribution corresponding to the undiffused layer shows a sharp peak as the main feature. The scan plotted after diffusion shows a broad low intensity curve superposed on a narrower distribution evidently representing the zone of diffusion. The broad background may readily be interpreted as due to the presence of a γ-ray component in the ^{51}Cr radiations in addition to x-rays and electrons which reproduce the actual distribution of ^{51}Cr with reasonably good resolution. A correction for this resolution was calculated from the width of the main peak in the 'undiffused' autoradiograph, and was found to be small, in the example shown it corresponded to a reduction of less than 1% in the measured diffusion coefficient. Correction for the γ-ray effect was not directly calculable, and several empirical methods of subtraction based on different extrapolations of the broad tail to the central maximum were tried. The method adopted in this work is illustrated in fig. 3, which shows an approximately linear tail in the density–distance squared curve. Linear extrapolation was used for this correction. When the log density was plotted against distance squared, the tail was again found to be nearly linear and an alternative correction could be based on a similar extrapolation. Both methods gave very nearly equal results.

Fig. 3

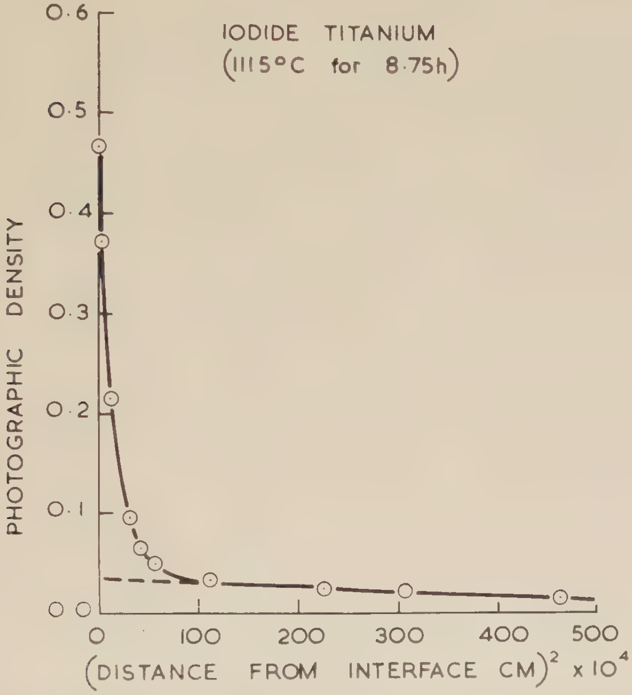

Method of subtracting the γ-ray contribution from the measured density curve.

A corrected curve of log density against distance squared is shown in fig. 4 and since the film calibration experiments showed that the density is linearly related to the specific surface activity, this curve is equivalent to the solute concentration distribution, $c(x)$. These curves were always found to be linear, corresponding to the appropriate solution

$$c(x)=c(0)\exp\left(-x^2/4Dt\right)$$

of Fick's differential equation where D is a unique diffusion coefficient, and t the diffusion time.

Fig. 4

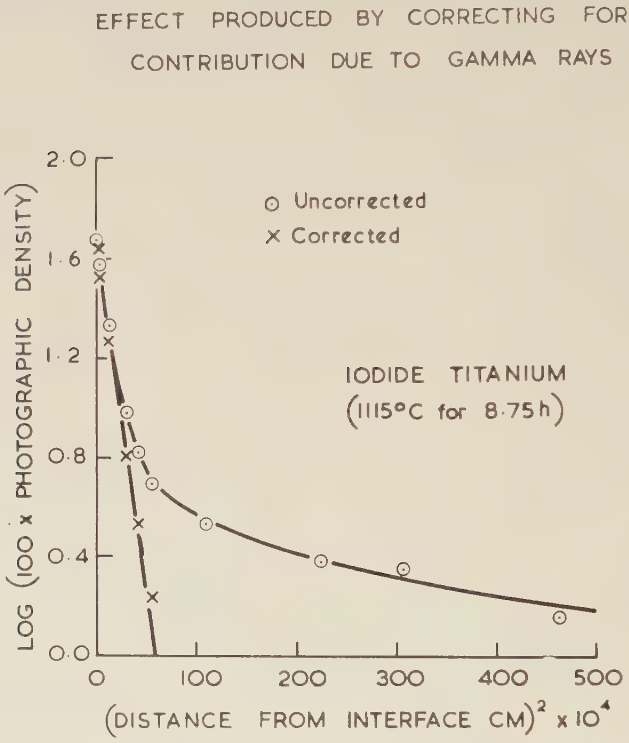

Corrected log–density against (distance)^2 plot.

Diffusion coefficients measured in this way for the different solvent metals at temperatures in the range 900°c to 1200°c are summarized in table 2, and plotted as log D against the reciprocal of the absolute temperature T in figs. 5, 6 and 7. In several cases two, and occasionally three, successive diffusion experiments were carried out with a given specimen in the way described previously (Mortlock and Tomlin 1956 a). Results obtained from such repeated experiments were usually consistent with those given by first heat treatments, beginning with a thin concentrated layer of solute, although some variation was observed with commercial Ti at 1000°c. In this particular case the average figure only has been

Table 2. Individual Diffusion Coefficients for the Diffusion of Cr in Ti and Ti–Cr Alloys

Specimen No.	Diffusion run No.	Time (hours)	Temperature (°c)	Diffusion coefficient (cm^2 sec^{-1}) × 10^9
Iodide Ti				
1	1st	10·0	1000	4·3
1	2nd	5·8	1177	23·5
2	1st	6·0	1176	20·5
2	2nd	28·0	1001	2·8
3	1st	8·0	1064	6·3
3	2nd	70·5	926	1·3
4	1st	8·8	1115	11·7
4	2nd	12·3	1193	20·6
Commercial Ti				
5	1st	6·0	1047	8·0
5	2nd	10·0	1000	3·7
5	3rd	10·0	1000	1·3
6	1st	10·0	1000	3·9
6	2nd	10·0	1000	6·8
7	1st	24·0	1067	9·0
8	1st	50·0	980	3·2
9	1st	23·0	1033	7·0
10	1st	24·0	1055	7·4
11	1st	6·0	1178	24·6
12	1st	11·0	1109	10·5
Ti + 10% Cr alloy				
1	1st	10·0	1000	2·4
1	2nd	5·8	1177	12·9
3	1st	8·0	1064	5·3
3	2nd	70·5	926	0·69
Ti + 18% Cr alloy				
5	1st	6·0	1047	3·9
5	2nd	10·0	1000	1·8
5	3rd	10·0	1000	2·2
6	1st	10·0	1000	2·0
6	2nd	10·0	1000	2·0
7	1st	24·0	1067	5·5
8	1st	50·0	980	1·6
9	1st	23·0	1033	4·1
11	1st	6·0	1178	18·3
11	2nd	44·3	925	0·73
12	1st	11·0	1109	8·2

Fig. 5

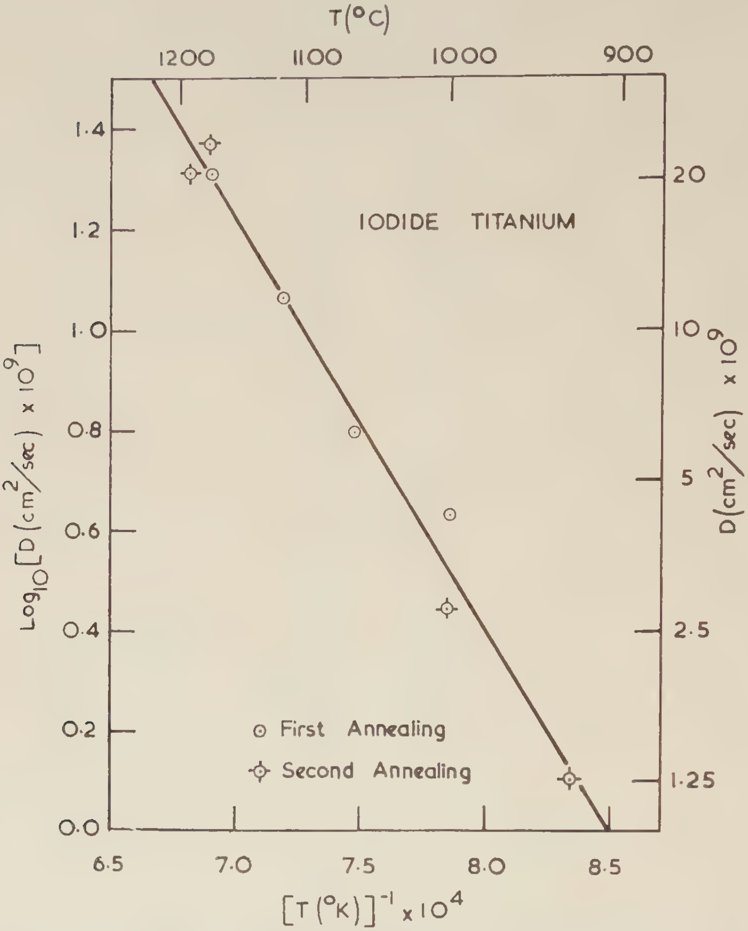

Dependence of diffusion coefficient on temperature for the diffusion of ^{51}Cr in iodide Ti.

Table 3. Frequency Factors and Activation Energies for the Diffusion of Cr in Ti and Ti–Cr Alloys

Solvent metal	Frequency factor D_0 (cm^2/sec)	Activation energy	
		Q (kcal/g mol)	E (ev/atom)
Commercial Ti	$0{\cdot}005^{+0{\cdot}009}_{-0{\cdot}003}$	$35{\cdot}3 \pm 2{\cdot}7$	$1{\cdot}53 \pm 0{\cdot}1$
Iodide Ti	$0{\cdot}010^{+0{\cdot}013}_{-0{\cdot}006}$	$37{\cdot}7 \pm 2{\cdot}2$	$1{\cdot}64 \pm 0{\cdot}1$
Ti+10% Cr	$0{\cdot}02^{+0{\cdot}06}_{-0{\cdot}01}$	$40{\cdot}2 \pm 3{\cdot}9$	$1{\cdot}74 \pm 0{\cdot}17$
Ti+18% Cr	$0{\cdot}09^{+0{\cdot}08}_{-0{\cdot}04}$	$44{\cdot}5 \pm 1{\cdot}6$	$1{\cdot}93 \pm 0{\cdot}07$

plotted. The linearity of the log D against $1/T$ plots allowed the diffusion coefficients to be expressed in the form

$$D = D_0 \exp(-Q/RT) = D_0 \exp(-E/KT),$$

where the frequency factors D_0 (cm^2/sec) and activation energies Q (cal/mol) or E (ev) were determined by least squares analysis. The results are given in table 3, together with calculated standard errors based on the observed scatter of the experimental results.

Fig. 6

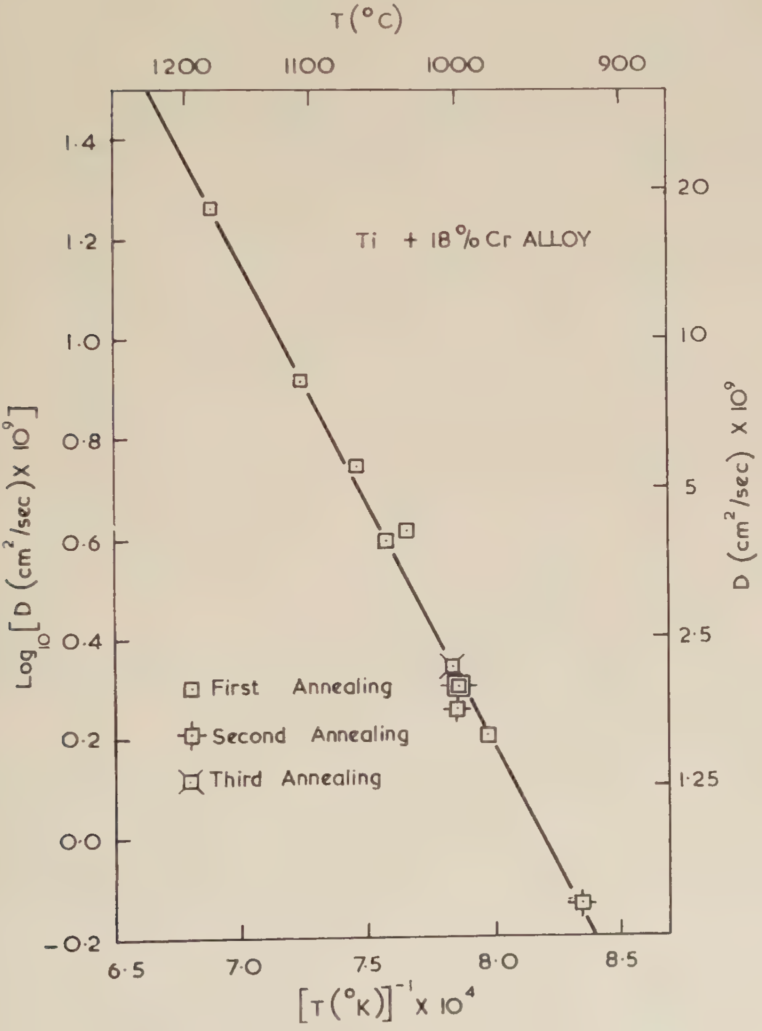

Dependence of diffusion coefficient on temperature for the diffusion of ^{51}Cr in Ti+18% Cr alloy.

Fig. 7

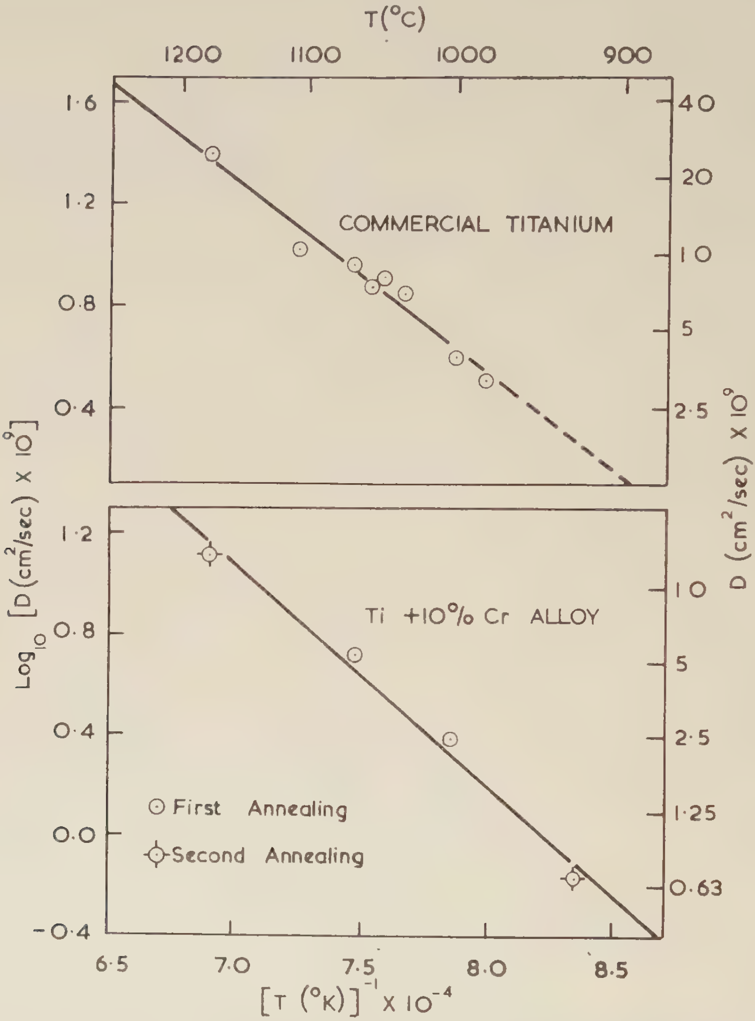

Dependence of diffusion coefficient on temperature for the diffusion of ^{51}Cr in commercial Ti and Ti+10% Cr alloy.

3.3. *Experiments at Temperatures close to the Transformation Point*

In all the experiments represented in the above results the autoradiographs showed a monotonic density variation in the direction of diffusion closely symmetrical about the initial interface, and were uniform in the transverse direction with no evidence of preferential diffusion along grain boundaries, or segregation of the solute and solvent elements. The rate at which the specimens cooled at the end of the heat treatment was apparently great enough in relation to diffusion rates to cause segregation during phase transformation on too small a scale for autoradiographic resolution.

One second annealing experiment with a commercial Ti specimen at 925°c did, however, yield a diffusion zone in which segregation of the solute was shown by the autoradiograph. A similar effect was found following the first heat treatment of an iodide Ti specimen at a temperature measured as 882°c, which is very close to the $\alpha \rightleftharpoons \beta$, phase transformation point.

The most likely interpretation of these results is that the temperatures of treatment corresponded to equilibrium $\alpha+\beta$ phase structures in which partition of the radioactive solute occurred between the α and β regions. The effects are consistent with the very low solubility of Cr in α Ti.

3.4. *Small Systematic Errors*

Probably the most important systematic error in this investigation lies in the absolute temperature determinations. The intrinsic sensitivity of the photo-electric control apparatus was about ±1°c, but it was necessary to allow for errors due to a measured temperature gradient in the furnace and in the absolute calibration of the measuring equipment. It was concluded that the total accuracy of temperature measurement could be safely estimated as ±4°c, corresponding to an uncertainty of ±4% in the diffusion coefficient at 1100°c.

End effects in heat treatment were not large, in a typical case the specimen temperature rose from 20°c to 1120°c in 12 min on being moved into the centre of the furnace, and fell to below 700°c in the same time when removed. Errors introduced by neglecting diffusion during heating up and cooling down were estimated by graphical integration from the temperature record and found to represent less than 1% of the measured diffusion coefficient.

Signs and magnitudes of other errors due to the systematic effects of thermal expansion and autoradiographic resolution were such that summation with the end effect temperature errors gave an approximately zero resultant for a typical case. Individual corrections were therefore considered to be insignificant. Considering the relative changes in these errors with temperature and duration of heat treatment the total accuracy of the finally calculated diffusion coefficients was estimated to be in the range ±5% to 10%. The scatter of the actual results largely confirmed this estimate though some determinations showed relative discrepancies larger than 10% (e.g. fig. 5).

§ 4. DISCUSSION

It is considered that the diffusion coefficients measured in this work may be interpreted as representing rates of diffusion of solute Cr atoms in the b.c.c. lattice of Ti–Cr alloys at essentially constant concentrations of 0, 10 and 18 wt %. The consistency of repeated experiments on a given specimen shows that the initial layer of solute was sufficiently thin in relation to the diffusion rates to give a negligible contribution to the total concentration during the time of heat treatment.

The possibility of interference by grain boundary diffusion is regarded as negligible on account of the large grain sizes of the specimens, particularly in the pure Ti, where very often the entire diffusion zone contained only two or three grains. Autoradiography provided a means of detecting any non-uniformity in the concentration distribution of diffused solute, but no such effects were found except at temperatures close to the $\alpha \rightleftharpoons \beta$ transformation point where phase separation was expected. The distributions were continuous across grain boundaries roughly parallel to the direction of diffusion, showing no observable dependence of diffusion coefficient on grain orientation and no enhanced diffusion along such boundaries. Although no significant curvature was found in the log concentration -(distance)^2 and in the log D -$1/T$ plots, this was not regarded as good evidence for non-interference by grain boundary diffusion because of the need to subtract the γ-ray components, and the rather limited temperature range available.

4.1. *The Activation Energies*

Accepting this interpretation, the most striking feature of the results is the rather low value obtained for the activation energy for the diffusion of Cr in pure Ti at tracer ($\simeq$ zero) concentration, in comparison with that expected for self-diffusion in Ti with a melting point as high as 1660°c.

Unfortunately, no measurements of self-diffusion in Ti have been reported up to the present; the element has no radioactive isotope with a period long enough for direct measurements to be made conveniently. It is possible only to estimate the activation energy of the process from empirical relationships which have been noted in other metals between this quantity and other physical constants. Kidson and Ross (1958) have collected data showing a close correlation between the activation energy for self-diffusion and the melting temperature T_m in metals of differing crystal structures, including the three b.c.c. metals Na, Li and α Fe. To be consistent with this correlation, it is necessary to assign an activation energy of 2·9 ev to the self-diffusion process in β Ti. Hoffman *et al.* (1956) show a correlation between the self-diffusion activation energy and heat of sublimation for a number of f.c.c. metals. If this is considered to apply also to metals with the b.c.c. structure, and applied to the present case, the heat of sublimation 112·7 kcal/mol determined for Ti by Edwards *et al.* (1953) would correspond to an activation energy of 3·2 ev.

Comparing these values with the experimental result of 1·6 ev for the tracer diffusion of Cr in Ti it is clear that the tracer solute and self-diffusion activation energies differ much more widely than in other systems which have been studied by tracer methods. For example, the diffusion of a number of solutes in Ag has been investigated by Tomizuka and Slifkin (1954) and the activation energies found to be within 15% of the value for self-diffusion in Ag. Work now in progress in this department on the tracer diffusion of Fe in Ti indicates that an activation energy even smaller that 1·6 ev is involved.

Such a large difference between the measured solute activation energy and that estimated for self-diffusion in Ti indicates that the mechanisms of the two processes are different. Since it is generally agreed that self-diffusion in metals takes place by a vacancy mechanism, and since also, lattice parameter measurements indicate that Cr enters into substitutional solid solution in β-Ti it would seem to be most satisfactory to suggest that Cr diffuses in this lattice by a modified vacancy mechanism.

Fig. 8

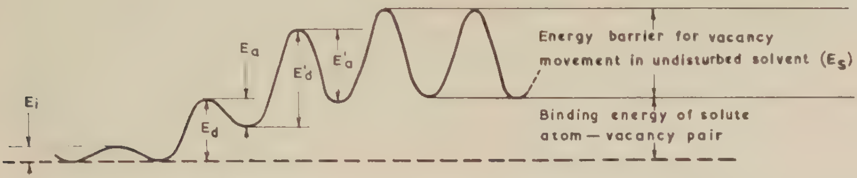
E_i
E_a
E_d'
E_a'
E_d
Energy barrier for vacancy movement in undisturbed solvent (E_s)
Binding energy of solute atom — vacancy pair

Diagram illustrating the proposed binding between impurity Cr atoms and vacancies in Ti.

Both Cr and Fe are small atoms compared with Ti, with size factors of about −13%. Swalin (1957) has recently calculated solute diffusion activation energies in the f.c.c. lattice by considering the dilation in the plane of atoms separating the initial and final sites in a solute atom-vacancy exchange, which together with a compression of the moving atom produces a hole large enough for this atom to pass through. It is of interest that in the b.c.c. lattice the corresponding hole is large enough without dilation for the passage of a solute atom with a size factor of −12%. In the f.c.c. lattice a size factor of −27% would be required to meet this condition. On this model, in which the activation energy is related to the work done against elastic forces to produce the necessary distortions, it follows that a small solute atom in a b.c.c. lattice can exchange with a vacancy with a very small activation energy. This does not at once imply a low activation energy for solute diffusion because of a strong correlation between successive solute-vacancy jumps. In fact this is precisely the situation in which diffusion of the solute atom is determined by the activation energy of solvent-vacancy jumps, i.e. of solvent self-diffusion. A reduced activation energy for solute diffusion could result if vacancies were preferentially bound to solute atoms when occupying both immediate and second nearest neighbour sites. The possibility then arises that a vacancy may remain associated with a solute atom for a long period by successive jumps into the second shell of six sites and back to a nearest neighbour site. This extension of Johnson's (1939) model of solute diffusion in f.c.c. lattices, in which only immediate neighbours needed to be considered, requires a distribution of potential barrier heights around a solute atom of the kind shown in fig. 8. The barrier heights E_i and E_s correspond respectively to exchanges between a solute atom and a vacancy and between a solvent atom and a vacancy in the pure solvent lattice. E_d and E_d' correspond respectively to the dissociation of a vacancy from a solute atom into one of the six second nearest neighbour sites, and from there to a site in the undisturbed solvent lattice. Similarly E_a, E_a' correspond to association jumps in which a vacancy becomes a first and second nearest neighbour respectively to a solute atom. The ratio E_a/E_d' will largely determine the mean lifetime of a solute atom-vacancy pair, and all the barrier heights will play a part in determining the solute diffusion coefficient and activation energy. A low resultant activation energy will arise from two considerations, through the possibility that $E_d \ll E_s$ because of lattice disorder around a solute atom-vacancy pair, and through the large binding energy of such a pair.

The tendency for the solute diffusion activation energy to increase at the relatively high concentrations of 10% and 18% Cr could be attributed to a breakdown of the proposed mechanism. The accompanying decrease in lattice parameter increases the effective size factor of the solute atom, and the binding energy of a solute atom vacancy pair may be reduced by the presence of other neighbouring solute atoms. It is of interest to note that the activation energies in pure Ti and in the Ti–Cr alloys do not show the relationship to melting temperature as found by Nachtrieb *et al.* (1957) in the silver–palladium system.

4.2. *The Frequency Factors*

The measured values of D_0 in this work are rather inaccurate because of the extensive extrapolation involved. The order of magnitude obtained suggests that the entropies of activation are positive, but small; a value of 0·3 cal/g mol °c was calculated for iodide Ti.

§ 5. CONCLUSION

The diffusion of Cr in Ti measured by tracer methods at effectively zero concentration does not appear to follow the close agreement between solute and self-diffusion activation energies usually found in such studies. It is suggested that a vacancy mechanism of diffusion may be retained if it is supposed that correlation between successive atom-vacancy jumps results in a high probability of a solute atom remaining a near neighbour of a vacancy. Though this can be justified to some extent in the present case on the grounds of the relatively small size of the solute atom and the open structure of the b.c.c. lattice, it must be admitted that a number of unsupported assumptions have been made. At all events it appears that some such modification of the simple vacancy model is necessary, and it is clearly desirable that the study of the effect of size factors on solute diffusion in b.c.c. lattices should be extended to clarify this situation.

ACKNOWLEDGMENTS

We wish to thank Dr. A. B. Lidiard for helpful discussions, and Professor R. W. Ditchburn for providing laboratory facilities.

REFERENCES

EDWARDS, J. W., JOHNSTON, H. L., and DITMARS, W. R., 1953, *J. Amer. chem. Soc.*, **75,** 2467.

HOFFMAN, R. E., PIKUS, F. W., and WARD, R. A., 1956, *J. Metals*, **8,** 483.

JOHNSON, R. P., 1939, *Phys. Rev.*, **56,** 814.

KIDSON, G. V., and ROSS, R., 1958, *Radioisotopes in Scientific Research*, **1,** 185 (London: Pergamon Press).

MORTLOCK, A. J., and TOMLIN, D. H., 1956 a, *Proc. phys. Soc. Lond.* B, **69,** 248 ; 1956 b, **69,** 250.

NACHTRIEB, N. H., PETIT, J., and WEHRENBERG, J., 1957, *J. chem. Phys.*, **26,** 106.

SWALIN, R. A., 1957, *Acta Met.*, **5,** 443.

TOMIZUKA, C. T., and SLIFKIN, L., 1954, *Phys. Rev.*, **96,** 610.

TOMLIN, D. H., and FAYERS, F. J., 1955, *J. sci. Instrum.*, **32,** 404.

WORNER, H. W., 1954, *Bull. Inst. Met.*, **2,** 131.

On the Release of Cold-work in Cadmium in Terms of Mechanical Properties†

By R. KAMEL‡ and E. A. ATTIA
Faculty of Science, Cairo University, Giza, Egypt

[Received December 2, 1958]

ABSTRACT

Three principal recovery processes were investigated by isothermal internal friction and elasticity measurements on heavily cold-worked Cd samples which had been annealed at various temperatures up to 280°c. The first recovery process is room temperature recovery and was observed immediately after shear deformation. The second process was studied after annealing below the re-crystallization temperature which is about 150°c, while the third was investigated above 150°c.

A tentative explanation is given for the structural changes that take place during the induction period which is activated with an energy of 32 ± 2 kcal/mole, and is possibly due to the recombination of extended dislocations with change in the orientation of the crystallites formed on deformation. It is concluded that for samples pre-annealed at temperatures lower than that of re-crystallization, re-crystallization is more likely to proceed by the growth of the particles formed on deformation.

§ 1. INTRODUCTION

THE study of the mechanisms involved in the release of cold-work in hardened metals may be conveniently approached by measuring changes in structure sensitive properties (Thorley 1950, Bowen *et al.* 1952). In previous publications (Kamel and Attia, 1957, 1958), the authors adopted the internal friction and elastic modulus changes to follow the course of softening of cold-worked metals. The aim of the present paper is to report further information concerning the release of cold-work in cadmium of 99·99% purity, and to identify the various stages involved in this process.

§ 2. EXPERIMENTAL

The internal friction Q^{-1} was measured by the resonance curve method, using clamped/free wire samples vibrating transversely at fixed frequencies in the low-sonic range. The vibrations were set up electrostatically *in vacuo* and were detected and measured by a micro-vibration pick-up of a type which has earlier been described by one of the authors (Kamel 1953). The square of the natural frequency was taken as a measure of elasticity. The maximum strain amplitude was in the range of 10^{-7}. Annealing was then carried out by subjecting the specimen to rectangular heat pulses of known magnitude. The frequency and the isothermal damping measurements were then made at room temperature (25°c).

---

† Communicated by the Authors.

‡ Now at H. H. Wills Physics Laboratory, University of Bristol.

§ 3. Results

3.1. *Room Temperature Recovery*

It was found that if fully annealed cadmium were deformed by plastic torsion, then immediately after deformation the internal friction assumes high values, but after standing for a few hours at room temperature, the internal friction of the cold-worked samples drops down to an asymptotic value (fig. 1). To investigate this type of recovery, we used samples of the same dimensions (8 × 0·082 × 0·082 cm) but having different grain sizes, viz. micro-crystalline, coarse-grained, and mono-crystalline samples.

Fig. 1

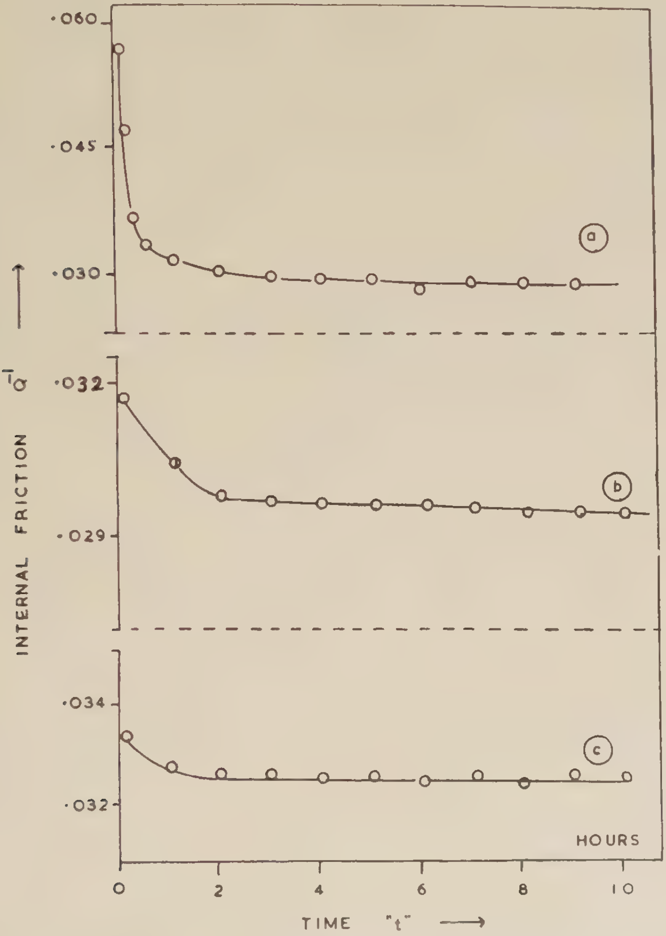

Internal friction versus time of rest at room temperature for Cd samples deformed by 10 twists: (*a*) Single crystal sample; (*b*) coarse-grained sample: G.D. = 0·05 cm; (*c*) polycrystalline sample.

Fig. 2

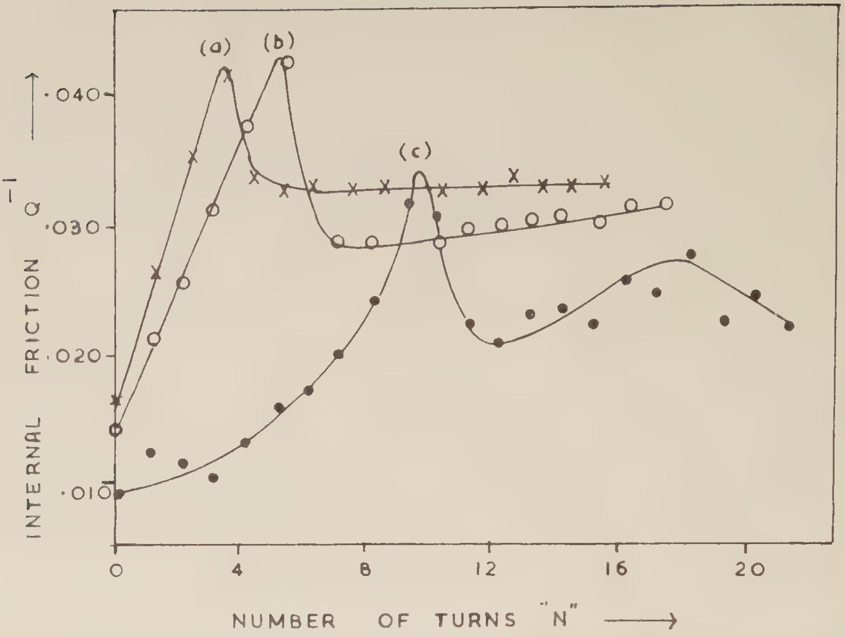

Change of internal friction as a function of number of turns twist: (*a*) for polycrystalline; (*b*) for coarse-grained G.D. = 0·05 cm; (*c*) for single crystal.

Fig. 3

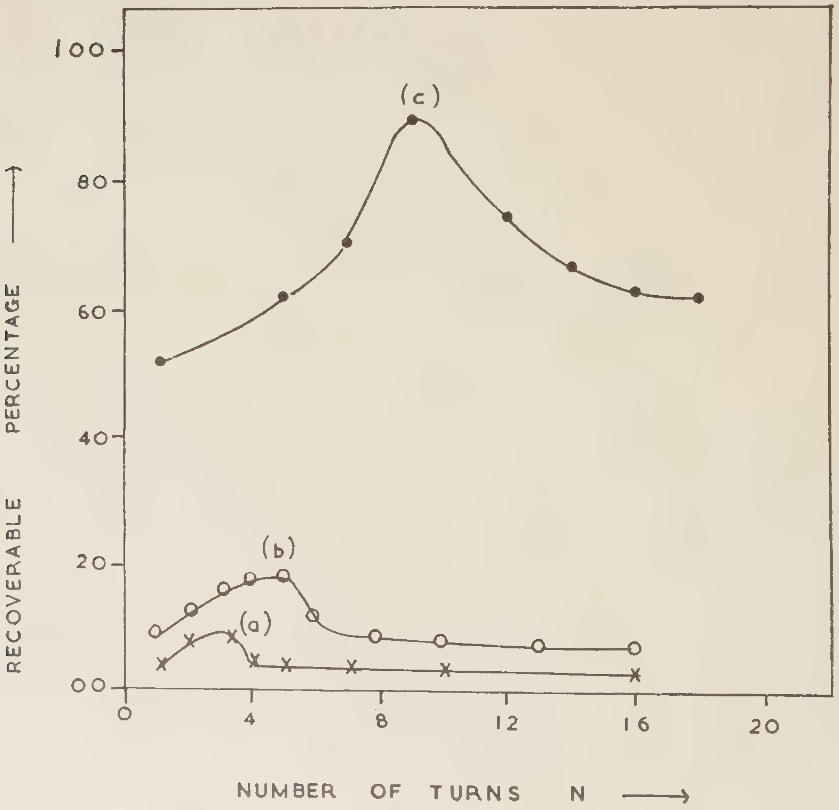

The recoverable percentage versus the degree of twist for different Cd samples: (*a*) polycrystalline; (*b*) coarse-grained; (*c*) single crystal.

Cold-work was performed by uniform twisting at room temperature, the number of twists being taken as a measure of the degree of deformation. The transverse internal friction was measured at 40 c/s as a function of the time elapsed since deformation: the first observation could not be made earlier than 5 min after deformation. We give in fig. 2 the value of Q^{-1} for different degrees of twist. Figure 3 represents the recoverable part of Q^{-1} as a percentage of the asymptotic value which is attained after 10 hours standing time.

Fig. 4

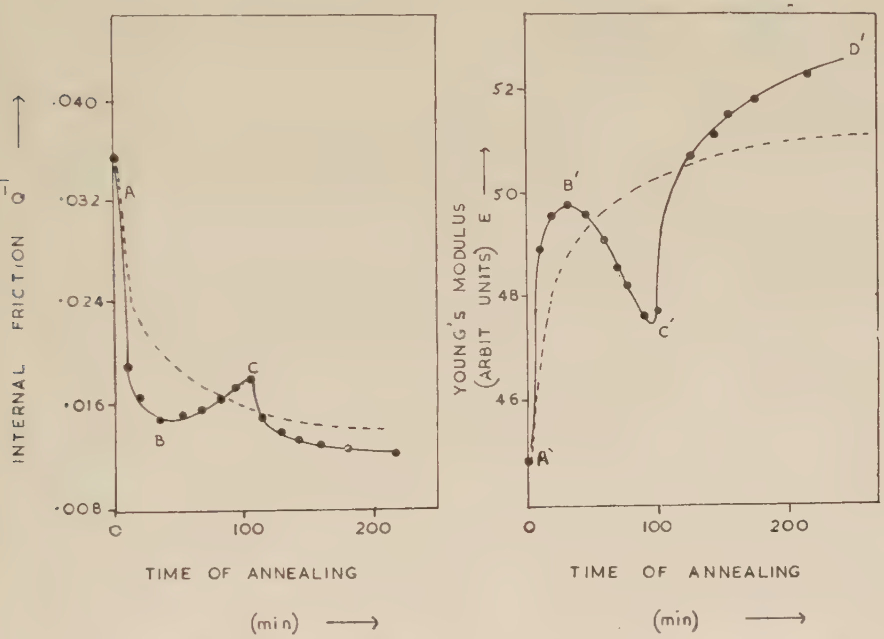

Change of isothermal internal friction and Young's modulus versus annealing time for a sample annealed at 280°c. The dotted curve represents recovery at 150°c, and is drawn for comparison.

3.2. *Recovery by Annealing above Room Temperature*

Cold-worked samples which had reached the asymptotic value of Q^{-1} at room temperature were heat-treated at temperatures between 50° and 280°c for various times. Measurements of the resulting changes of internal friction, and of elasticity were made at room temperature, at a frequency of 70 c.p.s. A series of curves were obtained showing these changes as a function of the annealing time, with the annealing temperature as a parameter.

The results for recovery between 50° and 150°c have already been published by the authors elsewhere (Kamel and Attia 1957, 1958). Assuming recovery to obey a reaction rate equation, the average

Fig. 5

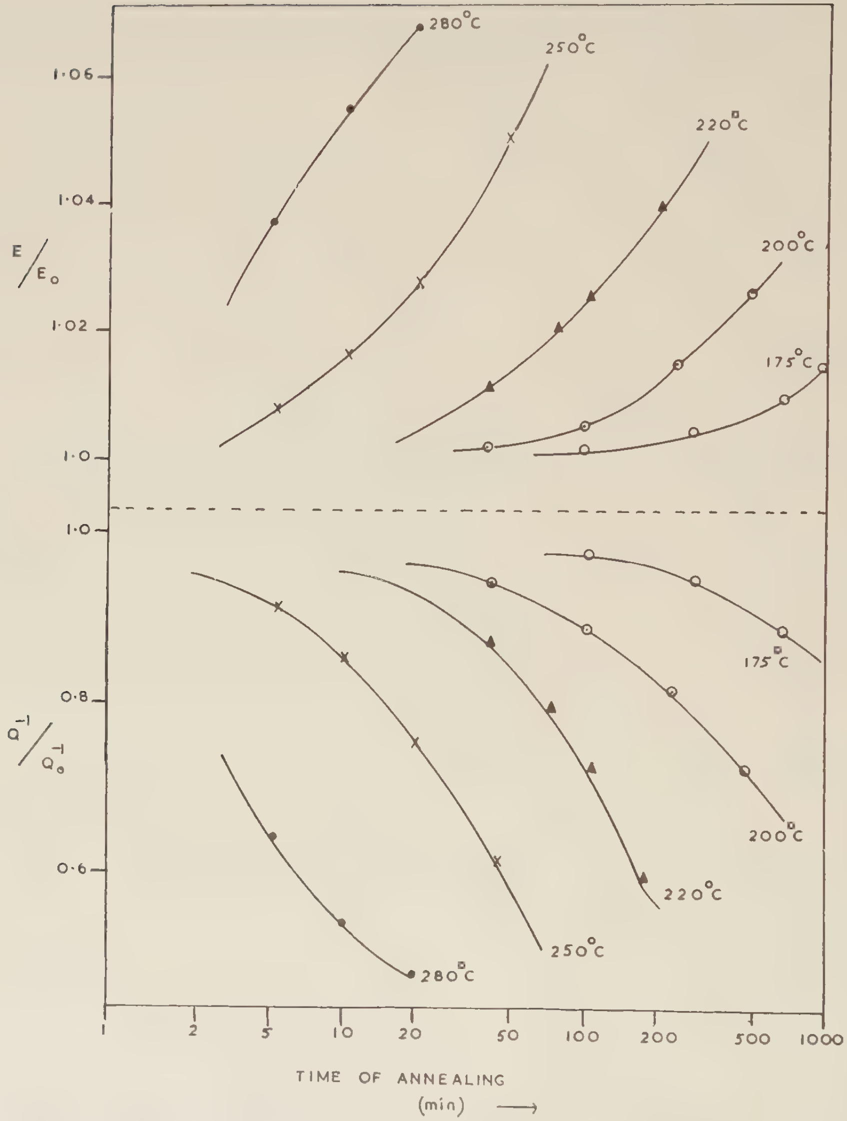

Change of relative isothermal internal friction and elasticity at different annealing temperatures between 175° and 280°C for cold-worked Cd pre-annealed at 100°C for 25 hours. The curves represent the initial behaviour before the characteristic hump.

activation energy† was found to be 21·5 kcal/mole and it was suggested that this was probably associated with the annihilation of dislocations during this stage of annealing.

Fig. 6

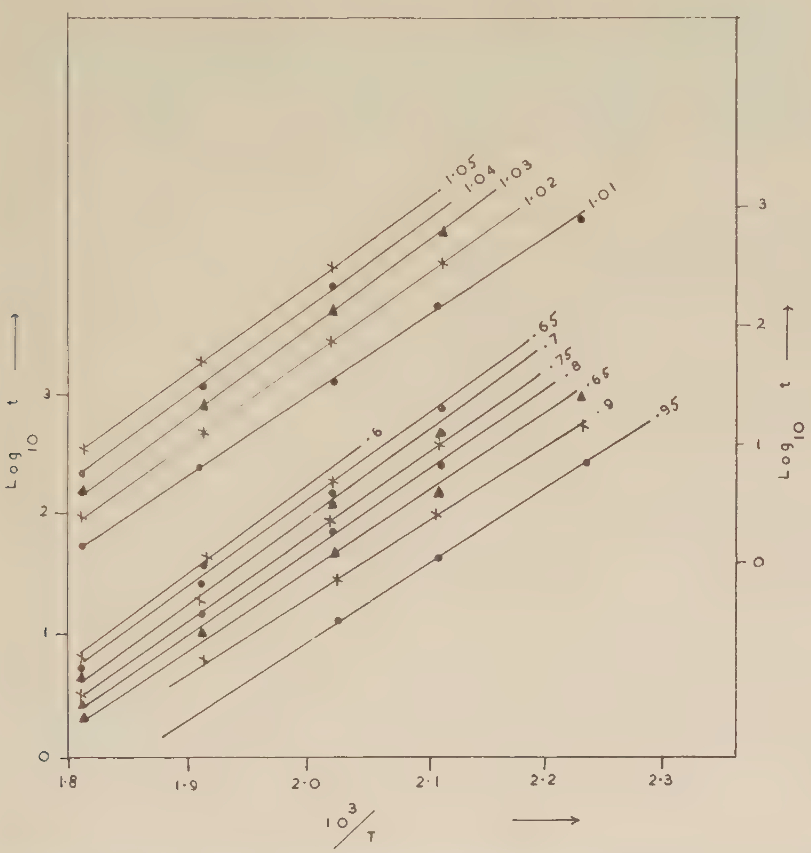

Reaction times and temperatures as deduced from the results of fig. 4. Average activation energy for the induction period is 32 ± 2 kcal/mole.

For recovery temperatures above 150°C, the graph of internal friction versus annealing time shows initially an abrupt fall, followed by a marked peak, after which the internal friction settles down to a steady value depending on the annealing temperature. The inverse behaviour is shown in the elasticity curves (cf. fig. 4). Our work on high temperature recovery has already been published.

---

† From an analysis of our results, Darling (1958) has noticed that, in support of his work on the recovery of slightly deformed high purity Cu (Darling 1956/7), the activation energy for the decrement change at higher degrees of recovery is different from the activation energy for the elasticity change, so that it is premature to ascribe the two changes to a single mechanism. The divergence, however, is of the order of the expected error, and a definite conclusion requires further investigations.

3.3. *Effect of Pre-annealing on the Re-crystallization Process*

Our previously observed (Kamel and Attia 1958) increase in activation energy with the increase in degree of recovery for low temperature anneal, suggests the simultaneous presence of another relaxation process different from that initially taking place.

In order to investigate the suspected process we used specimens which had been pre-annealed for 25 hours at 100°c to eliminate changes due to low-temperature recovery. Annealing was then made at different, higher temperatures. We give in fig. 5, curves showing on an enlarged scale, the recovery stage represented by the initial parts AB and A′B′ of the re-crystallization curves, cf. fig. 4, at some chosen elevated temperature of pre-annealed samples. The average heat of activation as calculated from these curves is (32 ± 2) kcal/mole (cf. fig. 6).

Fig. 7

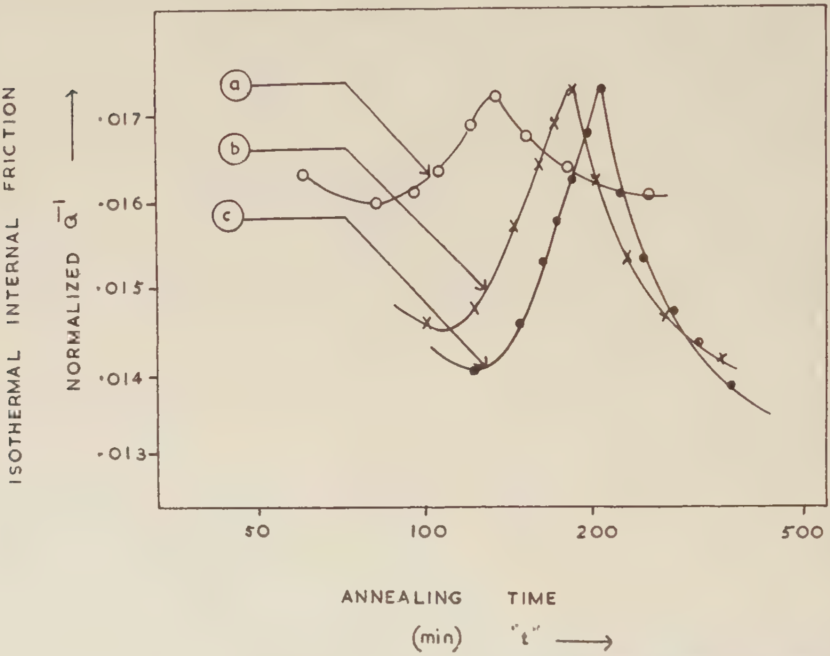

Curves showing room temperature internal friction changes versus annealing time at 250°c for cold-worked Cd samples:
(*a*) Received pre-annealing for 25 hours at 120°c; (*b*) Received pre-annealing for 25 hours at 100°c; (*c*) Received no pre-annealing.

The results of further study of pre-annealing are shown in figs. 7 and 8. These show the isothermal internal friction and modulus changes versus annealing time for Cd samples which had been initially heavily cold-worked. The samples were pre-annealed for the times and at the temperature quoted on the figures. The higher annealing temperature in all cases was 250°c.

For samples pre-annealed at temperatures of about 135°c, no peaks in the internal friction (or troughs in the elasticity curves) versus the annealing time could be observed.

Fig. 8

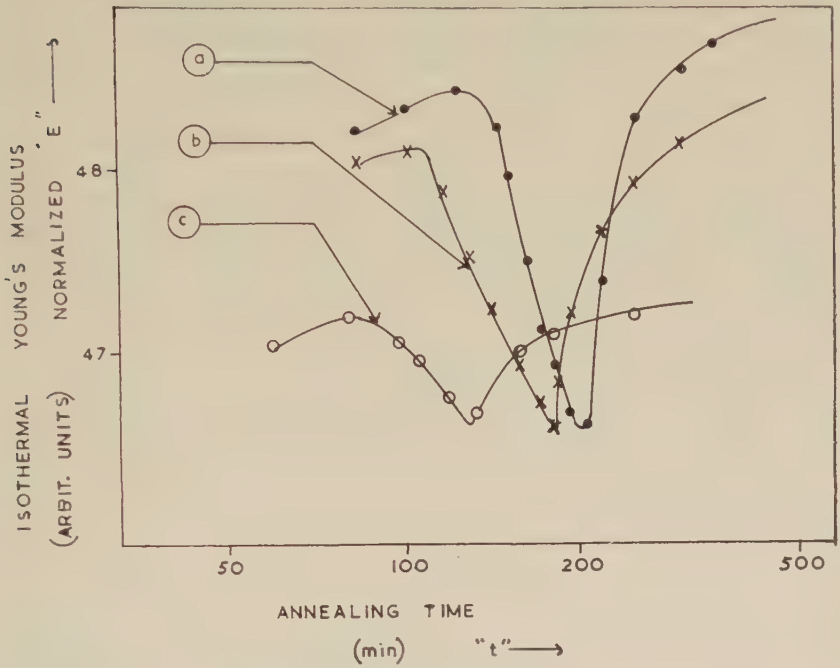

Curves showing room temperature modulus changes versus annealing time at 250°c for cold-worked Cd samples: (*a*) Pre-annealed for 25 hours at 120°c; (*b*) Pre-annealed for 25 hours at 100°c; (*c*) Received no pre-annealing.

§ 4. Interpretation and Discussion of the Results

The pronounced internal friction peaks which appeared at different degrees of deformation for samples with different crystalline states (fig. 2), may be explained by the continuous formation and subsequent locking of dislocations (Hasiguti and Hirai 1951, Hirone *et al.* 1955). The observed shift in this peak towards higher degrees of deformation as the sample tends towards a monocrystalline state, may be attributed to the enormous effect of grain boundaries on the locking of the newly born free dislocations.

4.1. *Room Temperature Recovery*

The rapid decrease in internal friction of the deformed sample with time of rest is probably caused by the presence of the newly born free dislocations. According to an explanation for room temperature recovery proposed independently by Nowick (1954) and Weertman (1955), it is believed that such dislocations are in continual striving to attain stable positions. As the equilibrium state is approached, the motion of the remaining free dislocations under an oscillatory stress decreases, and consequently the energy loss per cycle decreases too. The presence of grain boundaries in polycrystalline samples hinders the annihilation of free dislocations which contribute to internal friction, hence a smaller recoverable percentage is observed by room temperature annealing as evidenced from fig. 3. This conclusion agrees with that of Slifkin and Kauzmann (1952) and also Kennedy (1955), who studied the effect of recovery after creep in Zn and Pb.

4.2. *The Induction Stage*

The rising portion of the decrement curve and the associated inverse behaviour in the elasticity curve (fig. 4) may be interpreted as due to polygonization, whereas the descending part following the peak may be due to grain growth. The disappearance of the peaks in internal friction (or troughs in elasticity curves) versus the annealing time for samples pre-annealed at temperatures of about 135°c indicate that no polygonization has taken place. From figs. 5 and 6 the activation energy obtained for the induction period, assumed to precede polygonization (Anderson and Mehl 1945, Cahn 1950), lies reasonably well within the range of the reported values for grain boundary migration in Cd (Subrahmanyam 1956, Yousef and Kamel 1956).

According to Perryman (1954), the softening of metals during the induction period is probably due to the diffusion of dislocations, some cancelling out and others going to the sub-boundaries, thereby increasing the disorientation. This view accords with the proposal of Cottrell (1953) that the nucleus for re-crystallization is slightly disoriented from the surrounding matrix but, as it grows, the boundaries reach regions where the orientation is quite different.

It is noteworthy that in hexagonal metals, the edge dislocations are dissociated to form extended dislocations which must recombine to form unit dislocations before they can climb (Read 1953). The activation energy we obtained for the induction period falls also within the range required for the recombination of extended dislocations (Stroh 1954). Accordingly the mechanism responsible for the induction stage may be recombination of extended dislocations with change in the orientation of the crystallites of the sub-structure. Consequently, this induction stage brings about some sort of partial recovery of the boundary region which is necessary for the onset of the nucleation process.

4.3. *Effect of Pre-annealing on the Re-crystallization Process*

It may now be realized from the present results (figs. 7 and 8) that pre-annealing affects the re-crystallization process, thus enhancing the induction stage and decreasing the nuclei formation as evidenced by the suppression of the peaks. The effect is more marked as the pre-annealing temperature is raised. This behaviour could be, according to Cahn (1950), attributed to the fact that the highly distorted regions may be partially recovered, since recovery precedes re-crystallization. The density of dislocations will be diminished so that these regions will not favour nuclei formation. In agreement with Gay *et al.* (1954), it is likely that the original grain grows as a whole rather than by nuclei formation. Such a process is similar to that of the strain induced boundary migration reported by Beck (1954).

The present work on the effect of pre-annealing on recovery may throw some light on low temperature recovery. The noticeable increase of activation energy with the degree of recovery may probably originate from a mixed contribution between the changes occurring due to the induction period and those occurring in the genuine low temperature recovery. It looks obvious that low temperature recovery above about 120°C is markedly influenced by the incubation stage.

ACKNOWLEDGMENT

It is a pleasure for us to express our sincerest thanks to Professor Y. L. Yousef for his constant interest in this work.

REFERENCES

ANDERSON, W. A., and MEHL, R. F., 1945, *Trans. Amer. Inst. Mech. Engrs*, **161**, 140.
BECK, P. A., 1954, *Advanc. Phys.*, **3**, 245.
BOWEN, D., EGGLESTON, R. R., and KROPSCHOT, R. H., 1952, *J. appl. Phys.*, **23**, 630.
CAHN, R. W., 1950, *Proc. phys. Soc. Lond.* A, **63**, 323.
COTTRELL, A. H., 1953, *Prog. met. Phys.*, **4**, 254.
DARLING, A. S., 1956/7, *J. Inst. Met.*, **85**, 489; 1958, *Bull. Inst. Met.*, **4**, 92.
GAY, P., HIRSCH, P. B., and KELLY, A., 1954, *Acta Cryst.*, **7**, 41.
HASIGUTI, R. R., and HIRAI, T., 1951, *J. appl. Phys.*, **22**, 1084.
HIRONE, T., KUNITOMI, N., and ABE, M., 1955, *J. phys. Soc. Japan*, **10**, 96.
KAMEL, R., 1953, *J. appl. Phys.*, **24**, 1308.
KAMEL, R., and ATTIA, E. A., 1957, *J. appl. Phys.*, **28**, 1365; 1958, *Bull. J. Inst. Met.*, **4**, 56.
KENNEDY, A. J., 1955, *Proc. phys. Soc. Lond.* B, **68**, 257.
NOWICK, A. S., 1954, *J. appl. Phys.*, **25**, 1129.
PERRYMAN, E. C. W., 1954, *Acta Met.*, **2**, 26.
READ, W. T., 1953, *Dislocations in Crystals* (New York: McGraw-Hill).
SLIFKIN, L., and KAUZMANN, T. W., 1952, *J. appl. Phys.*, **23**, 746.
STROH, A. N., 1954, *Proc. phys. Soc. Lond.*, **67**, 427.
SUBRAHMANYAM, S. V., 1956, *Nature, Lond.*, **177**, 852.
THORLEY, N., 1950, *J. Inst. Met.*, **77**, 141.
WEERTMAN, J., 1955, *J. appl. Phys.*, **26**, 202.
YOUSEF, Y. L., and KAMEL, R., 1956, *J. appl. Phys.*, **25**, 1064.

On the Derivation of Cosmic Ray Specific Yield Functions†

By W. R. WEBBER‡ and J. J. QUENBY
Imperial College of Science and Technology, London

[Received November 29, 1958]

ABSTRACT

A series of revised differential response curves and yield functions have been deduced for the nucleonic and ionizing components of the secondary cosmic radiation at various atmospheric depths, using the most recent data on the primary spectrum and on geomagnetic cut-off rigidities.

§ 1. INTRODUCTION

UNTIL comparatively recently it has not been possible to study the time variations of the primary cosmic rays directly; instead it has been necessary to record the secondary radiation deep in the atmosphere at mountain altitudes or at sea-level, and then to deduce the nature of the variations in primary intensity from these observations. This can only be done in a satisfactory manner provided we know accurately the so-called specific yield functions which give the number of secondary particles produced at any given depth in the atmosphere as a function of the energy of the primary particles. In principle these yield functions can be calculated from a knowledge of the interaction processes involved in the atmosphere, but in fact this is not practicable because of the uncertainties involved. It is better to use an empirical approach which consists in taking the ratio of the measured differential latitude variation for the particular secondary component to the measured differential primary rigidity spectrum. This gives an average or ' gross ' yield function for all the charge components of the primary radiation.

Fonger (1953) used this approach to obtain yield functions for the nucleonic component at 680 g/cm^2 atmospheric depth and for the ionizing component at sea-level. Fonger's nucleonic component yield function has since been revised by Brown (1957), and Dorman (1957) has derived a comprehensive series of differential response curves for the nucleonic and ionizing components at various atmospheric depths.

Recently it has become clear, however, that calculated cut-off rigidities based on the dipole field of the earth may be seriously in error. These errors are such that they can substantially alter the previously derived response curves and yield functions as well as the interpretations based upon them. Moreover, recent work during the period 1954–58 (solar minimum to solar maximum) has led to a better understanding of the form of the primary spectra of the various charge components of the primary radiation. This is particularly true for the proton component and for the low rigidity end of the primary spectra for all the various charge components. This new information about the primary spectra leads to a substantial change in the form of the yield functions, particularly at the important low-energy end.

---

† Communicated by Professor P. M. S. Blackett, F.R.S.
‡ Now at the University of Maryland, U.S.A.

In view of these developments it seems appropriate at this time to re-examine the problem of differential response curves and yield functions. In this paper a series of new yield functions are derived for the nucleonic and ionizing components at various atmospheric depths using the modified cut-off rigidities derived by us (Quenby and Webber 1959) together with the most recent data on the spectrum of the primary radiation.

§ 2. CONSTRUCTION OF DIFFERENTIAL RESPONSE CURVES FOR SECONDARIES

Detectors of the secondary radiation located deep in the atmosphere respond mainly to the products of primary radiation incident near the vertical at the top. Thus, although the cut-off rigidity at any point depends on zenith and azimuth angle, the vertical cut-off rigidity is a reasonably good approximation to the lower limit of the primary rigidity spectrum capable of affecting a detector at that point. This approximation improves as the depth of the detector in the atmosphere increases. We can therefore write the total differential counting rate $dN(P,x,t)/dP$ of a nucleon or ionizing detector located a depth x, at time t and at a vertical cut-off rigidity P as

$$\frac{dN(P,x,t)}{dP}=\sum_z S_z(P,x)\frac{dj_z(P,t)}{dP} \quad . \quad . \quad . \quad . \quad . \quad (1)$$

where $dj_z(P,t)/dP$ is the differential primary rigidity spectrum in the direction of vertical incidence, defined as particles per unit solid angle per unit rigidity range per unit time, for the component of charge z and $S_z(P,x)$ is the specific yield function for the particular charge component at rigidity P and depth x.

From this it follows that

$$N(P,x,t)=\sum_z\int_P^\infty S_z(P,x)\frac{dj_z(P,t)}{dP}\,dP. \quad . \quad . \quad . \quad . \quad (2)$$

The quantity $N(P,x,t)$ is the experimentally measured response curve of the nucleonic or ionizing component as measured from latitude surveys. Equation (1) contains the yield functions for the individual charge components of the primary spectrum and none of these is at present known. We can, however, simplify eqn. (1) by assuming that the binding energy of nucleons in primary nuclei of $z>1$ is unimportant at cosmic ray energies and that the constituent nucleons interact independently in the atmosphere. Now for a given kinetic energy per nucleon it is easy to show that the rigidity of a nucleus of $z\geqslant 2$ is equal to twice the rigidity of a proton. Thus the yield function for a single nucleon in a nucleus of rigidity P is the same as the yield function for a free proton at a rigidity $\frac{1}{2}P$. Thus

$$S_z(P,x)=AS_p(\tfrac{1}{2}P,x) \quad . \quad . \quad . \quad . \quad . \quad . \quad . \quad . \quad (3)$$

for $z \geqslant 2$ where $S_p(P,x)$ is the proton specific yield function and A is the mass number of the particular nucleus. Then we have

$$N(P,x,t)=\int_P^\infty S_p(P,x)\frac{dj_p(P,t)}{dP}\,dP+\sum_z A\int_P^\infty S_p(\tfrac{1}{2}P,x)\left(\frac{dj_{z\geqslant 2}(P,t)}{dP}\right)dP. \quad . \quad . \quad . \quad (4)$$

Provided $N(P,x,t)$ and $[dj_z(P,t)/dP]$ are known $S_p(P,x)$, which is the only remaining unknown function in eqn. (4) can be deduced. In principle, $N(P,x,t)$ and $[dj_z(P,t)/dP]$ should be measured simultaneously in order to avoid difficulties due to time variations of the intensities. This has not yet been possible, but fortunately extensive cosmic ray measurements were made between mid-1954 and mid-1955 when solar activity was at a minimum and as a consequence only small variations in the cosmic ray intensity occurred.

In this period the neutron and ionizing intensities were measured as a function of latitude at sea-level (Rose *et al.* 1956) and neutron intensities were measured as a function of latitude at 680 g/cm^2, 312 g/cm^2 (also ionizing component) and 175 g/cm^2 (Meyer and Simpson 1955). Several measurements on the energy spectra of alpha particles and protons were also carried out at this time (McDonald 1956, McDonald and Webber 1959, Fowler *et al.* 1957, Waddington 1956). We shall therefore consider this as our ‘ base ’ period and use only data obtained at this time.

The differential response curves constructed from the above data on the nucleonic and ionizing components are shown in fig. 1. The curves are all normalized by requiring $N(15,x,t_0)=100$. The quantities $N(P,x,t_0)$ and $[dN(P,x,t_0)/dP]$ are also tabulated at intervals of 1 GV in table 1.

The sea-level differential response curve for the ionizing component at rigidities below 10 GV was derived by using data obtained during the flare of February 23, 1956. This was done by assuming the neutron differential response curve at sea-level to be correct at these rigidities, and comparing the relative flare increases for neutron and ionizing detectors at the same cut-off. The differential response curves for counter telescopes and ion chambers are indistinguishable for latitude survey data at sea-level, although at 312 g/cm^2 the ion chamber shows a noticeably larger response below 5 GV. This is confirmed by the relative responses of the two types of detector during the flare of February 23, 1956. For all types of variations other than the flares, however, this difference is immaterial. Consequently we have used the mean value of counter telescope and ion chamber results to represent the curves for the ionizing component at sea-level and at a depth of 312 g/cm^2.

Above 15 GV it is impossible to determine experimentally the differential response curves because of the limitations set by the earth’s field. However, in the region between 10–15 GV it is found that the differential response curves can be approximated by the power law

$$\frac{dN(P, x, t_0)}{dP} = KP^{-\gamma_1} \quad . \; . \; . \; . \; . \; . \; . \; . \quad (5)$$

Fig. 1

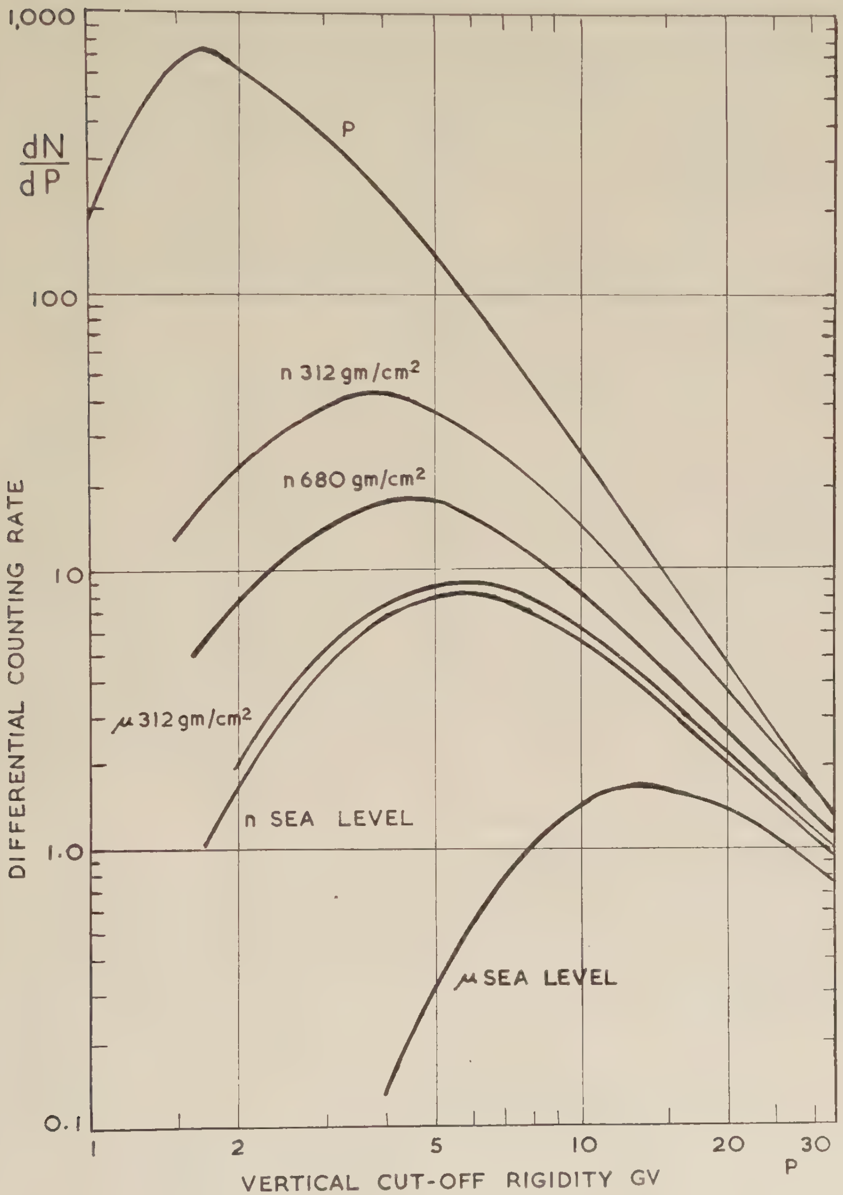

Differential response curves. Differential counting rates as a function of vertical cut-off rigidity for various detectors. All curves normalized such that $N(15, x, t_0) = 100$. n—neutron monitor, μ—ionizing component detector, P—primary radiation.

Table 1. $dN(P,x,t_0)/dP$ and $N(P,x,t_0)$ as a function of P for neutron and μ-meson detectors at various atmospheric depths and for the primary radiation. Curves normalized so that $N(15,x,t_0)=100$ in all cases

P (GV)	Sea-level nucleonic		680 g/cm² nucleonic		312 g/cm² nucleonic		Primary		Sea-level μ's		312 g/cm² μ's	
	dN/dP	N	dN/dP	N	dN/dP	N	dN/dP	N	dN/dP	N	dN/dP	N
1·0				244·8		400·3		2091				
1·5			4·0		13·1		640					
2·0		174·1		240·8		387·2		1451				184·2
2·5	3·2		11·2		32·4		495				3·8	
3·0		170·9		229·6		354·8		956				180·4
3·5	5·8		16·5		43·0		275				6·7	
4·0		165·1		213·1		311·8		681		112·8		173·7
4·5	7·6		18·7		41·2		172		0·21		8·6	
5·0		157·5		194·4		270·6		509		112·6		165·1
5·5	8·2		17·0		34·2		117		0·40		9·2	
6·0		149·3		177·4		236·4		392		112·2		155·9
6·5	8·1		14·6		28·2		80·0		0·65		9·1	
7·0		141·2		162·8		208·2		311·7		111·6		146·8
7·5	7·5		12·6		23·2		55·0		0·91		8·5	
8·0		133·7		150·2		185·0		256·7		110·7		138·3
8·5	6·7		10·5		18·8		41·5		1·18		7·6	
9·0		127·0		139·7		166·2		215·2		109·5		130·7
9·5	6·0		9·1		15·9		31·4		1·35		6·8	
10·0		121·0		130·6		150·3		183·8		108·1		123·9
10·5	5·2		7·9		13·5		24·3		1·51		6·0	
11·0		115·8		122·7		136·8		159·5		106·6		117·9
11·5	4·6		6·8		11·3		19·4		1·62		5·3	
12·0		111·2		115·9		125·5		140·1		105·0		112·6
12·5	4·1		5·9		9·7		16·0		1·65		4·6	
13·0		107·1		110·0		115·8		124·1		103·3		108·0
13·5	3·8		5·3		8·5		13·1		1·68		4·2	
14·0		103·3		104·7		107·3		111		101·7		103·8
14·5	3·3		4·7		7·3		11·0		1·66		3·8	
15·0		100		100		100		100		100		100
15·5	3·0		4·2		6·4				1·60		3·4	

and it seems reasonable to assume that at rigidities greater than 15 GV the differential response curves can similarly be represented by a power law of the form

$$\frac{dN(P,x,t_0)}{dP}=KP^{-\gamma_2}. \qquad (6)$$

(Note that this is not so for the differential response curve for the ionizing component at sea level which has a maximum in this region but which we assume to follow a power law above 25 GV.)

γ_2 can be calculated from the following considerations:

(1) The normalization condition which required

$$\int_{15}^{\infty} KP^{-\gamma_2}\,dP=100 \qquad (7)$$

and (2) the experimentally observed differential response curve at 15 GV

$$\frac{dN(15,x,t_0)}{dP}=C. \qquad (8)$$

Combining (7) and (8) we may write

$$\gamma_2=1+0{\cdot}15C. \qquad (9)$$

If we now require continuity of slope at 15 GV, then $\gamma_1=\gamma_2$. In practice we first calculate γ_2 from the experimental data, comparing this with the observed γ_1. In all cases they are very nearly equal and require only a slight readjustment of the experimentally determined quantities γ_1 and C to obtain continuity of slope at 15 GV. The adjusted values of $\gamma_1=\gamma_2$ are: 1·51 for neutrons at sea-level, 1·69 for neutrons at 680 g/cm^2, 2·12 for neutrons at 312 g/cm^2 (compare with 2·5 for the primary flux), 1·32 for the ionizing component at sea-level and 1·54 for the ionizing component at 312 g/cm^2.

§ 3. THE PRIMARY RIGIDITY SPECTRA

It is convenient in the discussion that follows to consider the primary rigidity spectra in two separate regions (1) above 5 GV. (2) below 5 GV.

In region (1) we shall assume that the primary spectra approach very closely a power law with a constant exponent. Table 2 lists the rigidity spectra for the various charge components as determined by Webber (1958). For convenience we also show the spectra as a function of total energy per nucleon.

These spectra have been discussed in detail in the preceding reference but it is of interest to note here that all charge components have the same exponent in either the differential rigidity or total energy expressions.

Using Webber's spectra the composition of the primary radiation in percentage of nucleons in a given interval of rigidity is as follows: protons = 49·5%; alphas = 33·0%; CNOF = 10·6%; and $Z\geqslant 10=6{\cdot}9\%$.

Thus for numerical purposes we may consider that in a given rigidity interval the number of nucleons brought in by protons is equal to the number brought in by heavier nuclei.

Fig. 2

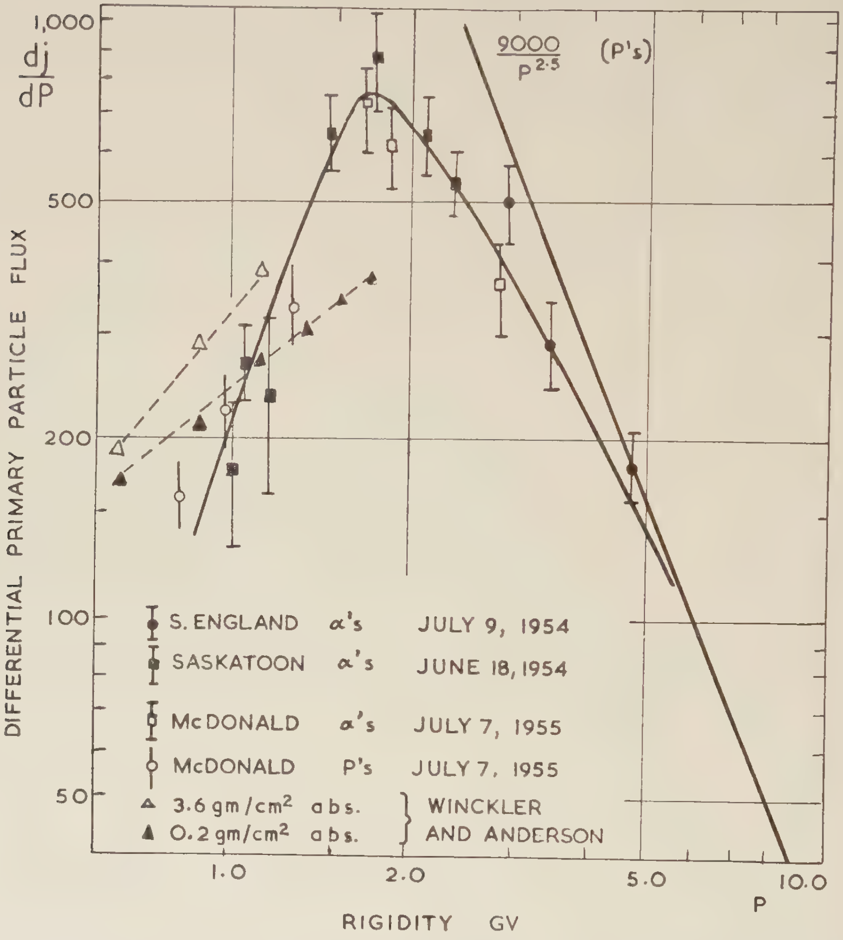

Differential primary spectrum at low rigidities. Alpha-particle intensities multiplied by 6. Proton curve normalized such that $j_p(15, t_0) = 100$.

In the region below 5 GV the primary spectra can no longer be approximated by a simple power law and are, in addition, considerably influenced by primary time variations. Because of the variability of the spectrum in this region we have chosen measurements made only in the period from mid-1954 to mid-1955. The alpha-particle spectrum has been measured in this rigidity region over Southern England (Waddington

1956) and over Saskatoon (Fowler *et al.* 1957) in 1954, using photographic emulsions. In 1955 McDonald (1956) measured the alpha-particle differential spectrum over Minneapolis using a Čerenkov–scintillation counter, obtaining close agreement with the emulsion results and thus indicating no major changes in the shape of the differential spectrum. On this same flight McDonald was able to measure the differential primary proton spectrum over a rather narrow range of rigidities (McDonald and Webber 1959). These proton intensities are shown in fig. 2 together with the alpha-particle intensities, which have been multiplied by six for ease of comparison with the protons. The proton spectrum as given in table 2 for $P>5$ GV is also shown and the normalization used is $j_p(15,t_0)=100$ which gives $dj_p(15,t_0)/dP=11$. The similarity in shape of the proton and alpha particle spectra at both high rigidities and in the region of 1 GV strongly indicates that the mechanism that produced the peak in the differential rigidity spectrum in 1954 affected the protons and alphas alike (and indeed the heavier nuclei as well as has been pointed out by Ellis *et al.* 1954) and seems to have been a rigidity dependent mechanism. This deduction has been strengthened and extended by measurements of McDonald in 1956 and 1958 (McDonald and Webber 1959) and is in agreement with the recent work of the Minnesota group (Frier *et al.* 1958) on the differential rigidity spectrum for alphas in 1957–58.

Table 2. Differential Spectra of Rigidity and Total Energy per Nucleon for the Various Charge Components in the Primary Radiation ($P>5$ GV)

	Rigidity	Total energy/nucleon
Protons	$\frac{9000}{P^{2\cdot5}}$	$\frac{9000}{E_T{}^{2\cdot5}}$
Alphas	$\frac{1500}{P^{2\cdot5}}$	$\frac{640}{E_T{}^{2\cdot5}}$
CNOF	$\frac{135}{P^{2\cdot5}}$	$\frac{42}{E_T{}^{2\cdot5}}$
$Z\geqslant10$	$\frac{45}{P^{2\cdot5}}$	$\frac{14}{E_T{}^{2\cdot5}}$

Spectra normalized such that integral proton flux is 100 at P or $E_T=15$.

We shall therefore conclude that the charge composition of the primary radiation remains the same at all rigidities, and that the shape of the low rigidity end of the primary spectrum for all charge components at sunspot minimum, 1954–55, is represented by fig. 2. This picture of the low-rigidity end of the primary spectrum is consistent with a series of measurements on the total radiation at the top of the atmosphere made by Winckler and Anderson (1957) in the summer of 1955. These measurements were made with counter telescopes with and without absorber between $\lambda = 51°$ ($P_M = 2{\cdot}05$ GV) and $\lambda = 65°$ ($P_M = 0{\cdot}30$ GV). The differential response curves of the two telescopes have been found at a fixed depth of 10 g/cm² using the vertical cut-off rigidities derived by us, and these should give an approximate measure of the differential rigidity spectrum of the total incident primary radiation. The counting rates of the telescopes at a vertical cut-off of 15 GV were found from previous equatorial latitude flights with similar telescopes. Thus it was possible to normalize the differential response curves such that the integral counting rate at 15 GV was equal to 100. The curves obtained by this procedure are shown in fig. 2.

§ 4. DETERMINATION OF SPECIFIC YIELD FUNCTIONS

Since the shapes of the primary differential rigidity spectra for all the charge components are the same we may re-write eqn. (1) in the following form by making use of eqn. (3):

$$\frac{dN(P,x,t)}{dP} = \left[S_p(P,x) + \sum_z K_z A S_p(\tfrac{1}{2}P,x)\right]\frac{dj_p(P,t)}{dP}. \qquad (10)$$

K_z is the abundance of nuclei of charge z in any rigidity interval relative to the proton abundance taken as unity. If we define the 'gross' yield function by

$$S_G(P,x) = S_p(P,x) + \sum_z K_z A S_p(\tfrac{1}{2}P,x) \quad . \quad . \quad . \quad . \quad (11)$$

we can find $S_G(P,x)$ by taking the ratio of the particular differential response curve as shown in fig. 1 and the differential primary proton spectrum as shown in fig. 2. It is more interesting, however, to find the proton specific yield function, $S_p(P,x)$, since from this the yield functions for all the charge components can be deduced using eqn. (3). Recalling that in a given interval of cut-off rigidity the number of nucleons contributed by nuclei with $z \geqslant 2$ is approximately equal to the number contributed by protons we may re-write eqn. (11) as

$$S_G(P,x) = S_p(P,x) + S_p(\tfrac{1}{2}P,x). \quad . \quad . \quad . \quad . \quad . \quad (12)$$

If we write $S_p(\frac{1}{2}P,x) = S_{z\geqslant 2}(P,x)$ then $S_{z\geqslant 2}(P,x)$ represents the yield from all nuclei of $z \geqslant 2$, taking into account the abundance of these nuclei relative to the protons. We can now deduce the function $S_p(P,x)$ from eqn. (12) by introducing a series of trial yield functions $S_p{}^i(P,x)$ and $S^i{}_{z\geqslant 2}(P,x)$ and this can be done separately for each type of detector and atmospheric depth. The first step is to assume that $S_p{}^1(P,x)$ is given by $S_G(P,x)$, the 'gross' yield function, which is directly derived from measured quantities. Then we have $S^1{}_{z\geqslant 2}(P,x) = S_p{}^1(\frac{1}{2}P,x)$. Remembering that (12) must be satisfied, a better approximation to $S_p(P,x)$ is obtained by finding

$$S_p{}^2(P,x) = S_G(P,x) - S^1{}_{z\geqslant 2}(P,x). \quad . \quad . \quad . \quad . \quad (13)$$

This allows us to deduce $S^2_{z\geqslant 2}(P,x)$ and the iteration is repeated until the process converges such that

$$S_G(P,x)=S_p^{\,n}(P,x)+S_p^{\,n}(\tfrac{1}{2}P,x) \quad . \; . \; . \; . \; . \quad (14)$$

Fig. 3

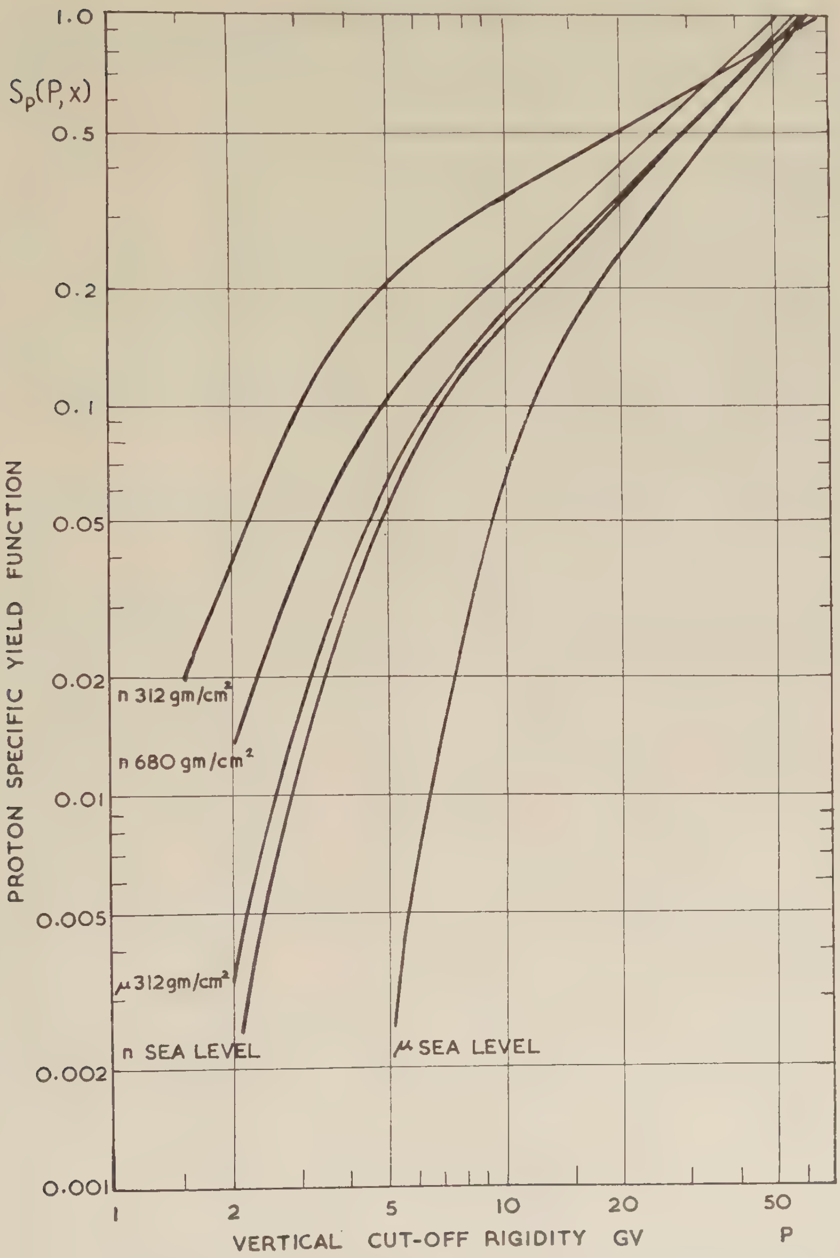

Proton specific yield functions as a function of vertical cut-off rigidity for various detectors. n—neutron monitor, μ—ionizing component detector.

is satisfied. The proton specific yield functions derived in this way are shown in fig. 3 for various detectors and atmospheric depths and both the 'gross' yield functions and the yield functions for $z \geqslant 2$ nuclei are easily deducible from these curves.

ACKNOWLEDGMENTS

The authors wish to thank Dr. H. Elliot for helpful discussions. Both the authors are indebted to the Department of Scientific and Industrial Research for financial support.

REFERENCES

Brown, R. R., 1957, *Nuovo Cim.*, **6,** 956.
Dorman, L. I., 1957, *Cosmic Ray Variations* (Moscow: State Publishing House for Technical and Theoretical Literature).
Ellis, R. A., Gottlieb, M. B., and Van Allen, J. A., 1954, *Phys. Rev.*, **95,** 304.
Fonger, W. H., 1953, *Phys. Rev.*, **91,** 351.
Fowler, P. H., Waddington, C. J., Frier, P. S., Naugle, J., and Ney, E. P., 1957, *Phil. Mag.*, **2,** 157.
Frier, P. S., Ney, E. P., and Fowler, P. H., 1958, *Nature, Lond.*, **181,** 1319.
McDonald, F. B., 1956, *Phys. Rev.*, **104,** 1723.
McDonald, F. B., and Webber, W. R., 1959, *Phys. Rev.* (in the press).
Meyer, P., and Simpson, J. A., 1955, *Phys. Rev.*, **99,** 1517, and references given therein.
Quenby, J. J., and Webber, W. R., 1959, *Phil. Mag.*, **4,** 90.
Rose, D. C., Fenton, K. B., Katzman, J., and Simpson, J. A., 1956, *Canad. J. Phys.*, **34,** 968.
Waddington, C. J., 1956, *Nuovo Cim.*, **3,** 930.
Webber, W. R., 1958, *Nuovo Cim. Suppl.*, **2,** 532.
Winckler, J. R., and Anderson, K., 1957, *Phys. Rev.*, **108,** 148.

Some Dislocation Interactions in Simple Ionic Crystals†

By B. H. Kear
The Franklin Institute Laboratories, Philadelphia 3, Pennsylvania, U.S.A.

A. Taylor and P. L. Pratt
Department of Physical Metallurgy, University of Birmingham, England

[Received March 11, 1959]

Abstract

Dislocation intersections in ionic crystals can produce both charged and uncharged jogs, as well as vacancies and interstitial ions. Dislocation reactions helped by the retarding effect of these jogs, can give rise to sessile dislocations by a zip-fastening mechanism. In this way the formation of boundaries during irrational twinning may be explained.

§ 1. Introduction

Ionic crystals having the sodium chloride crystal structure commonly slip on the $\{110\}$ planes in the $\langle 1\bar{1}0\rangle$ directions. Certain crystals in this class slip additionally upon $\{100\}$ and $\{111\}$ planes, and in the case of silver chloride, 'pencil-glide' occurs by slip simultaneously on all three planes containing a common $\langle 110\rangle$ direction. This paper considers the intersections and reactions that may occur between dislocations moving in these $\langle 110\rangle$ directions. For simplicity, the dislocations are considered to be moving on $\{110\}$ planes.

When one dislocation cuts through another, each dislocation acquires a jog equal to the component normal to its own slip plane of the other dislocation's Burgers vector (Read 1955). Thus for the sodium chloride structure, dislocations moving on orthogonal (110) planes will both acquire jogs of length $\mathbf{b}$ when they intersect, where $\mathbf{b}$ is the Burgers vector of the dislocations. In the particular case where the jog is acquired by a moving screw dislocation the result is the generation of a double row of alternately positive—and negative—ion vacancies, or interstitial ions, depending on the relationship between the Burgers vectors of the cutting dislocations. On the other hand, when dislocations moving on (110) planes inclined obliquely to one another intersect, jogs of length $\frac{1}{2}\mathbf{b}$ are formed, and these are charged electrostatically (Seitz 1951). Such a jog in a moving screw dislocation leaves a single row of alternately positive—and negative—ion vacancies (or interstitial ions) in its wake.

---

† Communicated by the Authors.

This result has been stated briefly by Fischbach and Nowick (1958), whereas Seeger (1954) has considered only the case of orthogonal intersection. It is of interest to consider the oblique intersections in some detail after the manner of Kear (1957) since they appear to play an important role in the plastic deformation of ionic crystals.

§ 2. INTERSECTION BETWEEN EDGE AND EDGE, OR EDGE AND SCREW DISLOCATIONS ON OBLIQUE PLANES

Consider an edge dislocation AB, fig. 1, gliding on (110) with Burgers vector $\frac{1}{2}\mathbf{a}[110]$, which cuts through another stationary dislocation CD on (011) with Burgers vector $\frac{1}{2}\mathbf{a}[011]$. The relationship of the latter to the glide plane (110) is shown in the unit cube (representing (100) faces) in the centre of the figure. The extra half-plane of the cutting dislocation experiences a shift at the point of intersection and the dislocation line becomes jogged. The jog PQ formed on intersection is best seen in terms of three components. The vector components of $\mathbf{b}$, resolved in and normal to the slip plane of the cutting dislocation are $\frac{1}{2}\mathbf{b}$, $\frac{1}{2}\mathbf{b}$ and $\mathbf{b}/\sqrt{2}$ (as shown in fig. 1) in relation to the unit cube. The figure shows that the vector $\mathbf{b}/\sqrt{2}$ merely increases the length of the dislocation line AB. Since $\mathbf{b}=\frac{1}{2}\sqrt{2}(\mathbf{a})$ where $\mathbf{a}$ is the side of the unit cell, the increment $\mathbf{b}/\sqrt{2}$ represents an extra layer of ions parallel to (001). The other two

Fig. 1

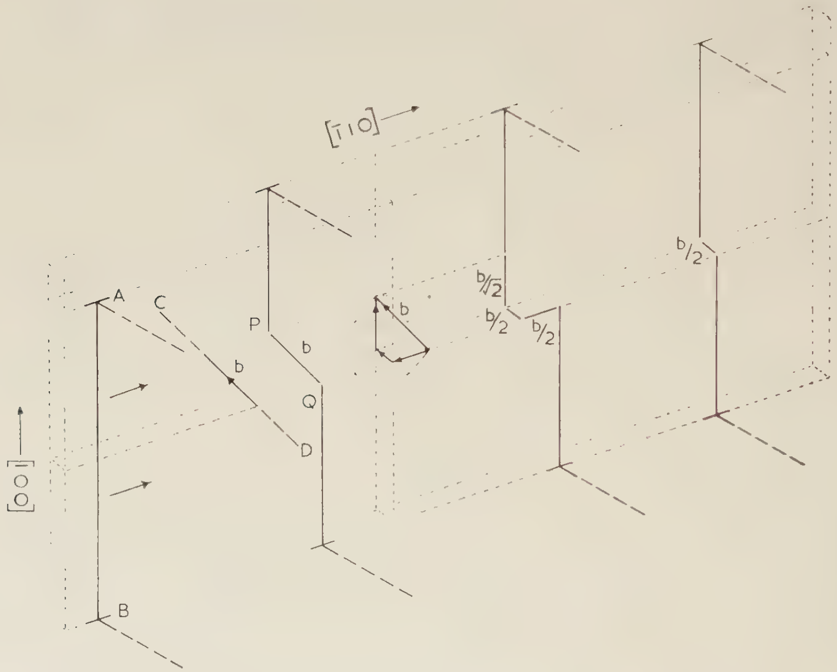

vectors form jogs, one of which is in the slip plane and the other perpendicular to it. The jog or kink in the slip plane can be eliminated by pure glide. The other jog, however, remains and must glide with its dislocations. Since this jog is a small segment of edge dislocation lying in the (100) plane, it can glide, with difficulty, with its dislocation.

§ 3. INTERSECTION BETWEEN SCREW AND EDGE, OR SCREW AND SCREW DISLOCATIONS ON OBLIQUE PLANES

A similar argument can be developed for the case in which the cutting dislocation is a pure screw dislocation. As before, the jog formed in the cutting dislocation of length $\mathbf{b}$ may be considered in terms of a three-component jog complex. One jog $\frac{1}{2}\mathbf{b}$ increases the length of the dislocation by adding an extra plane of ions perpendicular to the (110) slip planes, and the other displaces the line of the screw dislocation from one (110) plane to the next parallel one above. The jog $\mathbf{b}/\sqrt{2}$ advances one part of the line with respect to the other, which is equivalent to the spacing between two parallel (100) planes. This jog is in the slip plane and, as before, can be eliminated by pure glide. The net result is a screw dislocation with a single jog of length $\frac{1}{2}\mathbf{b}$ perpendicular to the slip plane. Such a jog will retard the motion of the screw dislocation since it will leave a trail of point defects in its wake.

§ 4. DISLOCATION REACTIONS

Possible reactions between dislocations capable of gliding on $\{110\}$ planes and having Burgers vectors $\frac{1}{2}\mathbf{a}\langle 110\rangle$ are of three types:

(i) $\frac{1}{2}\mathbf{a}[01\bar{1}]+\frac{1}{2}\mathbf{a}[0\bar{1}\bar{1}]\rightarrow \mathbf{a}[00\bar{1}]$,

(ii) $\frac{1}{2}\mathbf{a}[\bar{1}01]+\frac{1}{2}\mathbf{a}[0\bar{1}\bar{1}]\rightarrow \frac{1}{2}\mathbf{a}[\bar{1}\bar{1}0]$,

(iii) $\frac{1}{2}\mathbf{a}[10\bar{1}]+\frac{1}{2}\mathbf{a}[0\bar{1}\bar{1}]\rightarrow \frac{1}{2}\mathbf{a}[1\bar{1}\bar{2}]$.

Of these the first reaction is between dislocations on orthogonal slip planes, and the other two between dislocations on oblique slip planes. It is not certain that the first reaction will take place because the elastic energy is not reduced, although Amelinckx (1958) has observed this reaction experimentally in certain cases in potassium chloride. Dissociation of the $\mathbf{a}[00\bar{1}]$ dislocation into a pair of $\frac{1}{2}\mathbf{a}[00\bar{1}]$ dislocations is not possible in sodium chloride since it would necessitate the creation of a stacking fault of high energy. The second reaction is favoured since it leads to a reduction in elastic energy. However, the third reaction is unlikely since it involves an increase in energy.

Figure 2 (*a*) shows the formation of a new dislocation PQ by the association of two mixed edge and screw dislocations AB and CD, having Burgers vectors $\frac{1}{2}\mathbf{a}[\bar{1}01]$ and $\frac{1}{2}\mathbf{a}[0\bar{1}\bar{1}]$ which meet along the line of intersection PQ of their slip planes, (101) and $(0\bar{1}1)$ respectively. The new dislocation is pure edge with Burgers vector $\frac{1}{2}\mathbf{a}[110]$, and should be

Fig. 2

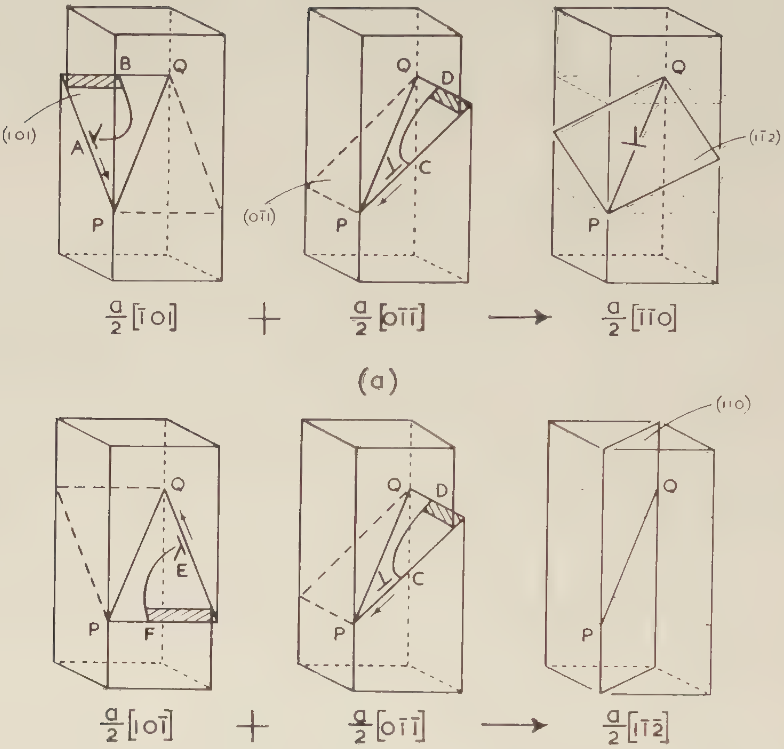
B
Q
(101)
A
P
Q
D
C
(01̄1)
P
Q
(11̄2)
P
$\frac{a}{2}[\bar{1}01]$ + $\frac{a}{2}[0\bar{1}\bar{1}]$ → $\frac{a}{2}[\bar{1}\bar{1}0]$
Q
E
P
F
Q
D
C
P
(110)
Q
P
$\frac{a}{2}[10\bar{1}]$ + $\frac{a}{2}[0\bar{1}\bar{1}]$ → $\frac{a}{2}[1\bar{1}\bar{2}]$

(a)

(b)

Fig. 3

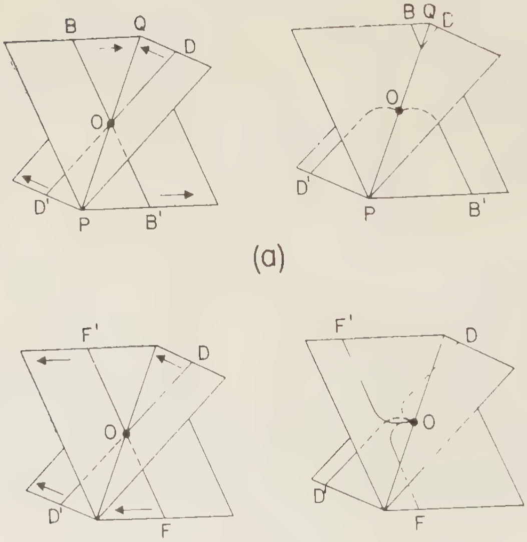

(a)

(b)

capable of gliding on the (112) plane, since this plane contains both its line and its Burgers vector. Since (112) is not a normal slip plane for sodium chloride, however, the new dislocation will be relatively immobile. The third reaction would produce a mixed dislocation PQ capable of gliding on (110) with Burgers vector $\frac{1}{2}\mathbf{a}[112]$, fig. 2 (*b*). Since this reaction involves an increase in elastic energy, it is unlikely to occur, and instead the two dislocations CD and EF will try to repel one another along the line of intersection PQ of their slip planes.

§ 5. MECHANISM OF REACTIONS

Since most of the dislocations gliding in intersecting planes are likely to intersect at points, it would appear at first consideration that the chances of a long segment PQ, fig. 2 (*a*), being formed by reaction (ii) is small. However, this is no longer the case, when the retardation due to the presence of a jog in the dislocation line is taken into account. Figure 3 (*a*), for instance, shows two pure screw dislocations BB′ and DD′ gliding towards one another under the applied stress. These dislocations are considered to be capable of reaction, according to fig. 2 (*a*). At the point of intersection O, the propagation of the screw dislocations will be checked, because the jogs subsequently formed are potential sources of vacancies, and therefore, they can glide only with difficulty. The unjogged parts of the dislocation line, however, are free to continue their glide motion. The result is that the segments OB and OD swing into the orientation OQ under the combined influence of the applied stress and the elastic attraction experienced by the dislocations. In this way, the formation of the new dislocation running in the direction OQ, fig. 3 (*a*), by a mechanism analogous to zip-fastening, is to be expected.

On the other hand, the repulsion between the two dislocations in fig. 2 (*b*) along the line PQ favours the formation of cusps in the dislocation lines by the mechanism shown in fig. 3 (*b*). Here the two pure screw dislocations DD′ and FF′, which could undergo reaction (iii), sweep past each other at the point of intersection O.

§ 6. FORMATION OF DISLOCATION BOUNDARIES BY SLIP ON INTERSECTING PLANES

So far reactions between individual dislocations on orthogonal and on inclined slip planes have been considered, and it has been shown how the jogs formed by intersection tend to favour the occurrence of these reactions. However, when slip occurs not on one plane alone but on many parallel planes of the two slip systems, the crystal may become divided macroscopically into blocks (see, for example, Taylor and Pratt (1958)). In the remaining part of this paper it is shown how dislocation intersections and reactions can lead directly to the formation of dislocation boundaries between these blocks, Slip on orthogonal planes can lead to two types of dislocation boundary under certain particular circumstances. In crystals deformed in the cube orientation slip may start independently in the two systems, one at each end of the crystal. As the deformation develops, so the two systems will grow out and meet each other in the middle of the crystal. The resulting boundary will take the form of a diffuse tilt boundary at right angles to the axis of loading since the leading edge dislocations of one slip system will have difficulty in passing through the stress field of edge dislocations in the orthogonal system.

Fig. 4

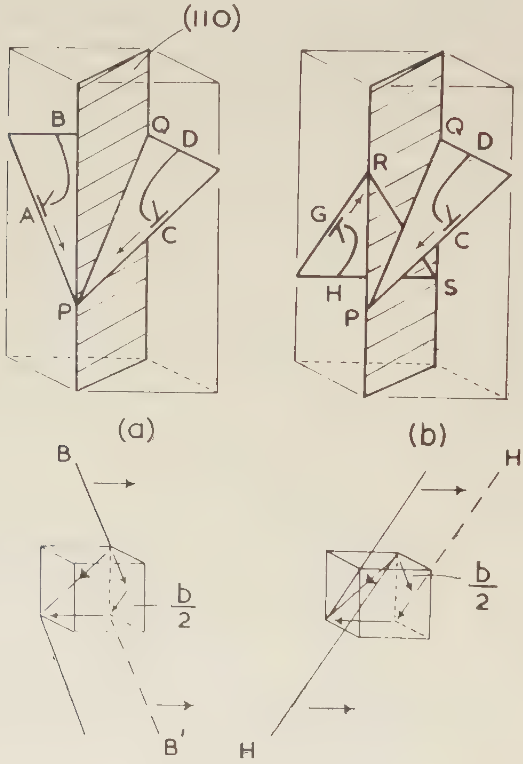

On the other hand, if slip starts in the two systems now at the same end of the crystal but on opposite sides, screw dislocations will have difficulty in intersecting those in the orthogonal system. In this case the crossed screw dislocations tend to line up into a simple twist boundary parallel to the axis of loading.

Slip on oblique planes similarly may give rise to two types of dislocation boundary, and these are commonly found during the irrational twinning of squat specimens in the cube orientation (Brilliantow and

Obreimow 1937, Taylor and Pratt 1958). In this case, however, both types of boundary may form in (110) planes parallel to the axis of loading. For slip on oblique planes of the type shown in fig. 4 (*a*), reaction (ii) will occur with the formation of edge dislocations along the lines of intersection of the slip planes of the two systems. These new edge dislocations will be in a position of minimum energy when they are lined up one above the other in a (110) plane as indicated in the figure. Such a wall of edge dislocations gives rise to a pure tilt about the [111] direction, and this is in agreement with the experiments on irrational twinning in squat specimens.

Slip on oblique planes may also occur in the manner shown in fig. 4 (*b*). Here no dislocation reactions are possible, since the dislocations can meet at a point only and not along a line. Slip on many parallel planes will produce a crossed grid of mixed edge-screw dislocations which can only intersect with difficulty. The result is a complex dislocation boundary lying in the (110) plane, with both a twist and a tilt in this plane. When equal numbers of dislocations are present on the two slip systems, this boundary may be described by a rotation about the [221] axis (Whitworth 1959, private communication).

§ 7. BREAK-UP OF BOUNDARIES

Under a sufficiently large stress, the dislocations originally held up in the boundaries will be able to continue their glide motions, even though this must involve complicated intersections between the dislocations in the two systems. The lower part of fig. 4 (*a*) shows that the intersection of the screw component of dislocation AB with the dislocation CD leads to the formation of a jog $\frac{1}{2}\mathbf{b}$, which becomes a source of vacancies, and likewise for CD following intersection with AB. On the other hand, fig. 4 (*b*) shows that when the screw component of dislocation GH intersects the dislocation CD, the jog $\frac{1}{2}\mathbf{b}$ formed becomes a source of interstitial ions; likewise for the jog in CD following intersection with GH. Thus the dissociated dislocations from the original tilt boundary are potential sources of vacancies, whereas the mixed dislocations constituting the complex boundary are potential sources of interstitial ions.

Experimental evidence showing the importance of these dislocation intersections and reactions in relation to work-hardening, and to changes in physical properties, of deformed ionic crystals will be presented shortly.

ACKNOWLEDGMENTS

The authors wish to thank Professor G. V. Raynor for providing research facilities in the Department of Physical Metallurgy, and for arranging financial support for one of us (B. H. K.). One of us (A. T.) wishes to thank the University for a Research Fellowship during the period in which this paper was being written.

REFERENCES

AMELINCKX, S., 1958, *Acta Met.*, **6,** 34.
BRILLIANTOW, N. A., and OBREIMOW, I. W., 1937, *Phys. Z. Sowjet*, **12,** 7.
FISCHBACH, D. B., and NOWICK, A. S., 1958, *J. Phys. Chem. Solids*, **5,** 302.
KEAR, B. H., 1957, Thesis, Birmingham University.
READ, W. T., 1955, *Dislocation in Crystals* (New York : McGraw-Hill), p. 85.
SEEGER, A., 1954, *Report of Bristol Conference on Defects in Crystalline Solids* (London : The Physical Society), p. 391.
SEITZ, F., 1951, *Rev. mod. Phys.*, **23,** 341.
TAYLOR, A., and PRATT, P. L., 1958, *Phil. Mag.*, **3,** 1051.

[*The Editors do not hold themselves responsible for the views expressed by their correspondents.*]

Fig. 1

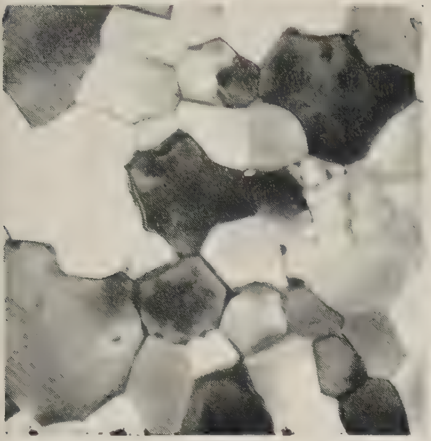

Thin foil of pure α-iron. (×80 000.)

Fig. 2

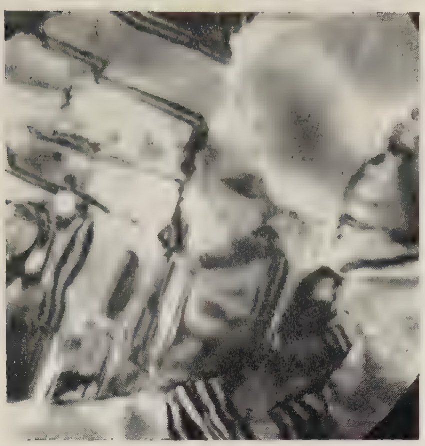

Thin foil of iron–nitrogen–austenite. (×60 000.)

Fig. 3

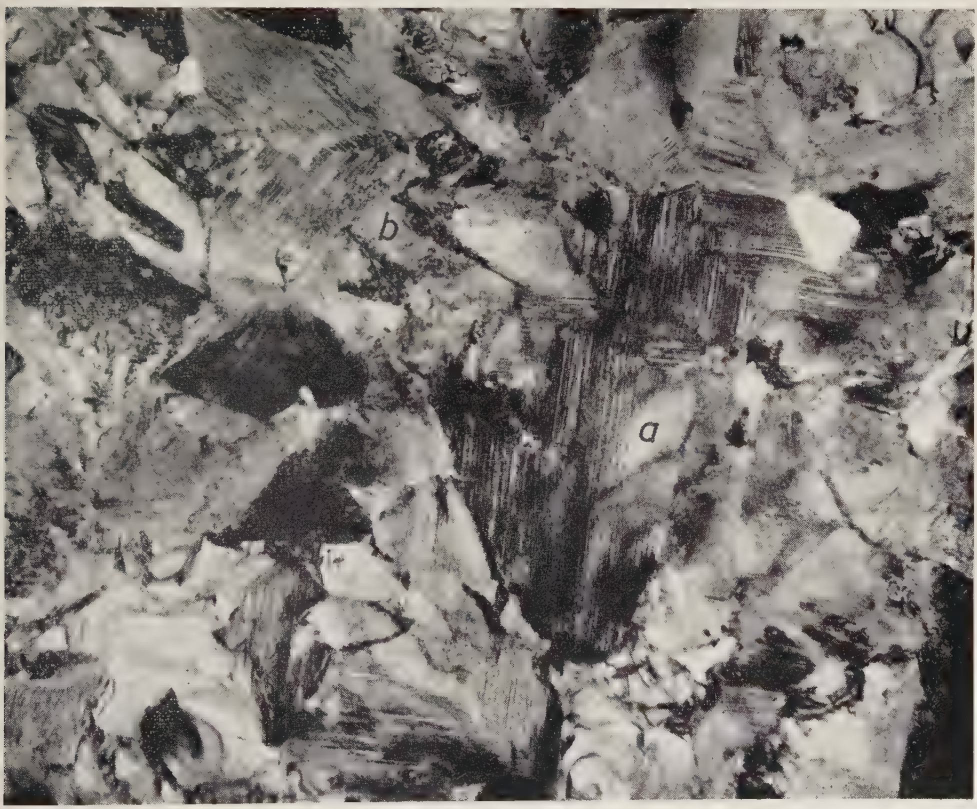

Thin foil of iron–nitrogen–martensite. (×60 000.)

Fig. 4

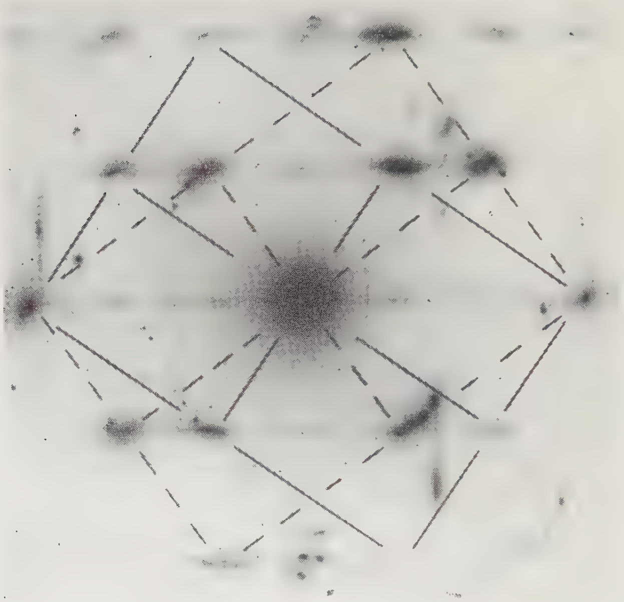

Electron diffraction of area (*a*) in fig. 3. Two schemes are drawn into the diagram in order to demonstrate the twin arrangement of the spots.

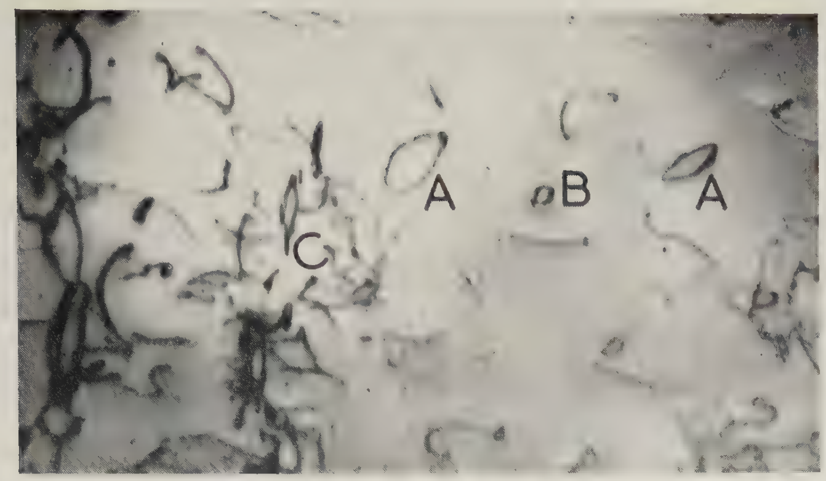

Fig. 1

Dislocations in aluminium–zinc–magnesium alloy quenched from 520°c. Large loops can be seen at A and a spiral at B. There are complex networks at C. Mag. × 30 000.

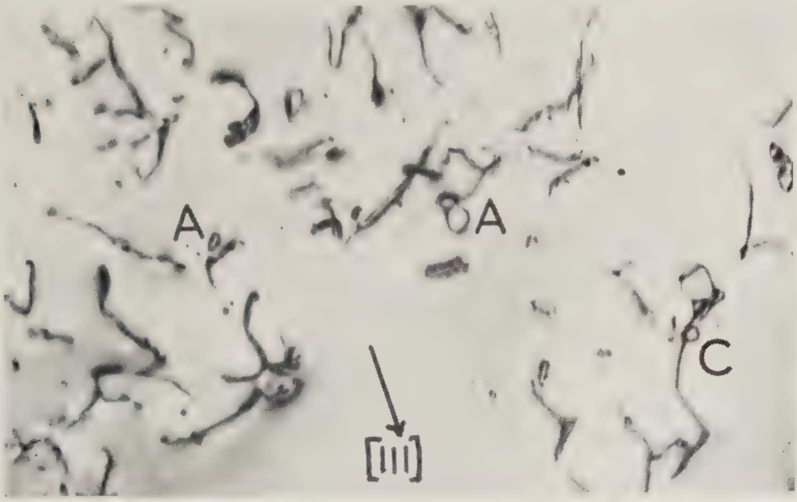

Fig. 2

As fig. 1 but showing smaller loops at A and complicated dislocation arrangements at C. Mag. × 30 000.

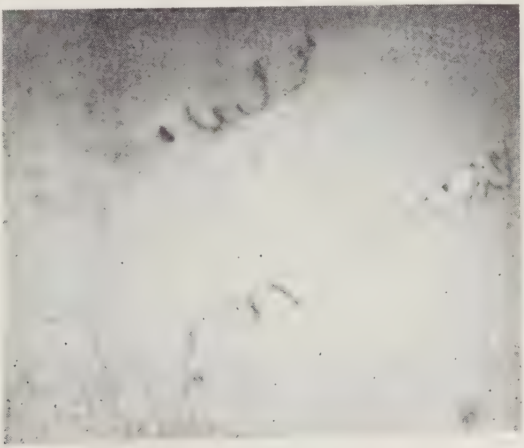

Fig. 3

Spiral or helical dislocations in aluminium–zinc–magnesium–copper alloy water-quenched from 475°c. Mag. × 40 000.

Fig. 4

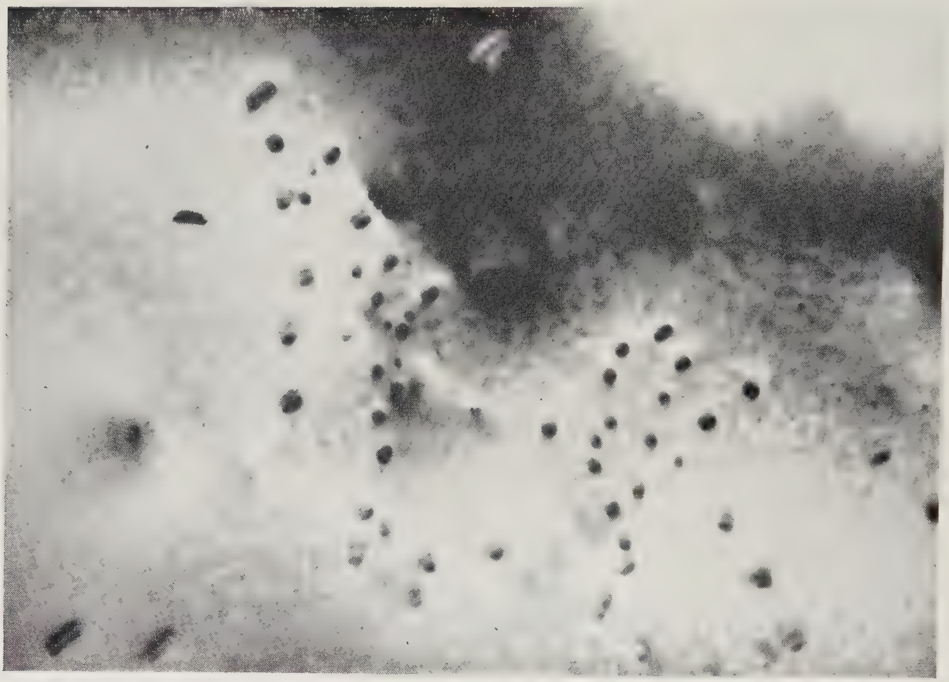

Dislocation loops—200 Å diameter in quenched ternary alloy. Note absence of dislocation lines in this area. Mag. × 70 000.

Fig. 5

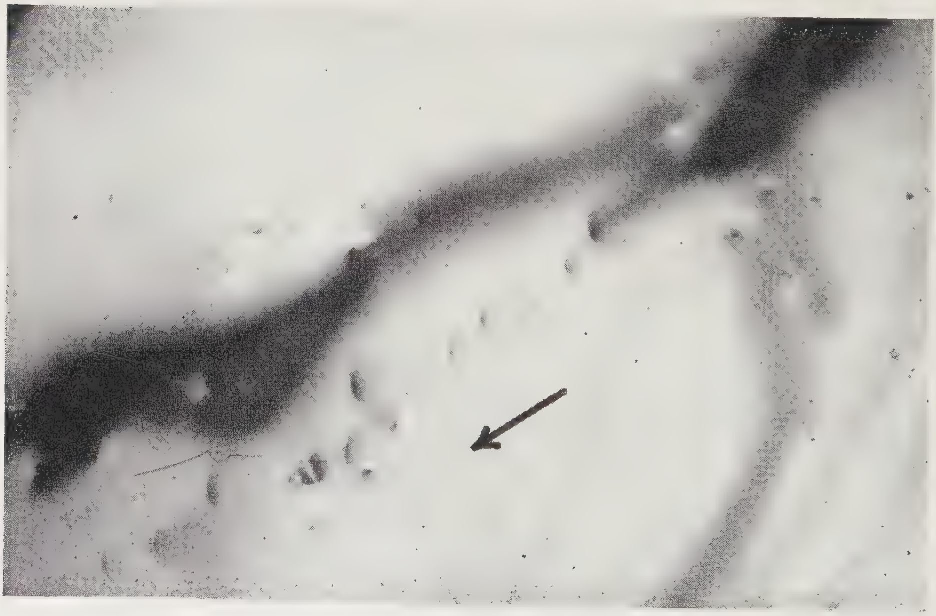

Successive dislocations moving away from the edge of a foil of quenched ternary alloy. Mag. × 40 000.

Fig. 6

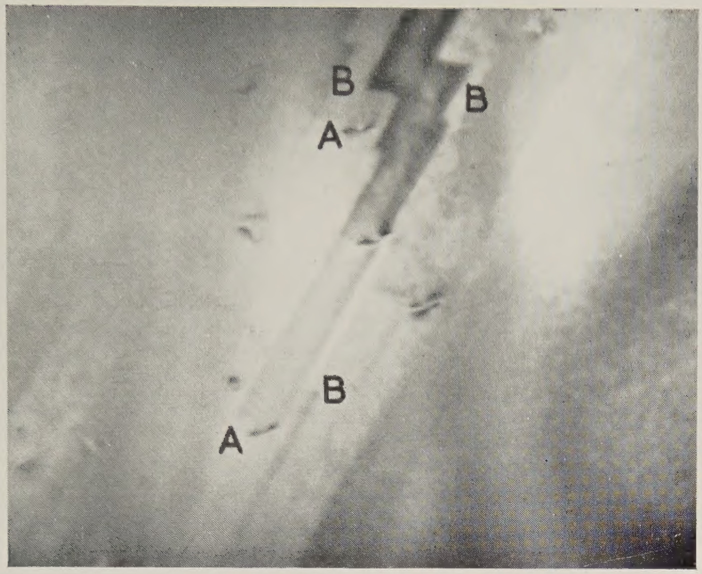

Cross-slip at BB in quenched alloys. Dislocations at A may act as obstacles to slip. Mag. × 60 000.

Fig. 7

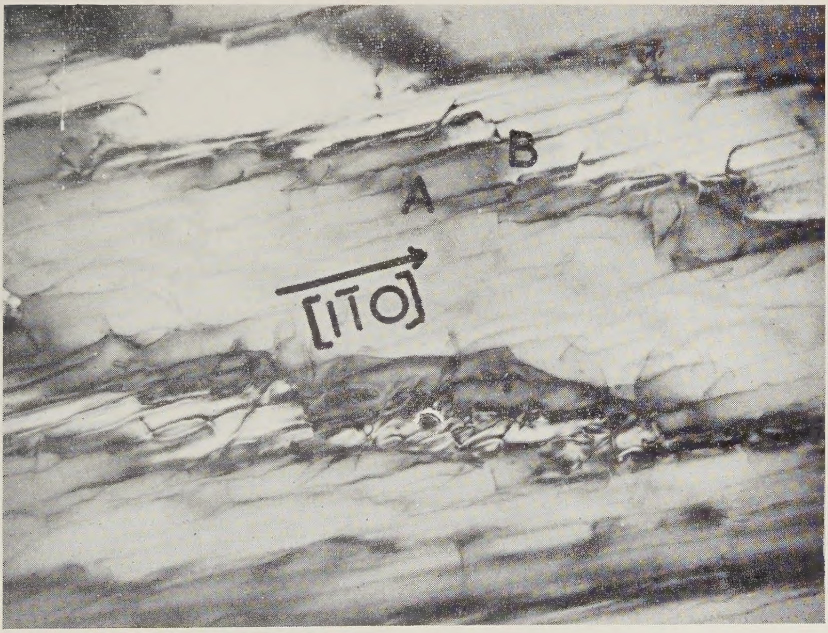

Movements of segments of dislocations A in the [1$\bar{1}$0] slip direction. Mag. × 30 000.

Fig. 8

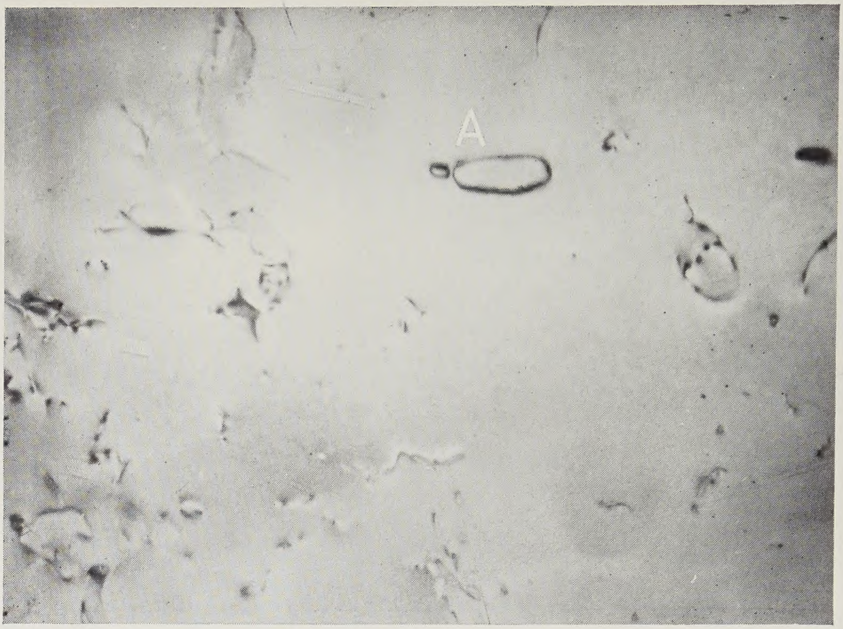

Dislocation loops A after ageing ternary alloy for 1 week at room temperature. Mag. × 30 000.

Fig. 9

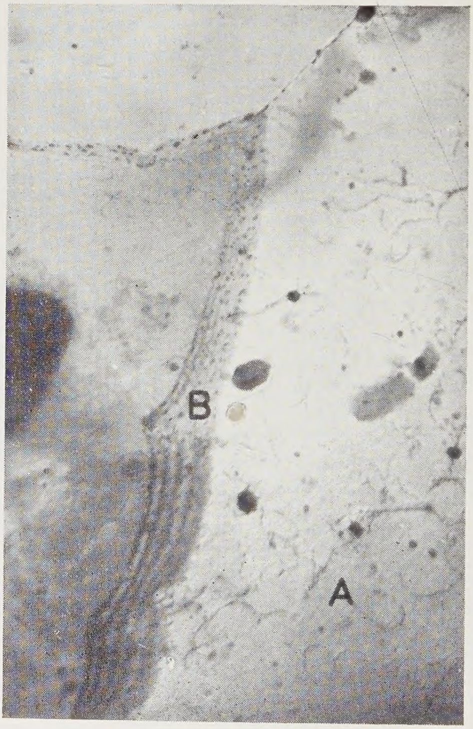

Precipitates on large loops A and along the low angle grain boundary B in quaternary alloys after ageing 1 hour at 160°c. Mag. × 12 000.

Fig. 10

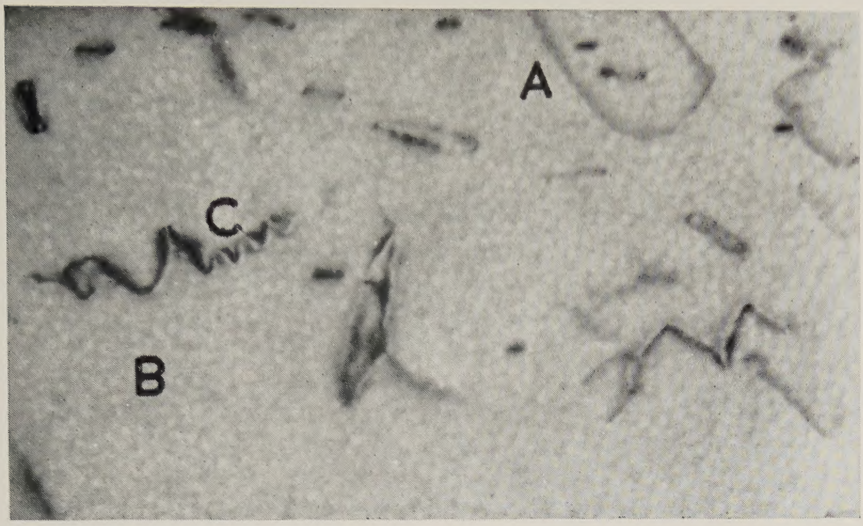

Precipitates on large loops A. The G.P. zones—50 Å diameter can be seen in the matrix at B. Dislocations at C may be spirals. Quaternary alloy aged 2 hours 120°c. Mag. × 60 000.

Fig. 11

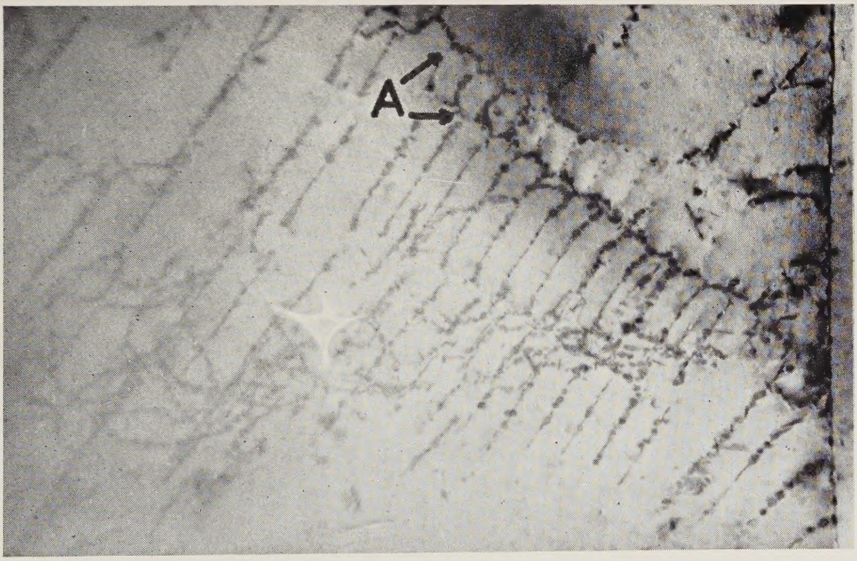

Precipitates formed on a hexagonal array of dislocations near a grain boundary. Dislocation nodes at A. Quaternary alloy aged 1 day 160°c. Mag. × 12 000.

Fig. 12

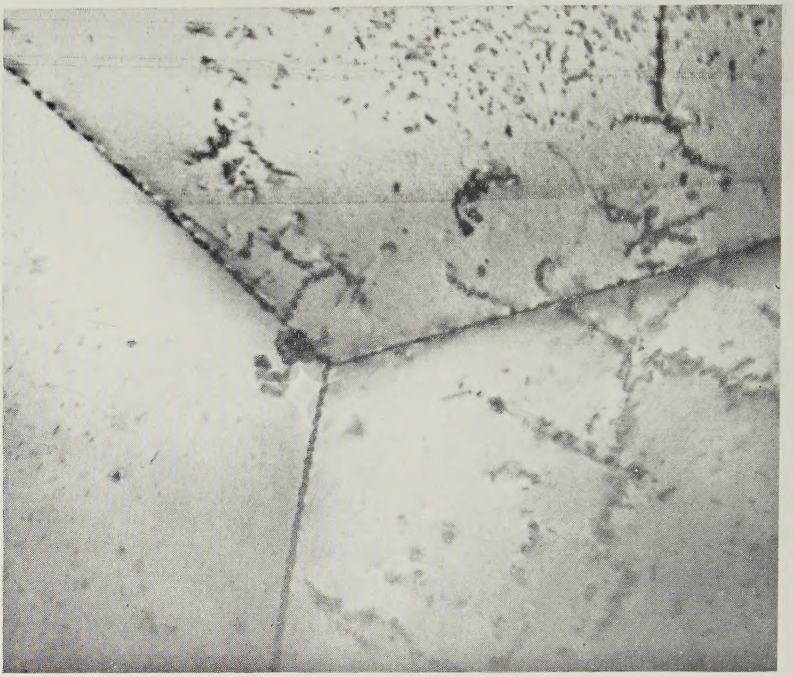

Denuded zones after precipitation along grain boundaries and on dislocations. Ternary alloy aged 1 day 160°c. Mag. × 12 000.

Fig. 13

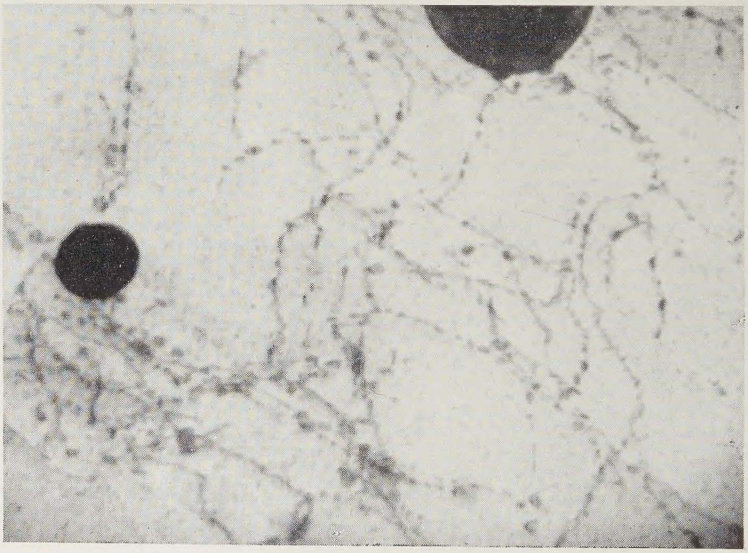

Precipitates in the matrix and along dislocation lines. The separation of precipitates is ~100 Å. Quaternary alloy aged 1 day 160°c. Mag. × 60 000.